Dipl.-Ing. Patrick Grüneberger

Analysis methods for Irregular Combustion events in SI engines

DOCTORAL THESIS

to achieve the university degree of
Doktor der technischen Wissenschaften

submitted to

Graz University of Technology

first Supervisor
Univ.-Prof. Dipl.-Ing. Dr. techn. Helmut Eichlseder
Institute of Internal Combustion Engines and Thermodynamic - TU Graz

second Supervisor
Univ.-Prof. Dipl-Ing. Dr. techn. Christian Beidl
Institute of Internal Combustion Engines and Powertrain Systems - TU Darmstadt

Graz, July 2019

"The important thing is not to stop questioning. Curiosity has its own reason for existing."

Albert Einstein

Acknowledgments

This doctoral thesis is the product of my work at AVL List GmbH in the department of optical measurement technologies.

I want to thank Dr. Ernst Winklhofer, who gave me the opportunity to work on this theme and for his supervising my work.

In that context I want to thank Dr. Harald Philipp, Dr. Alois Hirsch, Dr. Heribert Fuchs, DI Martin Kortschak, DI Bernhard Jocham, Thomas Dampf and Michael Trifterer for their help, theoretical and practical experiences and their patience to support me with my experiments and evaluations. Many thanks to all members of the department MIC and all employees of AVL for the help, the support and the great working ambience.

I want to thank Prof. Dr. Helmut Eichlseder for interesting conversations on these topics and his guidance on experiments and measurements.

Furthermore I thank my family, who enabled the path for my education and my friends who made my time great.

Finally I want to thank my wife for the big support, the tolerance and the motivation during the time of the thesis.

Patrick Grüneberger Graz, July 2019

Table of Content

Symbols, Indexes and Abbreviation

Latin symbols

$a = \lambda/(\varrho \cdot c_p)$	m²/s	Thermal diffusivity
A	m²	Surface
c	m/s	Velocity
$c = \delta q_{\mathrm{rev}}/\mathrm{d}T$	J/(kg·K)	specific heat capacity
c_m	m/s	Piston speed
c_{S}	m/s	Sonic sound
c_p ; c_v	J/(kg·K)	Specific isobar; isochoric heat capacity
d	m	Diameter, distance
E	J	Energy
h	W/(m²·K)	Heat transfer coefficient
k		Thermal conductivity
l	m	Length
m	kg or mol	Mass
$\dot{m}$	kg/s	Mass flow
n	rpm	Engine speed
p	bar, Pa	Pressure
p_{i}	bar	Indicated mean effective pressure
$\dot{Q}$	W	Heat transfer
s	m	Distance
s_l, s_t	m/s	Flame speed
t	s, min	Time
T	K	Thermodynamic temperature
u	m/s	Combustion speed
V	m³	Volume

Constants

$R = N_{\mathrm{A}} \cdot k_{\mathrm{B}} = 8{,}3145$	J/(mol·K)	General (molar) gas constant

Greek symbols

α	W/(m²·K)	Heat transfer coefficient
α	° ; rad	Angle
ε	–	Compression ratio
η	–	level of efficiency
κ	–	Isentropic exponent
λ	–	Air-fuel ratio
ρ	kg/m³	Density
τ	s	Ignition delay time
φ	deg CA	Crank angle

Additional Indexes and Abbreviations

0	Reference state; start
1	State 1; low
2	State 2; mid
3	State 3; high
1500rpm	At engine speed 1500 rpm
2000rpm	At engine speed 2000 rpm
boost	Boosting
comp	Compression
const	Constant
e	End
f	Flame propagation
g	Gas
glow, gp	Glow plug
i	Ignition
l	laminar
max	Maximum
p	Under constant pressure
PK	Peak
ref	Reference
S	Surface
SP	Spark plug
t	turbulent
TC	Turbo charger
v	Under constant volume

1D	One-dimensional
3D	Three-dimensional
CA	Crank angle
CAD	Computer-aided design
CH	Hydro carbon
CR	Compression ratio
Cyc	Cycle
Cyl	Cylinder
DI	Direct Injection
ECU	Engine control unit
EGR	Exhaust gas recirculation
ETU	Engine timing unit
EX	Exhaust
FIFO	Fist in first out
GDI	Gasoline direct injection
HCCI	Homogeneous charge compression ignition
HP	High pressure
IC	Internal combustion
IN	Intake
ID	Ignition delay
IGN	Ignition
IMEP	Indicated mean effective pressure
INJ	Injection

IR	Infra-red
LP	Low pressure
LW	Livengood-Wu
LSP	Low speed pre-ignition
MFB	Mass fraction burned
ON	Octane number
PFI	Port fuel injection
PI	Pre-ignition
RoHR	Rate of heat release
RON	Octane number
SA	Spark Advance
SCRE	Single cylinder research engine
SI	Spark ignition
SOC	Start of combustion
SP	Spark plug
TDC	Top dead centre
WOT	Wide open throttle

List of Figures

List of Tables

AFFIDAVIT

Ich erkläre an Eides statt, dass ich die vorliegende Arbeit selbstständig verfasst, andere als die angegebenen Quellen/Hilfsmittel nicht benutzt, und die den benutzten Quellen wörtlich und inhaltlich entnommenen Stellen als solche kenntlich gemacht habe. Das in TUGRAZonline hochgeladene Textdokument ist mit der vorliegenden Dissertation identisch.

I declare that I have authored this thesis independently, that I have not used other than the declared sources/resources, and that I have explicitly indicated all material which has been quoted either literally or by content from the sources used. The text document uploaded to TUGRAZonline is identical to the present doctoral thesis.

Dipl.-Ing. Patrick Grüneberger

Abstract

This thesis is about self ignition events in SI engines. The central question on self ignition is related to the source of activation energy required to ignite the in-cylinder charge. Activation energy on the "receiving" side depends on the igniting molecular species: the reactive molecules as are present in the charge such as fuel and lube oil constituents, or reactive residuals in deposits and on surfaces. The "delivery" of activation energy is related to compression of the charge, the heat of residual gas, the heat input from surfaces into the charge and hot "leftovers" from previous combustion cycles such as deposits or even burning gas. As activation of chemical reactions needs time, engine speed in combination with thermodynamic processes before self ignition are key parameters.

In combustion system development, the understanding of above mechanisms is essential to reduce the risk for pre-ignition (PI). Such understanding is supported by combustion analysis based on cylinder pressure and ignition location evaluation. The methods to accomplish such evaluation are described in this thesis in some detail, as well as their applicability to the analysis of normal engines under risk of PI.

A particular result of this work is related to the analysis of "weak" or borderline PI events. The procedure to detect such events is simply based on pressure and spark timing measurements. The benefit is seen in the evaluation of PI risks in situations which appear to show normal combustion behavior, but are under risk of escalating into mega knock cycles.

Kurzfassung

Die vorliegende Arbeit befasst sich mit Selbstzündungsphänomenen in fremdgezündeten Motoren. Die zentrale Frage betrifft dabei die Zündwilligkeit der Zylinderladung und die Herkunft der für die Zündung notwendigen Aktivierungsenergie. Die Zündwilligkeit wird durch die molekulare Zusammensetzung der Zylinderladung bestimmt. Aktivierungsenergie wird bereitgestellt durch die Kompression der Ladung, den Wärmeinhalt des Restgases sowie den Wärmeeintrag von den Brennraumoberflächen und heißen Überresten aus vorrangegangen Verbrennungszyklen. Da das Einleiten von Zündreaktionen neben der Aktivierungsenergie auch kraftstoffabhängige Zeitintervalle erfordert ist die Motordrehzahl ein maßgebender Einflussfaktor.

In der Entwicklung von Verbrennungsmotoren ist es wichtig zu verstehen wie die Vorentflammungen eingeleitet werden um diese durch geeignete Entwicklungsmaßnahmen hintanhalten zu können. Unter realen motorischen Bedingungen wird Kenntnis über Selbstzündungsvorgänge durch Druckindizierung und optische Zündortbestimmung erzielt. Die dafür nötigen experimentellen Analysemethoden werden im Detail in dieser Arbeit dargestellt und mit Beispielen aus entsprechenden Motorversuchen belegt.

Ein Teilergebnis dieser Arbeit ist die Analyse von „schwachen" bzw. grenzwertigen Vorentflammungsereignissen. Deren Analyse erfolgt durch eine genaue Messung von Zylinderdruck und Zündzeitpunk. Damit werden Vorentflammungsrisiken bereits bei scheinbar normalem Motorbetrieb erkannt und die Eskalation in den „Mega Knock" -Motorbetrieb kann frühzeitig abgefangen werden.

1 Introduction

This dissertation is about pre-ignition and irregular combustion events in spark ignition (SI) engines. Ignition in SI engines is initiated by the input into the fuel-air mixture of "activation energy" provided by the spark plasma. Any other input of sufficient activation energy into the fuel – air mixture would result in self-ignition, or pre-ignition. Such pre-ignition, potentially can destroy an engine. Consequently, as such events may occur in highly boosted modern engines to increase the efficiency, measures must be found to reduce or altogether avoid the risk of pre-ignition (PI).

In order to conclude on most effective measures to prevent PI, a procedure has been developed to measure and analyse PI processes.

At any given engine, this procedure starts with the assessment of conditions leading up to PI and consequent "irregular combustion". Main input to such assessment is the evaluation of combustion pressure signals at engine operation under risk of PI. Clarification of engine boundary conditions, such as temperatures, gas exchange, fuel and oil conditions as well as fuel injection modes contribute to such assessment. Finally, as PI is an event introduced at fairly random conditions at an unknown location of the combustion chamber, the measurement of location and time of PI events is a central part of any PI events analysis.

The chapters of this manuscript are arranged along a typical analysis procedure of PI events in a modern, mostly direct injection SI engine, see Figure 1-1.

- In order to be able to relate the analysis procedures and techniques to basic ignition and combustion processes, combustion basics are described in chapter 2
- The measurement techniques developed and applied to the study of PI are listed in measurement techniques chapter 3 to 5. Some of these techniques which may be less well known from open literature are described in more detail as may be required to understand their specific application to PI analysis.
- Data and results of the analysis cases are given in the examples chapter 6.
- The manuscript then concludes in chapter 7 and 8 with a synthesis of procedures applied to the measurement, analysis and improvement of SI engines at risk of PI and irregular combustion

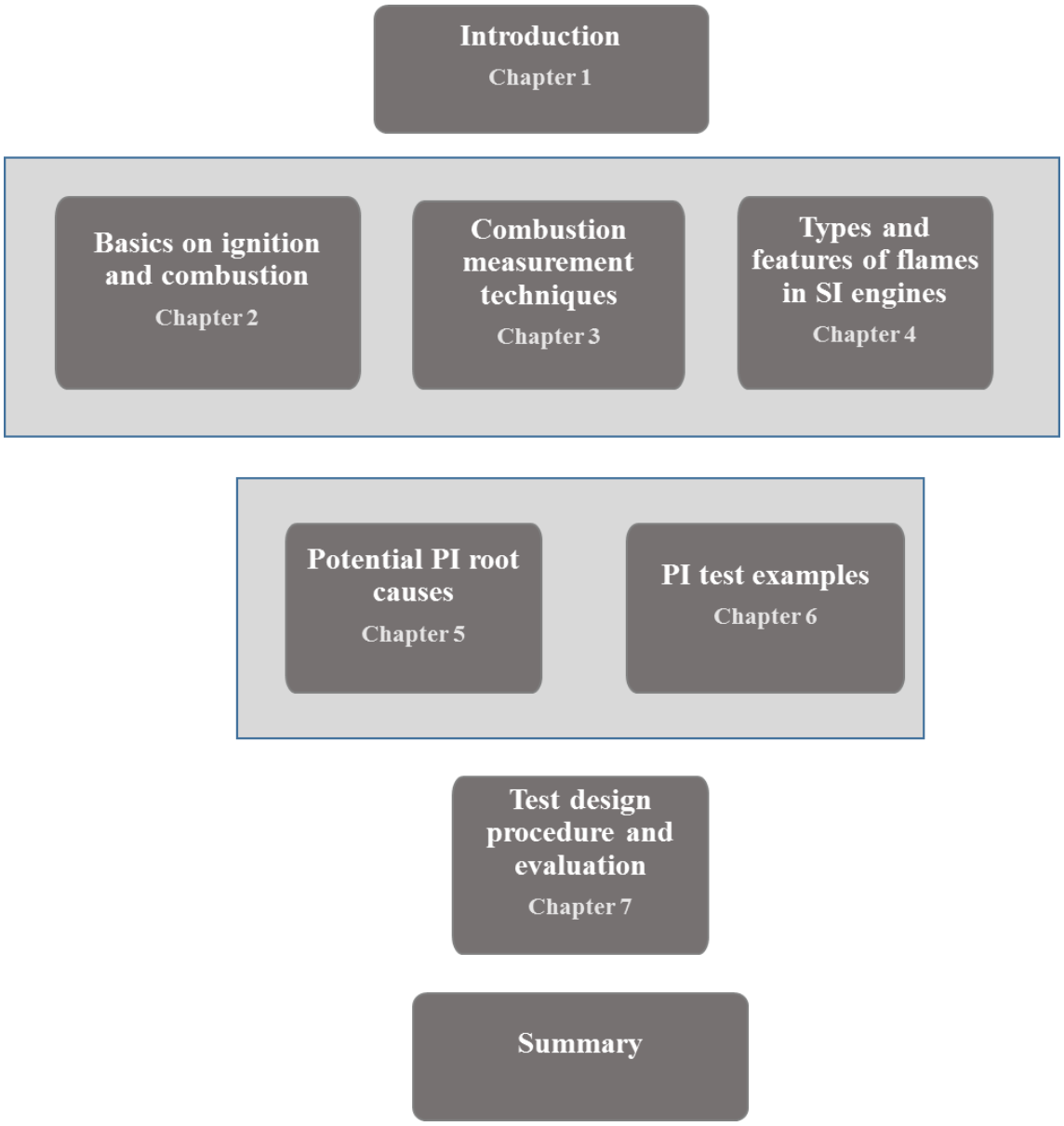

Figure 1-1 PI analysis, the structure of this thesis

2 Basics

A typical “regular” combustion in SI engines proceeds under pre-mixed stoichiometric conditions of the combustible charge after ignition at a defined ignition time by the plasma of the spark plug.

In this chapter the basic features of regular ignition and combustion are described. This serves to define and understand the difference to irregular ignition and irregular combustion as will be the main topic in this manuscript.

2.1 Ignition: Providing activation energy to premixed stoichiometric charge

2.1.1 Regular Ignition and flame propagation

The fuel-air mixture needs activation energy to initiate exothermal molecular reactions and initiate combustion. The ignited fuel-air mixture then responds with a flame propagating across the volume of the combustion chamber.

In a “regular ignition” situation, activation energy is provided by the spark plasma. Molecular diffusion of the plasma particles (ions, electrons) into the surrounding charge provides activation energy for excitation and ionisation of the compressed gas. Recombination of ions produced by this activation process to combustion intermediates and products yields thermal activation of nearby gas molecules. This process of thermal activation of the unburned gas molecules and release of thermal energy by the enthalpy of the reactions is terminated when all unburned charge is consumed or when the reaction enthalpy is insufficient to compensate for the thermal dissipation before achieving activation of unburned molecules. Such “quenching” of the flame front can arise in high turbulence situations and in charge comprising high levels of inert gas (EGR and lean mixtures). (2) (3)

The molecular diffusion process results in a macroscopic flame front progressing through and consuming the unburned mixture. The main part of reaction enthalpy is released in this flame front with the rest of the overall enthalpy being released in the post flame front reactions. As the exothermal reactions result in the production of heat, the gas reacts with an increase of pressure. This pressure rise is a source of “compression heat” rising the temperature of the unburned gas ahead of the flame front. (2)

This concept of ignition and flame front progress is illustrated in the diagram of Figure 2-1. The charge before ignition is characterised by its internal energy as provided by the compression process. The activation energy required to start combustion is specific for each type of fuel. The activation energy available in the spark discharge plasma must be sufficient to initiate local combustion by plasma particle diffusion as described above. Then, activation energy released by exothermal flame front reactions promotes the progress of the flame front through the unburned charge.

As the pressure rise, generated by the heat released in the flame, progresses at the speed of sound, the internal energy of the unburned gas rises before being consumed by the flame front reactions. The schematic in Figure 2-1 summarizes these energy – flame relations. (2) (3)

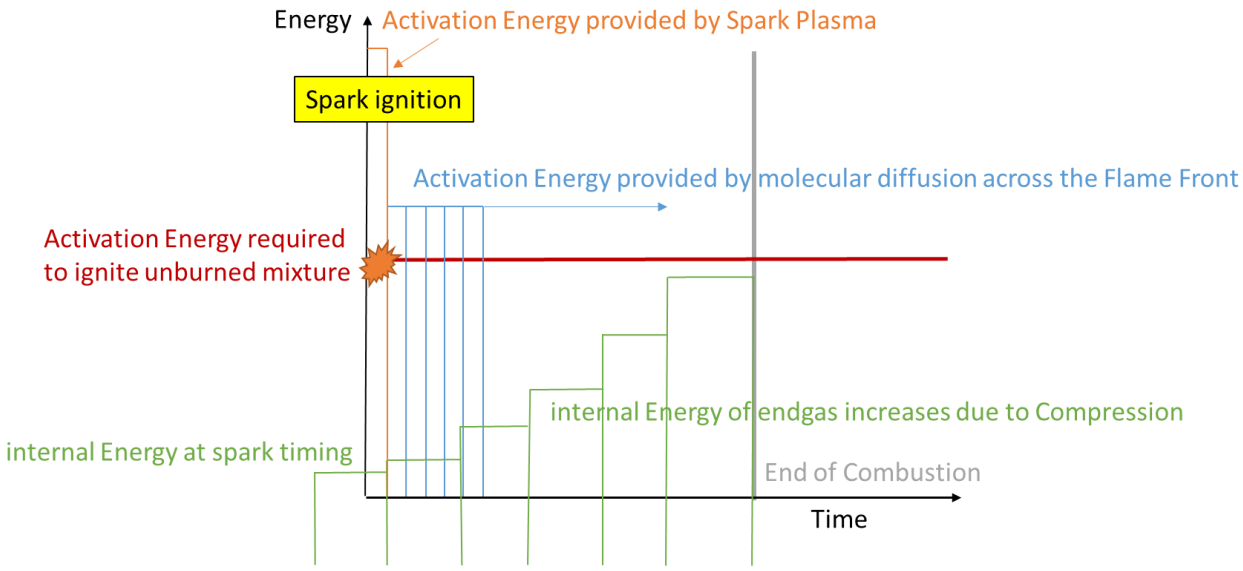

Figure 2-1 Activation energy scheme for regular ignition and combustion in SI engines

In summary, "regular combustion" starts with "regular ignition" at the time selected by spark discharge and progresses in a "turbulent flame front" until all charge is converted to products.

Table 2-1 Definition of regular and irregular combustion and ignition

	regular	irregular
ignition	Timing and location defined	Self-ignition with unknown timing and location
combustion	By the progress of the flame front	By flame front, by HCCI type combustion or by their combined effects

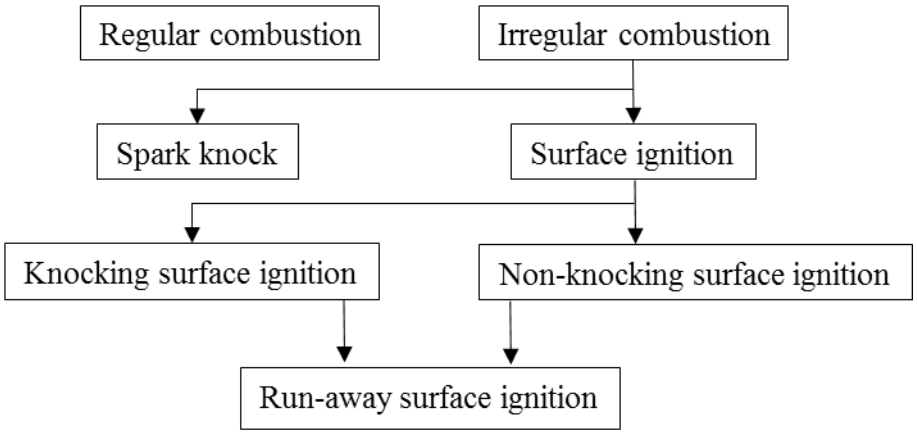

Figure 2-2 Classification of combustion phenomena as per Heywood (4)

Heywood (4) described the mentioned phenomena as:

- *Regular combustion:* is a process where a timed spark ignites the charge and a flame front propagates throughout the combustion chamber
- *Irregular combustion:* is the result of a self-ignition event before or during regular combustion.
- *Spark knock*: is a result of self-ignition of "end gas" as compression heating of end gas initiates ignition before the arrival of the flame front. Spark knock is under control of spark timing.
- *Surface ignition:* ignition of the fuel-air charge due to hot components and particles, the ignition time can occur before or after spark
- *Knocking surface ignition:* knock starting due to surface ignition, which is not controllable by the spark timing
- *Non knocking surface ignition*: very early start of combustion, charge is consumed before end gas can self-ignite
- *Run-away surface ignition:* Knock in cycle 1 initiates heating of combustion chamber surface spot which promotes knock in cycle 2 and so on, until hot surface leads up to self-ignition

Which are now the sources of activation energy other than the regular spark discharge?

Which events promote combustion other than the normal turbulent flame front propagation?

2.1.2 Spark knock

"Spark knock" as defined by Heywood starts with regular combustion, and ends with self-ignition of the end gas. The energy – time schematic in Figure 2-3 explains the rise of the end gas internal energy: in high load operation, the compression heating by the ongoing combustion raises the internal energy of the end gas above the self-ignition limit.

This schematic allows discussion of parameters influencing the end gas self-ignition event:

1. Lower risk of spark knock by reducing compression heating via
    a. Lower load
    b. Lower compression ratio
    c. Later ignition: reduces compression heating in the late combustion phase by shifting combustion into the later phase of the expansion stroke. Such retarded spark timing is the common response of any engine control system whenever knock is detected.
2. Higher risk of spark knock by heat input from external sources
    a. Intake air temperature
    b. "Hot spots" in the combustion chamber such as exhaust valves provide local heating of the end gas
    c. Residual burned gas (EGR) as source of heat
3. Fuel composition
    a. Defines the end gas activation energy and is summarized by the fuel's octane number.
    b. Defines the fuel's ignition delay time

4. Engine speed: has influence via turbulent flame front velocity and the time available for end gas heating
5. Combustion chamber design
    a. By its influence on flame front progress to burn off end gas areas before self-ignition can occur
    b. By its influence on cooling of combustion chamber surfaces
6. Ignition delay time and engine speed: Temperature – time effects are discussed in Chapter 5

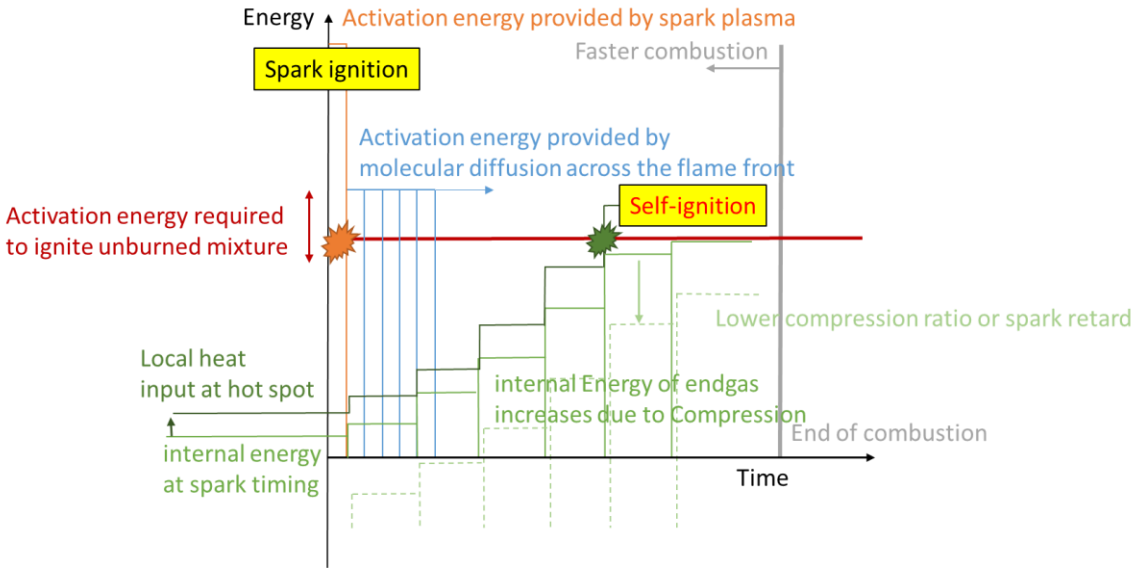

Figure 2-3 Internal gas energy scheme in spark knock situation

The fast heat release by the end gas self-ignition event introduces a pressure wave starting at the self-ignition location which then progresses through the combustion chamber at the speed of sound. Multiple reflection of this pressure wave at the combustion chamber walls results in gas oscillations which create the typical knocking sound as gas oscillations are transmitted through the engine structure to the surrounding air. (4) (5) (6)

For best combustion efficiency in high load operation, engine calibration aims at providing ignition conditions to operate the engine at its knock limit. This limit is arbitrarily defined by different manufacturers. A widely accepted guideline for the knock limit without engine damage potential is defined with:

$$Knock\ limit\ [bar] = \frac{engine\ speed\ [rpm]}{1000}$$

2.1.3 Pre-ignition

Pre-ignition is most relevant to engine operation whenever it occurs at high load with the ignition event well before spark timing. The resultant irregular combustion can introduce structural damage to the engine.

A number of potential root causes with resulting combustion phenomena are summarized in Heywood's classification in Figure 2-2. Pre-ignition, essentially is the event of providing activation energy other than by the spark discharge. This includes pre-ignition of end gas as appears in spark knock, HCCI type ignition as well as ignition by any local source in the combustion chamber.

Pre-ignition especially is of concern to engine operation as it may lead up to strong knock or "mega-knock" and the risk of engine damage.

Activation energy for pre-ignition can be provided by: (7) (8)

Local heat sources

- Hot surfaces such as spark plug, exhaust valves, etc.

Leftovers from previous combustion cycles:

- Glowing deposits: free moving or on surfaces
- Residual gas

The risk for pre-ignition is under influence of: (8) (6) (9)

- Chemical properties of
  - the fuel (auto-ignition temperatures)
  - lube oil
  - deposits (of unspecified composition)
- compression ratio
- engine operation
  - load
  - speed
  - gas exchange and fuel injection at transient load change
- the time available for heating the charge
  - the accumulated influence of activation energy is described by the Livengood Wu integral, see Chapter 5

The energy – time schematic in Figure 2-4 shows the influence of some of above parameters.

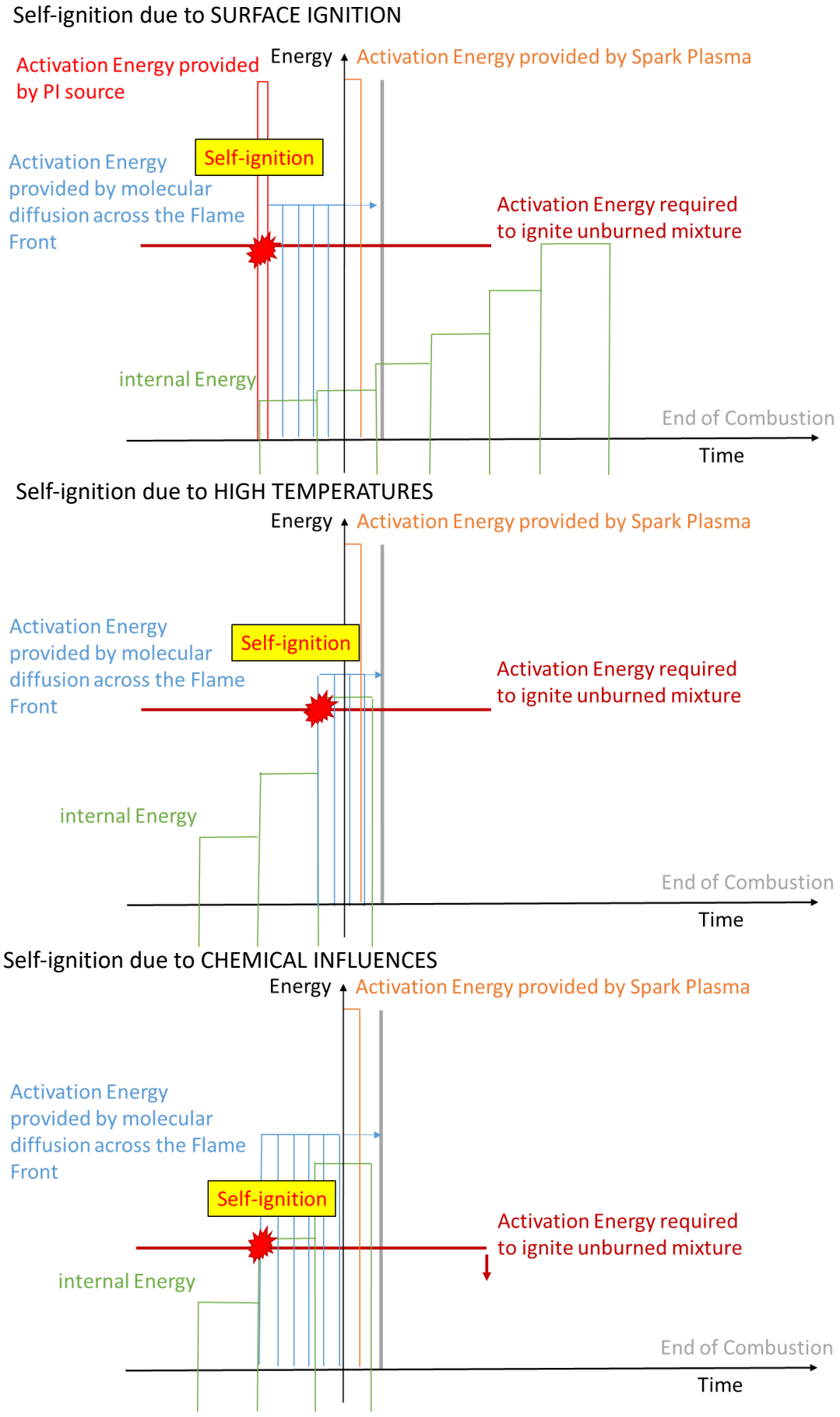

Figure 2-4 Energy schematic of in pre-ignition situations.

Figure 2-5 shows various cylinder pressure signals including

- Regular ignition and combustion
- Regular ignition followed by weak knock (spark knock)
- Pre-ignition with knock
- Pre-ignition with “mega-knock”

In all cases spark timing was set to 4 $deg\ aTDC$.

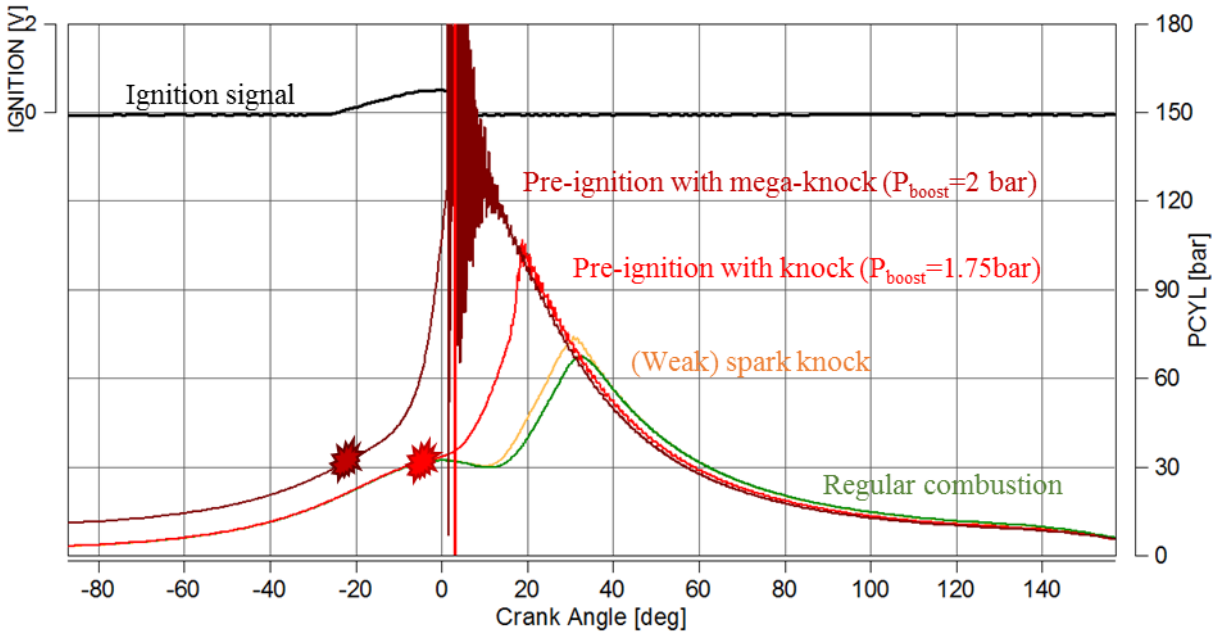

Figure 2-5 Cylinder pressure signal examples: pre-ignition with mega-knock, pre-ignition with knock, spark knock and regular combustion.

In engine development, it is the task for combustion analysis to identify root causes for each type of irregular combustion events. In Chapters 4 and 5 methods and procedures are presented to first identify location of PI events and furthermore to identify root causes, see Chapter 6, in order to provide specific advice for improvements.

In engine calibration, as pre-ignition introduces uncontrolled heat transfer to combustion chamber surfaces, and this raises the risk for consecutive PI cycles, an engine must be protected against such escalating PI events. A systematic procedure for such tasks is given in Chapter **7**.

2.1.4 Runaway knock

Runaway knock is a self-enhancing mechanism with an initial knocking cycle providing heat to raise the temperature of some area on the combustion chamber surface. Such temperature rise can lead to knock in the consecutive cycle with a repetition of surface area heating. In ongoing cycles such repeated heating of a “hot spot” may advance and enhance the knock event until the hot spot itself leads up to pre-ignition and mega-knock.

In modern SI engines such runaway sequences are interrupted by retarding spark timing whenever borderline knock is detected.

However, in case of a PI event, spark retard is ineffective and the cycle’s heat input can start a runaway sequence. The correct response to PI cycles thus must be found with intervention via fuel injection modes such as fuel cut, late cycle injection or else.

2.2 Pre-mixed flame features

Figure 2-6 shows the sequence of a flame kernel growing out of the spark discharge plasma and progressing into the unburned charge. An image of such "premixed, turbulent flame" shows the flame kernel's distorted surface which forms as a result of turbulent motion of the cylinder charge.

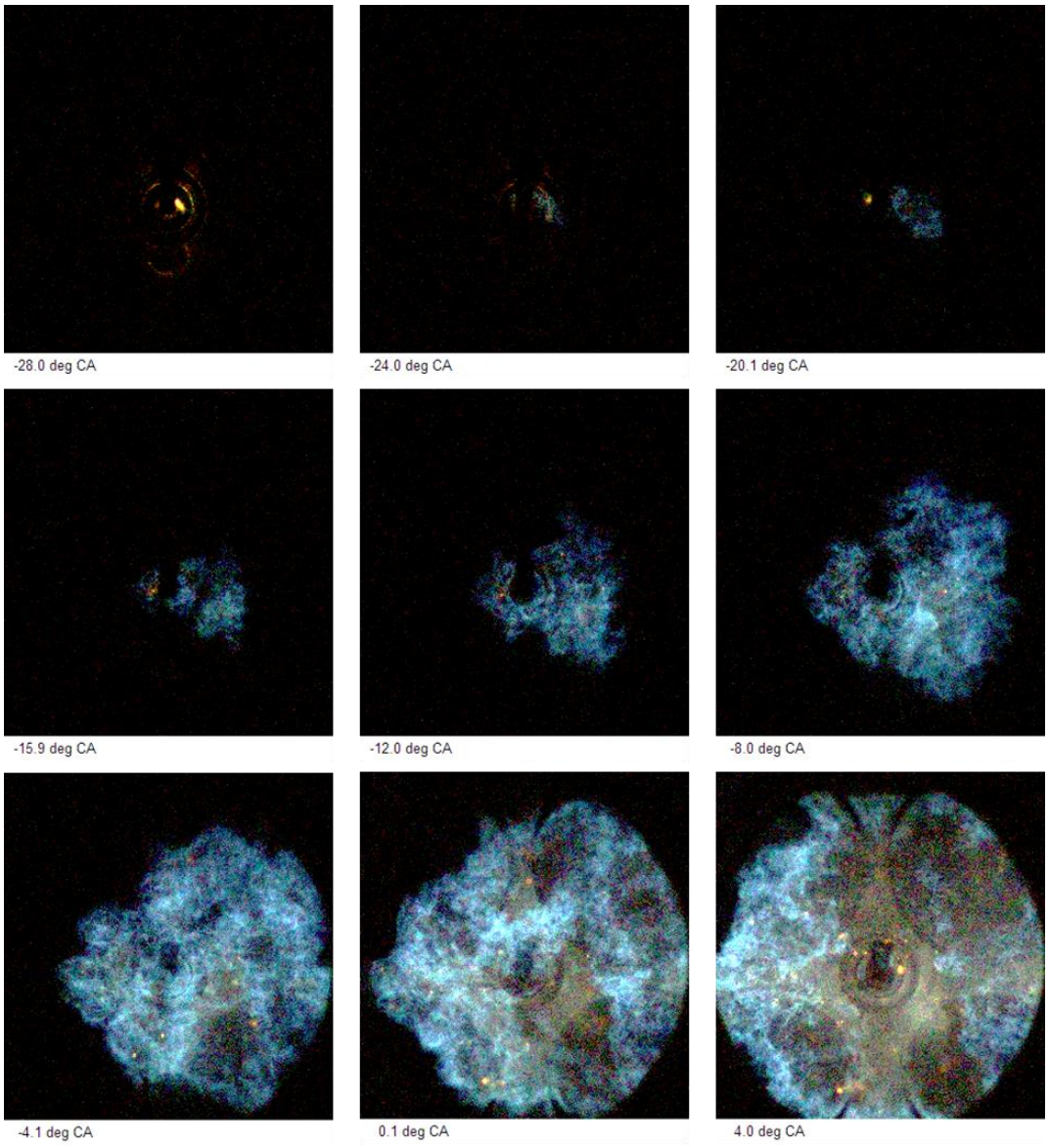

Figure 2-6 Flame growth of SI-combustion with spark timing at -28 deg CA at 2000 rpm 8bar IMEP

On microscopic scales, the boundary between burned and unburned gas is defined by molecular diffusion of products into the unburned gas and of reactants into the burned gas regime. These transport mechanisms are governed by molecular diffusion. Diffusivity is specific for the gas molecules involved and their temperature and density conditions. Consequently a laminar flame front is formed, see Figure 2-7. The progress of this flame front into unburned gas is described by the laminar flame front velocity. (5) (6)

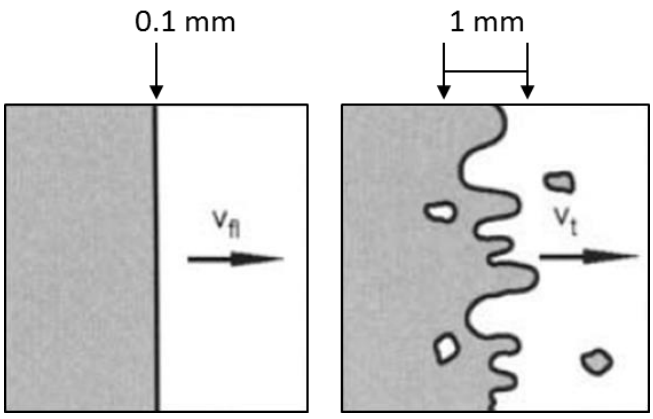

Figure 2-7 Model graph of a laminar and turbulent flame front (right) (6)(modified)

Typical values for these flame properties are given in (4)

Laminar flame front thickness: $0.1\ mm$

and laminar flame speed: $\sim 30\ \frac{cm}{s}$

at gas conditions of: $Lambda\ = 1$ at ambient pressure

Turbulent gas motion as is present in internal combustion (IC) engines has a twofold effect on such laminar flame progress:

1. It distorts the smooth laminar flame front into turbulent flame front "wrinkles", thus enlarging the surface between burned and unburned gas, see Figure 2-7. This wrinkled "turbulent flame front" extends over a typical length of $1\ mm$.
2. The enlarged contact surface enhances the overall rate at which burned and unburned gas is mixing. Consequently, overall combustion speed and turbulent flame velocity increase significantly above laminar velocities. (4)

2.3 Flame front velocity

Flame speed in SI engines is described by laminar diffusivity and turbulent enhancement of the flame front.

A formula for laminar flame speed has been proposed by Metghalchi and Keck (10) on basis of experimental data gained in combustion bomb reaction tests (11). At reference conditions ($T_0 = 298K, p_0 = 1\ atm$) laminar flame speed for gasoline type fuels was found to be

$$s_{l,0} = 28\ \frac{cm}{s}$$

Variations of temperature and pressure take influence on molecular diffusivity. Their combined effect yields the empirical formula (11)

$$s_l = s_{l,0} \left(\frac{T}{T_0}\right)^{\alpha} \left(\frac{p}{p_0}\right)^{\beta} \qquad (2\text{-}1)$$

with $\alpha = 2.18$, $\beta = -0.16$.

For engine conditions of $T = 650\ K$, $p = 35\ bar$ this yields a laminar flame velocity of about 93 cm/s.

Damköhler (12) extends this laminar flame concept for a turbulent gas environment as is relevant in engines. The turbulent flame speed is then calculated with Damköhler's equation

$$s_t = \left(1 + C\frac{u'}{s_l}\right)^n s_l. \tag{2-2}$$

With the constant $C = 2.05$ and $n = 0.7$ (5) the laminar flame speed s_l and the turbulent fluctuation velocity u'. For u' the approach (2-3) of Wirth (13) is used:

$$u' = \frac{1}{2}\, c_m \tag{2-3}$$

with mean piston speed:

$$c_m = 2 \cdot n \cdot s_m \tag{2-4}$$

where n in $[rpm]$ is the engine speed and s_m in $[mm]$ is the stroke.

This yields a turbulent flame speed for $1500\ rpm$ $\quad s_t = 14\ \frac{m}{s}$.

In an analysis of flame photographs taken in an optical research engine, Winklhofer et al. (3) have evaluated turbulent flame velocities for a range of parameters shown in Fig. 2-8. For stoichiometric mixtures turbulent flame front velocities have been found to scale with engine speed at about the rate given by

$$v = \frac{engine\ speed}{100}\ \left[\frac{m}{s}\right] \tag{2-5}$$

For an example of $1500\ rpm$ the turbulent flame speed is about $15\ m/s$.

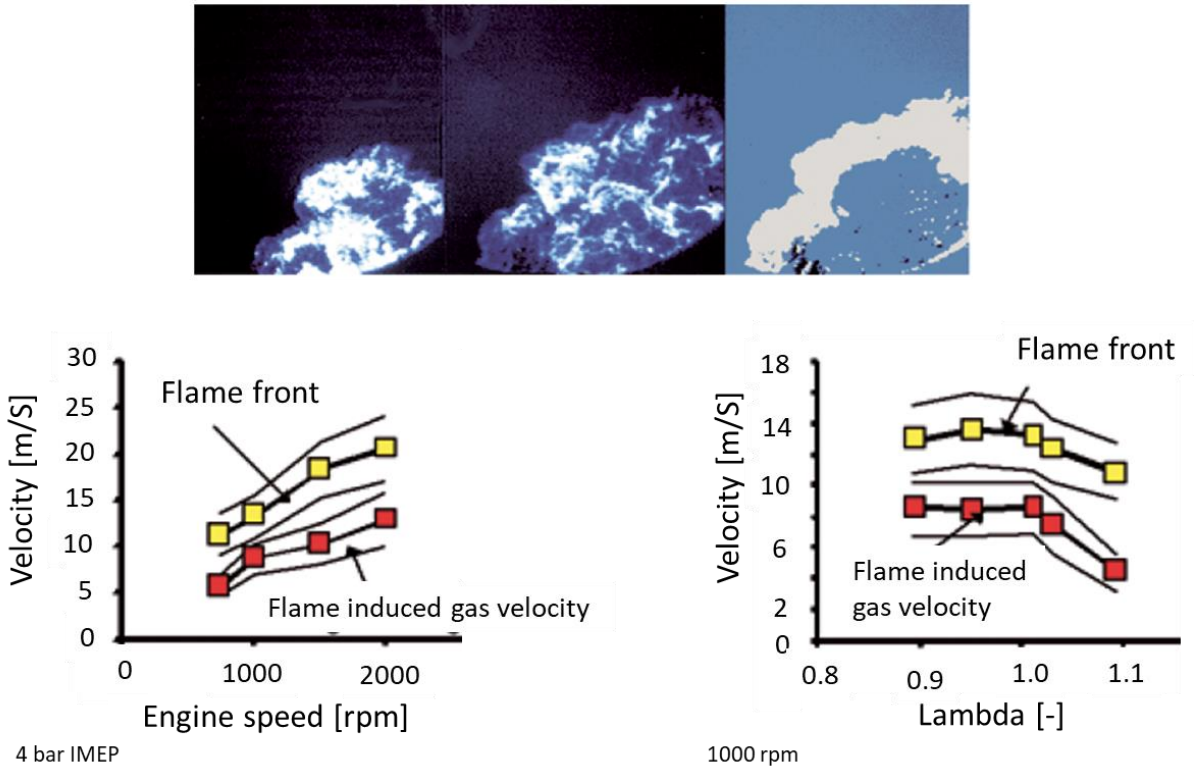

Figure 2-8 Flame front propagation velocity is evaluated from time delay flame image pairs (3)(modified)

3 Measurement methods for pre-ignition phenomena

Whenever engine development has to deal with pre-ignition and mega-knock events, the need arises to identify their root causes and to find improvements for these irregular combustion situations. For this purpose, test engines are operated under conditions at risk of PI events and data are taken to evaluate event statistics and to locate the positions where PI combustion is initiated. With knowledge of operating conditions leading up to PI and with understanding of in-cylinder areas at risk to start PI, improvements are expected to be found for engine calibration (gas exchange and injection), handling of heat transfer issues or in the re-design of critical components.

A central part in these efforts is engine operation at high load in borderline situations at risk of irregular combustion. Here, any sensor or test procedure must not interfere with original engine operation. In particular, geometry and heat transfer of original engine components must be maintained, as well as engine operation sequences in stationary and in transient mode within the speed and load range of interest.

The following chapters describe measurement and visualization techniques to support analysis of PI test situations.

3.1 Thermodynamic single cylinder research engine (SCRE)

A single cylinder engine with a displacement of around 0.5 liter has been used to initiate and study pre-ignition events. Engine features are listed in Table 3-1, design details are shown with some CAD drawings in Fig. 3-1.

Table 3-1 Engine data of the PI-engine

Fuel	Gasoline RON95
Bore	82 mm
Stroke	86 mm
Compression ratio	11.5
GDI system	Bosch GDI central position, 6 holes up to250bar
PFI system	2x VW type 022 906 031 L for oil and fuel injection
Ignition coil	VW type 6N0 905 104 with spark plug BMW type: 12 12 0 034 098
Engine management system	Open ECU to access actuators
Pressure sensor	AVL type GU22C, M5 without cooling, pressure $< 250 bar$
Endoscope	IR-Endoscope 0°, 4 mm outer diameter
Glow plug bore	Glow plug (BERU) with temperature sensor

PI events are initiated with:

- Engine operation near critical PI conditions
- A glow plug acting as hot spot ignition source
- Injection of lube oil into the intake port

Analysis of PI events is accomplished with sensors for

- Glow plug temperature
- Cylinder pressure
- Flame kernel imaging by means of an IR sensitive endoscope and camera
- Flame radiation measurement by means of a multichannel fiber optic spark plug sensor

The cylinder head has been adapted with access bores to allow insertion of above mentioned sensors. Sensor details are given in relevant chapters of this thesis.

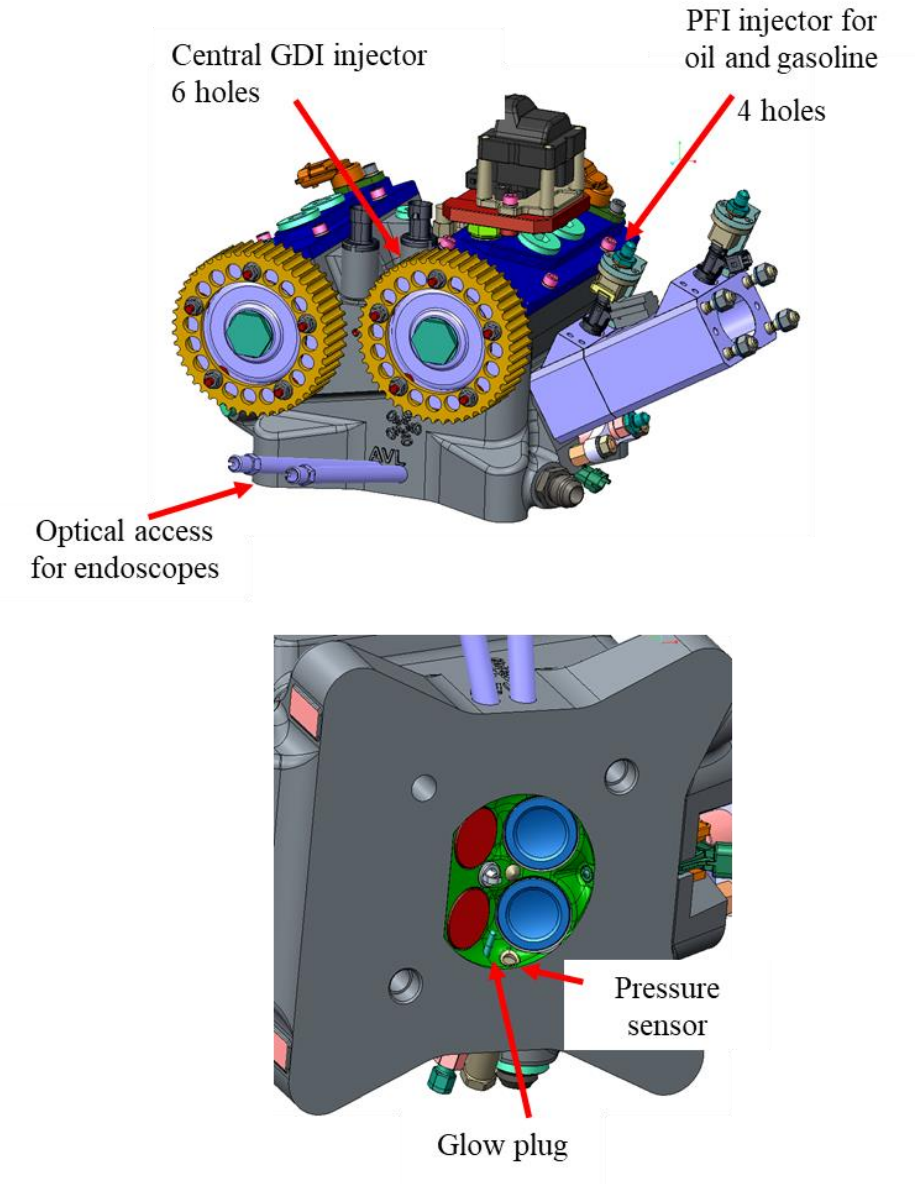

Figure 3-1 SCRE with various sensor access bores and actuators for fuel and oil injection

Table 3-2 Glow plug specifications

Glow plug	BERU ISS Glow plug with Thermocouple
Time to 1000 °C	$< 3\ s$
Temperature at 60 s	$980 - 1040\ °C$

Typical engine operation sequences comprise:

- Engine conditioning at prescribed test temperature
- Engine start and speedup
- Engine operation at target load
- Initiation of pre-ignition:
    - By means of glow plug
    - By means of oil injection
- Use of an engine "safeguard" device to terminate fuel injection in case of critical pressure conditions

A signal sequence including glow plug operation, the appearance of PI cycles and termination of fuel injection in response to a PI event is shown in Fig. 3-2.

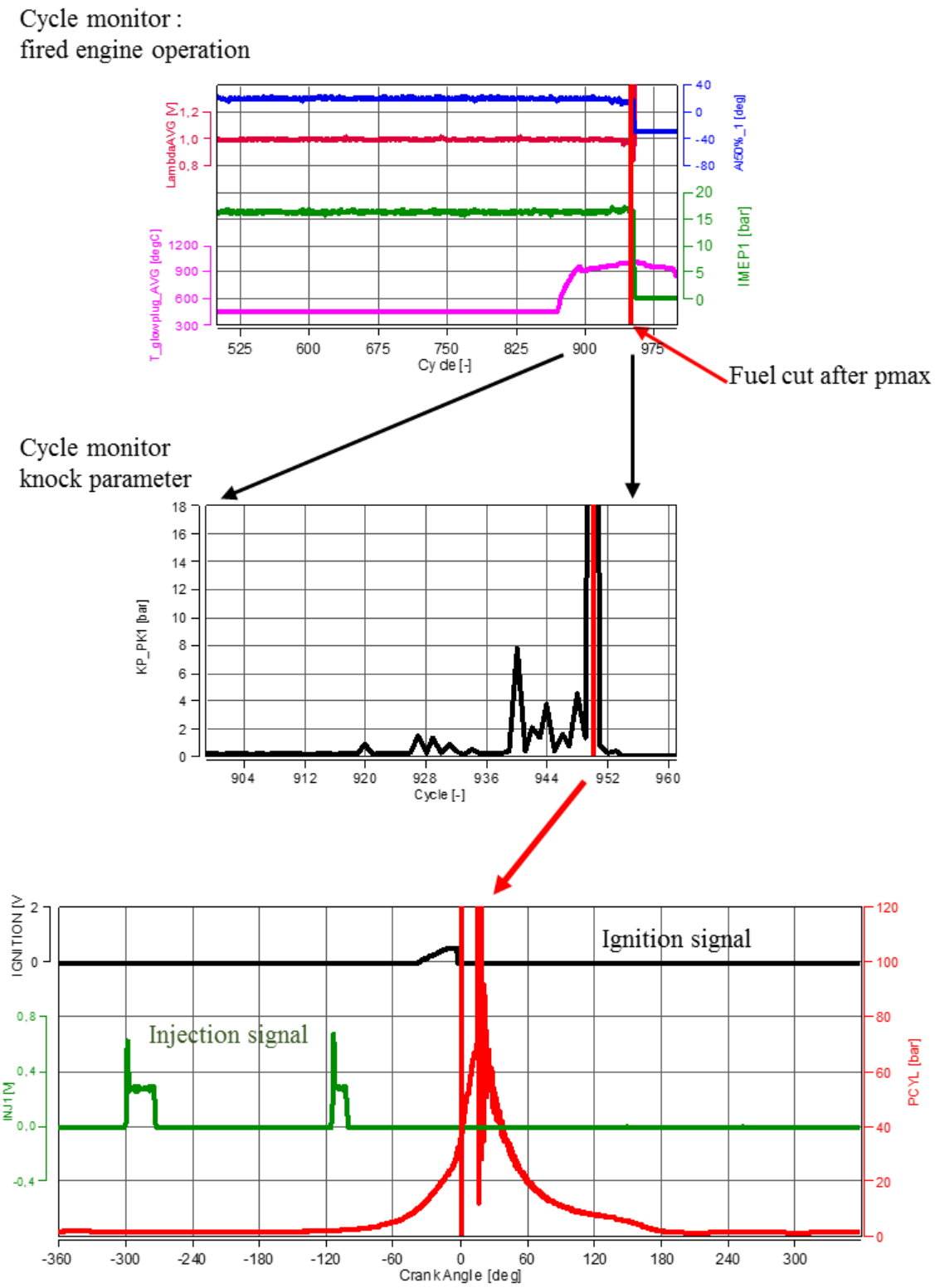

Figure 3-2 Indicating data with cycle monitor for knock parameter and a performed fuel cut

3.2 Cylinder pressure measurement

Cylinder pressure measurement is prerequisite for any analysis of combustion events in normal and irregular combustion situations. As mega-knock may introduce high pressure load on pressure sensors, they are selected for their high load capabilities.

Following pressure sensor types have been used for cylinder pressure measurements in the test cases of this work:

Table 3-3 Pressure sensor types for selected test engines

Sensor type	Specific features	Test engine
AVL - GH12D	P_{max} ~250 bar Compact dimensions M5 thread No cooling required	Transparent engine
AVL - GU22C	P_{max} ~250 bar Precise thermodynamic analysis Small dimensions No cooling required	SCRE for high load
AVL – GU24D	P_{max} ~250 bar High accuracy, Size for M8 thread No cooling required	Full engine at test bed
AVL - Spark-plug pressure sensor	P_{max}~200 bar High reliability Simple installation No cooling required	Full engine at test bed

Reference information on cylinder pressure measurement can be found in (14).

3.3 Optical methods and instrumentations

The purpose of optical flame analysis is to identify locations in the combustion chamber where PI starts. Such information, together with thermodynamic and statistical combustion cycle analysis, is expected to provide conclusions on specific root causes of PI events in the engine under test.

Potential optical methods to visualize self-ignition in a combustion chamber include:

- Imaging of flame radiation through windows in the combustion chamber wall
  - With large windows in optical research engines
  - With small windows in engines adapted for endoscope access
- Recording flame radiation with an array of optical fibres and reconstructing the origin of radiation signals by means of sensor geometry and time sequence data

Each of these techniques has been applied in the course of this thesis. Requirements and preferences in any given test situation are described in the following chapters 3.3.1 and 3.3.2.

In addition to optical requirements, each of above techniques must also be adopted to the specific features of a PI event as are:

- Unknown, sporadic appearance
- Spontaneous ignition at an unknown location
- Formation of a flame kernel with low initial brightness and gradual growth of this turbulent flame

Adoption of any technique to such engine and combustion features is in detail described in chapter 5.5 and 6.

3.3.1 Flame imaging

3.3.1.1 In an optical research engine with large windows

Basic studies of PI combustion were done in an optical research engine, see Figure 3-3. Optical access is provided with a glass cylinder and a window in the piston. Imaging of PI situations and flame kernel growth was accomplished with a high speed camera observing the combustion chamber via a 45° mirror and a piston window.

The complete test configuration comprises

- Shaft encoder
- Cylinder pressure sensor
- High speed camera (Phantom type “v7.3”, specifications see Table 3-4)
- Engine control unit (AVL “ETU - engine timing unit”)
- Signal recorder (Indication system - AVL “Indimodul”)
- Camera controller (AVL “VisioScope”)

Table 3-4 Specifications of the high speed camera (15)

Camera type	Phantom v7.3
Sensor	CMOS with $800x600\ pixels$
Frame rate	6,688 fps up 500,000 fps (with selected resolution)
Trigger	Via Engine Timing Unit (ETU)

PI events have been captured spontaneously with continuous signal recording as the engine was operated in borderline high load operation.

The images used in this document are captured with view through the piston to the roof of the cylinder head, see Figure 3-3.

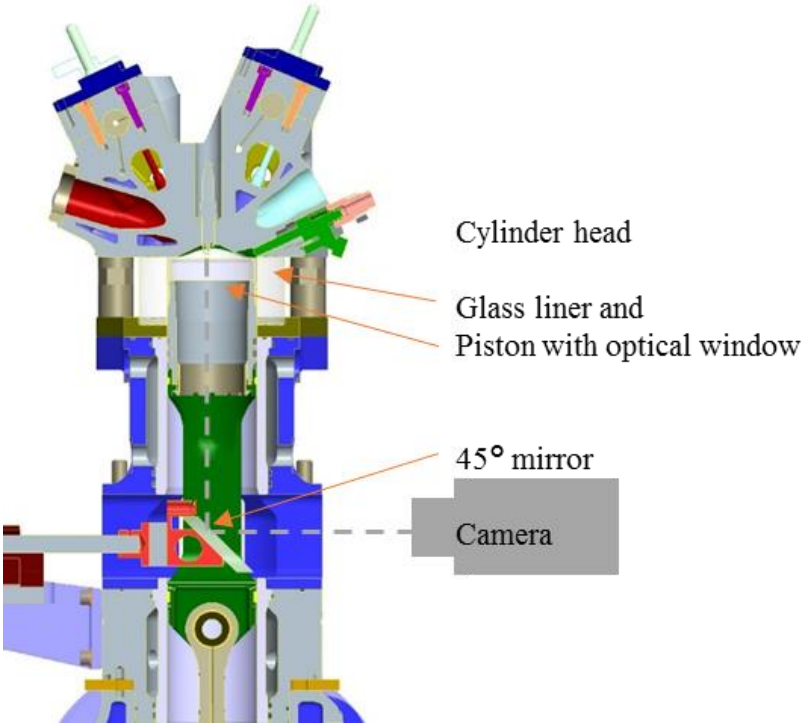

Figure 3-3 Optical engine with high speed camera set-up

For basic PI studies, the benefit of using an optical research engine is seen in following points:

- Visual access to a large portion of the combustion chamber
- The piston window and 45° mirror provide high optical access
- This allows to use a camera lens f-number of 2.8 which enables high image sensitivity
- The high speed camera records every $2\,\mathrm{deg}\,CA$ a picture with an exposure time of $20\ \mu s\ -50\ \mu s$, depending on the load point

3.3.1.2 In a combustion chamber accessed with endoscope bores

Flame kernel imaging via endoscope access suffers from the low optical throughput of endoscope optics with typical f-numbers of 48 and higher (16). For this reason, a normal high speed camera or a single shot colour camera is unsuited for flame kernel detection. Consequently, attempts for flame kernel imaging were made with a camera sensitive in the near infrared part of the spectrum and thus better suited to record low intensity flame radiation.

Table 3-5 Specifications of the infrared camera (17)

Camera type	Xeva 1.7 320
Spectral sensitivity	900 nm – 1700 nm
Frame rate	Max. 100 Hz
Trigger	Via Engine Timing Unit (ETU)
Endoscope	Storz IR 0°, endoscope diameter 4 mm with cooling channels
Endoscope windows	0° combustion chamber window with sapphire glass

As the frame rate is limited to a maximum of 100 fps, only 1 image per combustion cycle can be recorded.

In the current study, camera trigger timing was set to 1 $deg\ CA$ before spark discharge with a camera recording duration (shutter duration) of 100 µs. For results see Chapter 6.2.

Purpose of this endoscopic study was to visualize “hot spot” PI events. For this, a cylinder head has been prepared with a glow plug acting as hot spot ignition source. This hot spot together with any occasional self-ignition flame kernel was observed with the endoscope. Design of access bores and glow plug location is shown in Figure 3-4. The photograph in Figure 3-5 shows the combustion chamber before assembly. The engine with endoscope and camera installation is shown in Figure 3-6.

Figure 3-4A shows the endoscope position. A view into the combustion chamber is shown in Figure 3-4B.

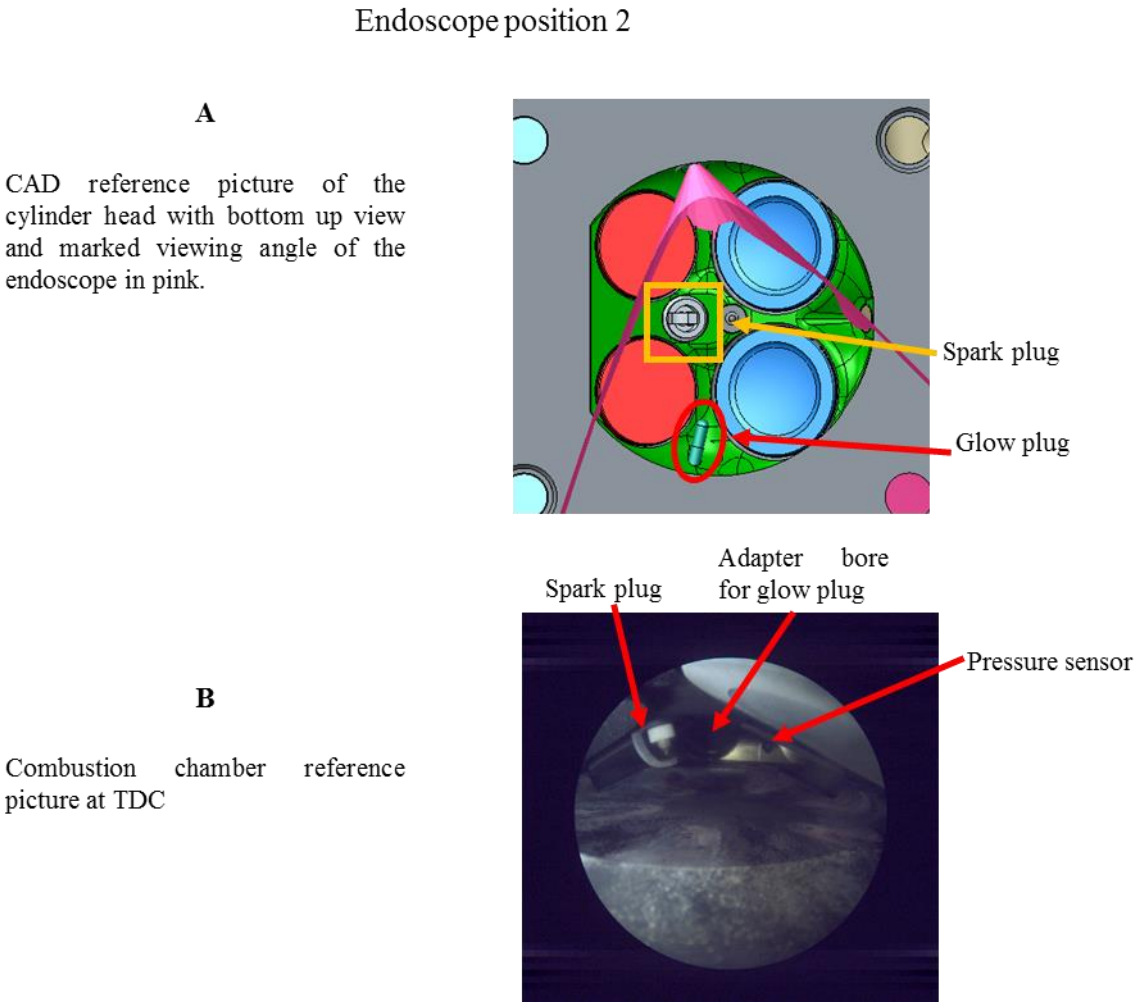

Figure 3-4 Reference picture of the endoscope view 2, A CAD picture with viewing angle of the endoscope in pink, and B reference picture at TDC

Figure 3-5 and Figure 3-6 show photographs of the cylinder head and engine test bed setup.

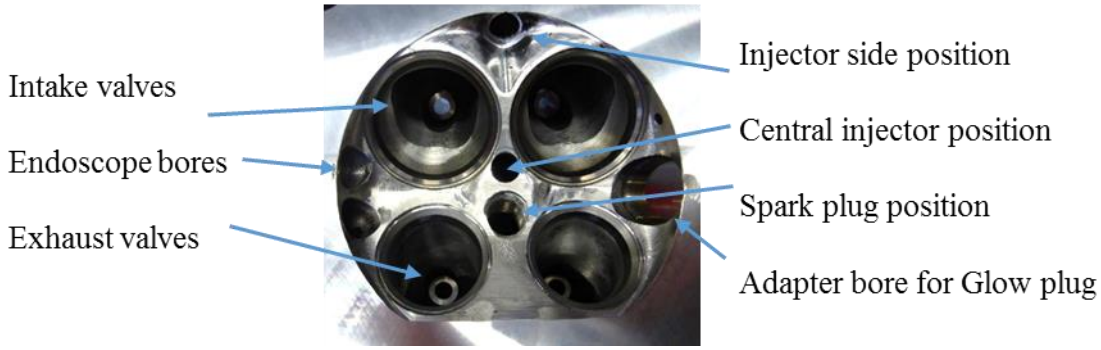

Figure 3-5 Photograph of cylinder head with access bores; view from the bottom

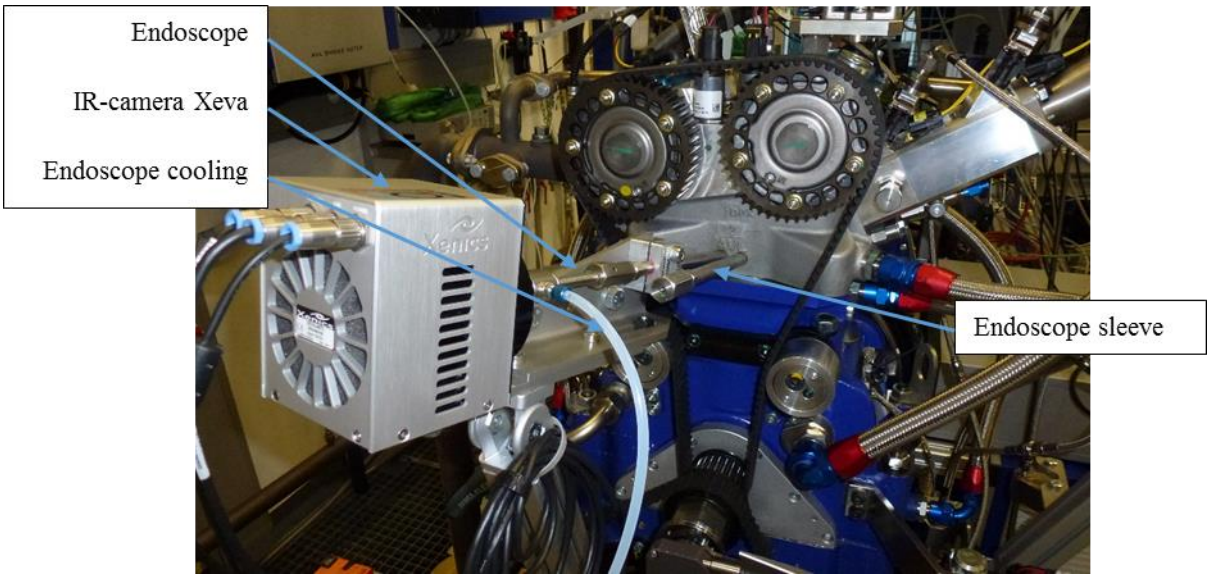

Figure 3-6 Measurement set up with IR-camera

3.3.2 Flame radiation measurement with optical fibre sensor arrays

Obviously, the request for PI analysis in normal engines cannot be satisfied if any PI event recording system needs insertion of endoscope bores or even large size windows as is done in research engines. Meeting such request, however, is accomplished with fibre optic sensors implanted in the body of spark plugs. (3)

As such “Visiolution” fibre optic spark plug sensors are extensively used in this work, sensor design and sensor variants are described here in more detail.

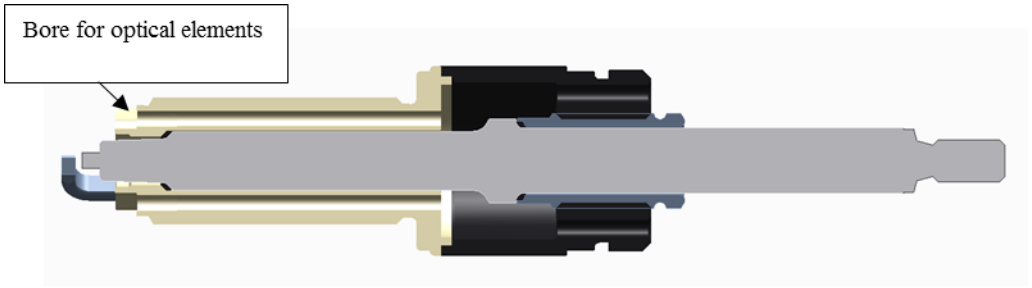

Figure 3-7 Spark plug body with center electrode and bores for optic elements

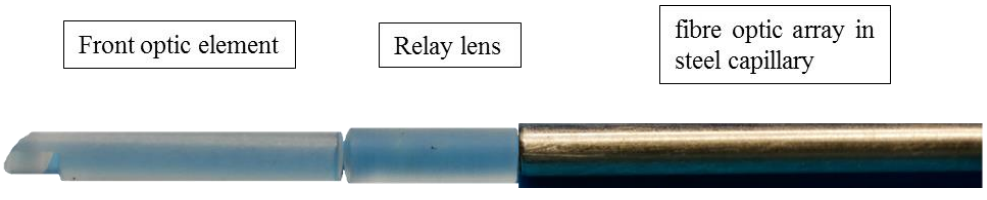

Figure 3-8 Optical elements of Visiolution sensors

The combination of optical fibres and front lenses inside the body of spark plugs as shown in Figure 3-7 and Figure 3-8 allows the recording of radiation within the aperture cone of each sensor channel. Radiation within the volume accessed by the sensor aperture contributes to the signal converted by photodiodes and transferred to a signal recorder, see Ref. (3) .

The configuration of multiple sensor channels provides information on flame appearance within the individual aperture directions. Such directional information together with flame velocity is used to locate the appearance and growth of flame events along the length of individual aperture cones. This feature is applied in identifying the location of PI events, see chapter 4.5.

The number of fibre optic sensor channels and their configuration defines the directional resolution. The benefit of high channel numbers, furthermore, is also seen in signal redundancy providing high signal confidentiality even in situations with poor signal to noise ratios.

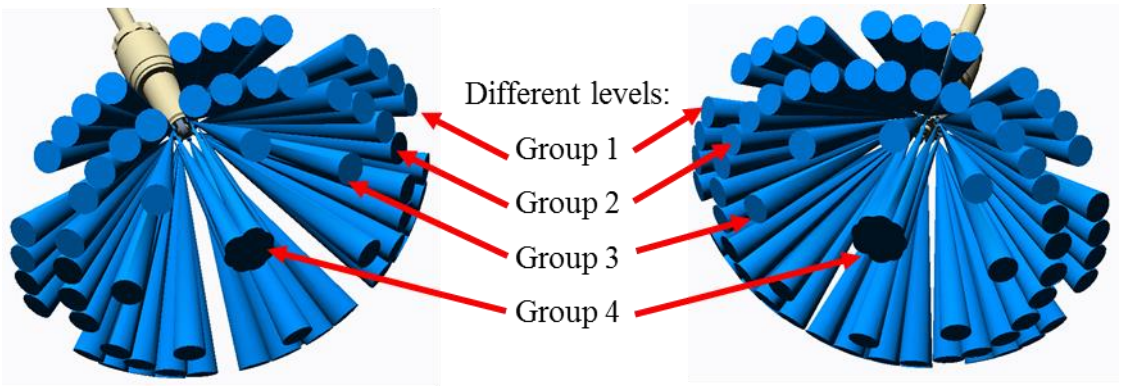

Figure 3-9 Fibre optic channel orientation of a M12 Visiolution spark plug with 70 (left) and M14 with 80 channels

When such multichannel spark plug sensors are mounted in an engine, it is mandatory to understand the orientation of each sensor channel with respect to the combustion chamber geometry. This is accomplished as follows:

I. The spark plug sensor is mounted in the spark plug thread applying a pre-described mounting torque.
II. Orientation angle "α" of the sensor index direction against the engine intake side is measured with an angular scale.
III. The sensor channel with orientation towards the intake side is given the sensor channel number 1.

Thus, in a "data box" for a 4-valve combustion chamber, sensor channel 1 is always pointing in the direction between the intake valves.

For the example of a 70- channel spark plug sensor, the angular orientation is given by the schematic of Figure 3-10:

Group 1 – Sensor Channel-Nr 1…28

Group 2 – Sensor Channel-Nr 29…56

Group 3 – Sensor Channel-Nr 57…63

Group 4 – Sensor Channel-Nr 64…70

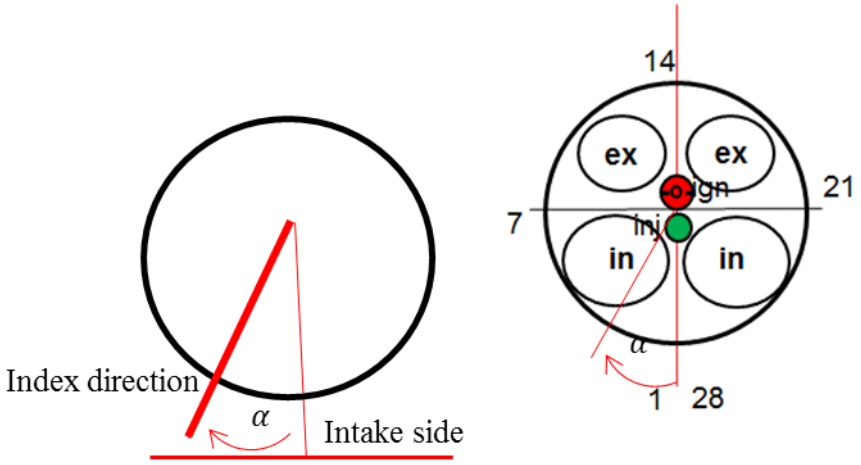

Figure 3-10 Index direction 1 is related to the spark plug sensor, signal channel nr. 1 is related to the direction between the intake valves. Orientation angle α is measured with angular scale after sensor mounting.

Calibration of the sensor channels is required in order to yield same output signal of each channel (in Volt) for any given input radiation intensity (in arbitrary units, as light intensity is not measured in absolute scales). For this purpose, an input source signal is provided by irradiating the sensor channels in an Ulbricht sphere (18). The design of the Ulbricht sphere ensures uniform illumination of each sensor channel. Thus, each channel is exposed to the same input radiation, whereas output signals are specific for each channel's optical transmission.

Thus, the calibration, or more precisely, "equilibration" procedure comprises of:

Step 1: "black background": recording of background noise levels with Ulbricht sphere switched off

Step 2: "reference brightness": With Ulbricht sphere on, recording of reference brightness signal per channel.

Step 3: "equilibration": each sensor's output signal is multiplied with a sensitivity factor to yield same output signal for same input brightness

This procedure ensures identical relative sensitivity per sensor channel. However, as the sensor input surfaces can be contaminated during engine operation, individual sensors may change their sensitivity. This effect is corrected by means of "recalibration with flame signals".

Step 4: "recalibration with flame signals": combustion cycles with premixed flame signals at a given IMEP level are used as reference light sources. This recalibration applies the same equilibration technique as is described in step 3. The method is justified under the assumption of homogeneous and isotropic radiation of premixed flames and it requires identification of premixed combustion cycles at given IMEP levels.

4 Types and features of flames in SI engines and their recording with fibre optic spark plug sensors

This chapter gives a description of premixed and diffusion flames as found in SI engine combustion. Identification of these flame types by means of fibre optic sensors and the analysis of combustion features such as flame kernel growth, knocking combustion and finally the identification of pre-ignition locations comprise the main part of this chapter.

4.1 Pre-mixed flames and flame signals

Homogenization of stoichiometric (and slightly rich or lean) gaseous fuel – air mixture during the intake and compression stroke, by definition results in a "pre-mixed" flame. Radiation of this premixed flame is dominated by the recombination of excited molecules resulting in the typically blue (or white) flames as shown in Figure 4-1. The geometrical structure of a premixed flame and its growth is the result of molecular diffusion and the enhancement of the flame front by turbulent gas motion as was described in chapter 2.3 and 2.4.

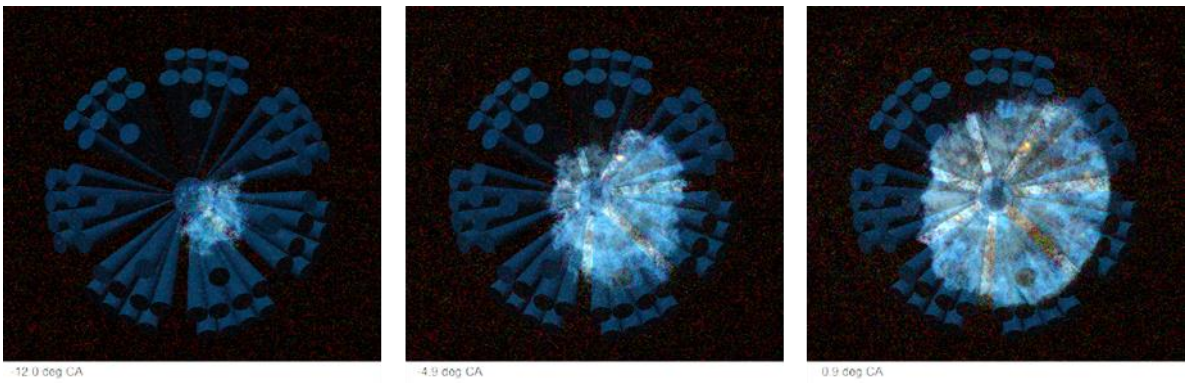

Figure 4-1 Flame kernel growth seen in an optical research engine. Aperture cones of a fiber optic spark plug sensor are superimposed on the flames to show the fields of view for each sensor channel.

Measurement of such premixed flame radiation along the multiple aperture cones of a fibre optic spark plug yields radiation signals as shown in Figure 4-2.

Such premixed flame signals are characterized by

1. Overall features:
    a. Signal shape (start, growth, peak and decay) is similar to the rate of heat release.
    b. Signal peak at about the time of maximum combustion pressure (19)

These overall features a and b are similar for each sensor channel.

2. Signal details:
    a. At start of combustion flame growth can be non-symmetric. This results in a differentiation of signal start and growth in individual sensor channels.
    b. Signal peaks may differ in timing and level due to asymmetric flame growth.
3. Signals are furthermore under influence of sensor front contamination. This is of minor concern in premixed combustion situations, however it must be considered in presence of diffusion flames, see chapter 4.2.

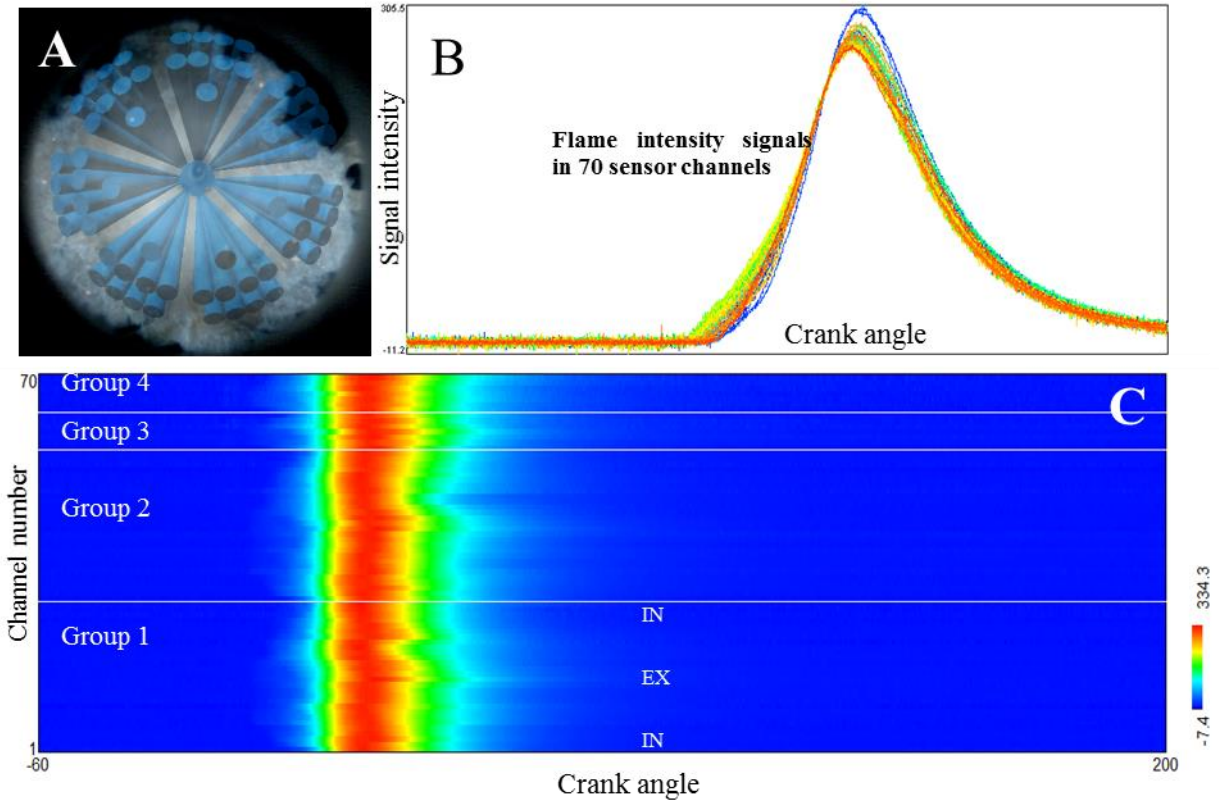

Figure 4-2 Example of pre-mixed combustion signals: (A) pre-mixed flame recorded in an optical research engine superimposed on the sensor aperture cones of a Visiolution sensor, (B) Visiolution signals shown in a line plot, (C) same Visiolution signals displayed in a colour coded signal box

4.2 Diffusion flame signals

In SI engines with incomplete fuel evaporation and insufficient fuel – air mixing prior to combustion, areas with liquid fuel (droplets or wall film) and rich (Lambda < 0.5) fuel vapour result in diffusion flames. Such diffusion flames comprise of soot particles which are heated by the premixed flame environment. As flame temperatures may be as high as $2000\,K$, soot particle radiation comprises of broadband continuum radiation. Due to the high specific density of soot particles as compared to the gaseous environment, local radiation intensity is high and easily seen with a camera or with fibre sensors, see Figure 4-3.

The fibre sensor signal records of diffusion flames embedded in the background of premixed flames (Figure 4-3) are characterized by

1. Overall features:
    a. Each sensor shows a mostly similar premixed flame background signal
    b. individual sensor channels show various degrees of additional radiation
    c. such additional radiation is unrelated to combustion pressure or rate of heat release

Specific features of such diffusion flames include following

2. Signal details:
    a. as opposed to premixed flame signals, diffusion flame radiation can pertain long into the expansion stroke
    b. signals are highly localized
3. Sensor front contamination must be considered in presence of diffusion flames

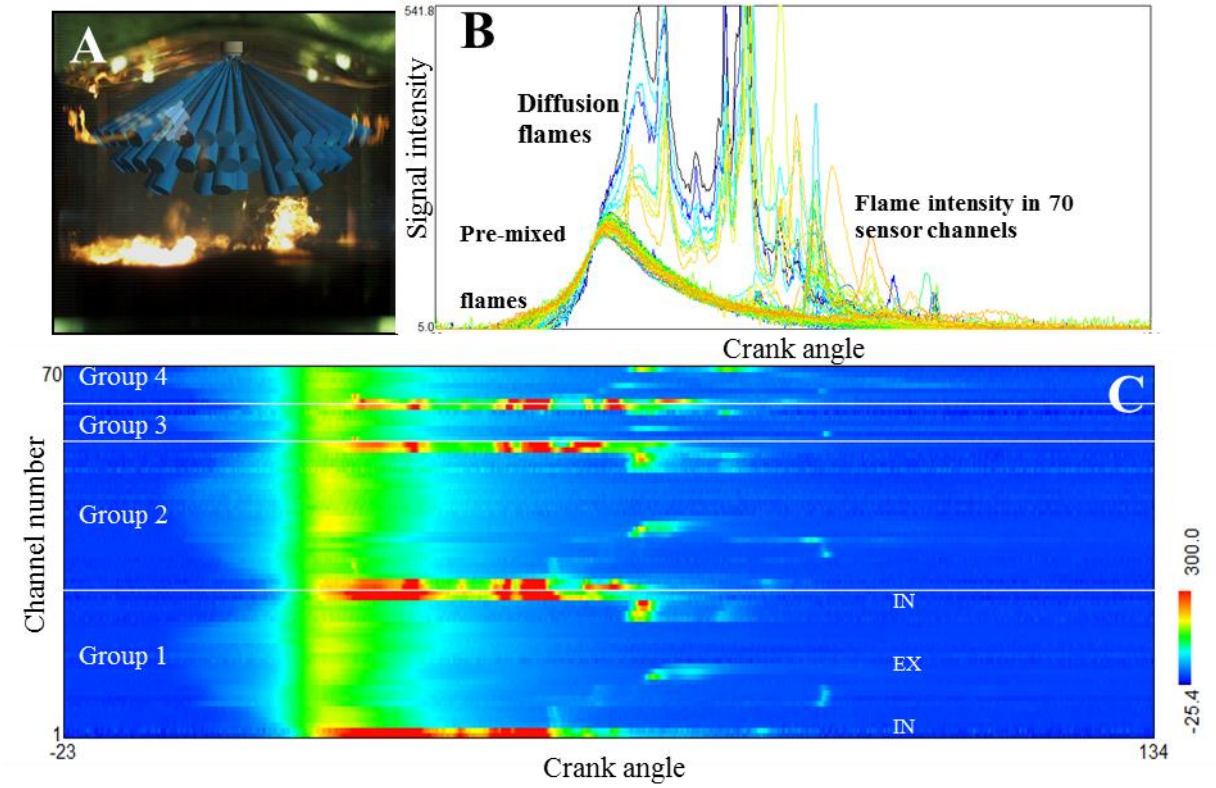

Figure 4-3 Example of diffusion combustion signals: (A) diffusion flame recorded in an optical research engine superimposed on the sensor aperture cones of a Visiolution sensor, (B) Visiolution signals shown in a line plot, (C) same Visiolution signals displayed

4.3 Diffusion flame localization

The sensor channels allow identification of the direction at which diffusion flames are located. As is shown in Figure 4-4. The signal chart with radiation versus degree crank angle signals is evaluated for any given deg CA in a polar sensor channel diagram. For the same deg CA, graphics show the position of piston and the intersection of sensor channel apertures on the liner and piston surface. Again, the radiation signals have no resolution along the aperture cones. However, the deg CA sequence of polar diagrams allows conclusions about the location of diffusion flame clouds attached to the piston surface, the liner or being close to the spark plug. The diffusion flames of the example given in Figure 4-4 and Figure 4-5 show the occurrence of soot (diffusion flames) near the piston bowl surface.

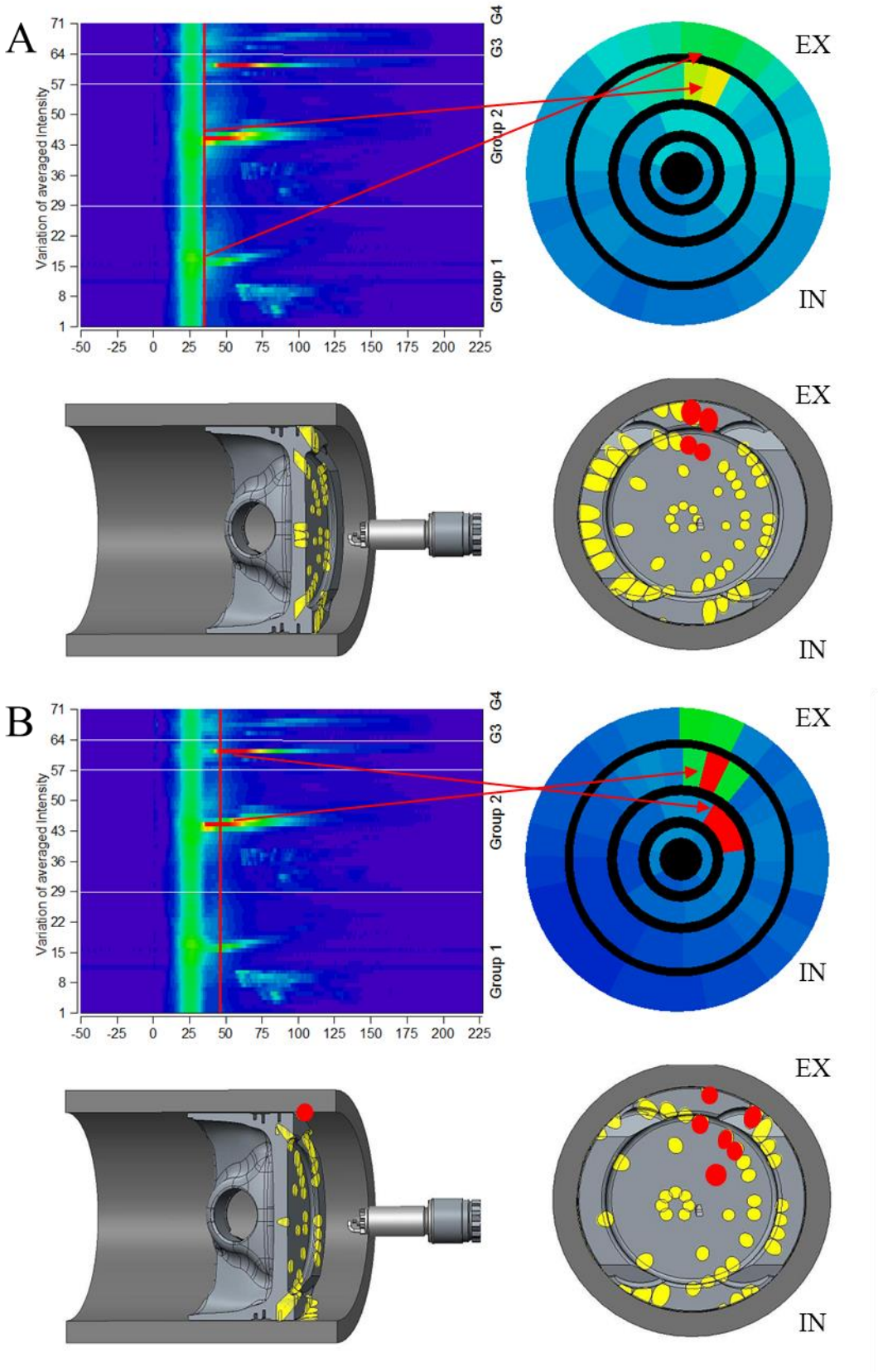

Figure 4-4 Section of a signal sequence of consecutive time points (A,B) show the appearance of diffusion flame signals. Diffusion flame location is evaluated from the polar signal diagram and the sensor channel positions at the actual deg CA position.

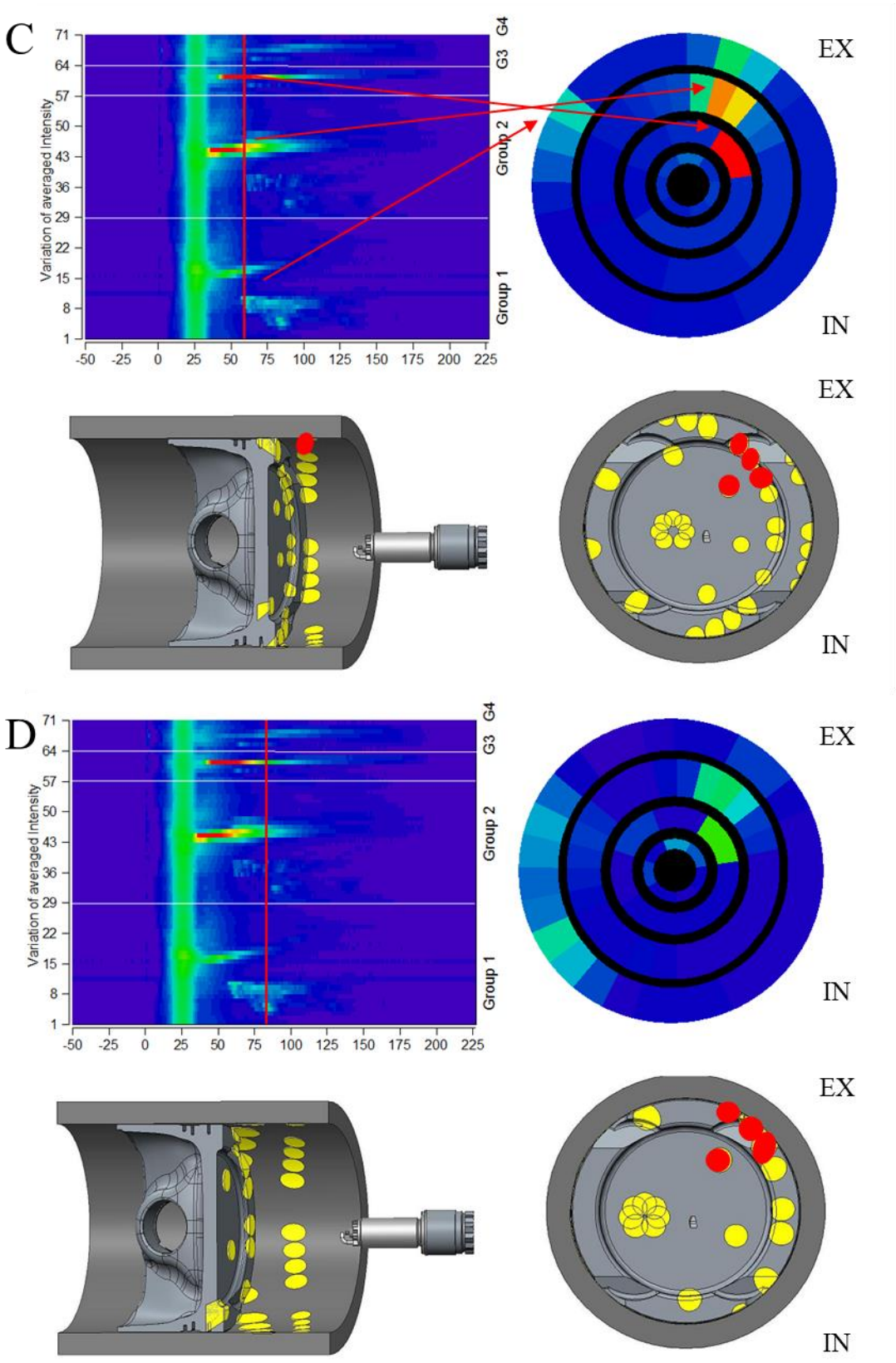

Figure 4-5 Section of a signal sequence of consecutive time points (C, D) show the appearance of diffusion flame signals. Diffusion flame location is evaluated from the polar signal diagram and the sensor channel positions at the actual deg CA position.

4.4 Pre-ignition combustion

The central request in pre-ignition combustion situations is to understand possible root causes in order to find improvements. Identification of PI locations supports such understanding and, consequently, contributes a significant part to PI root cause analysis.

Identification of PI centres is accomplished with flame radiation measurement using multichannel fibre optic spark plug sensors. The concept to identify flame kernel location and flame growth is shown in the schematics of Figure 4-6.

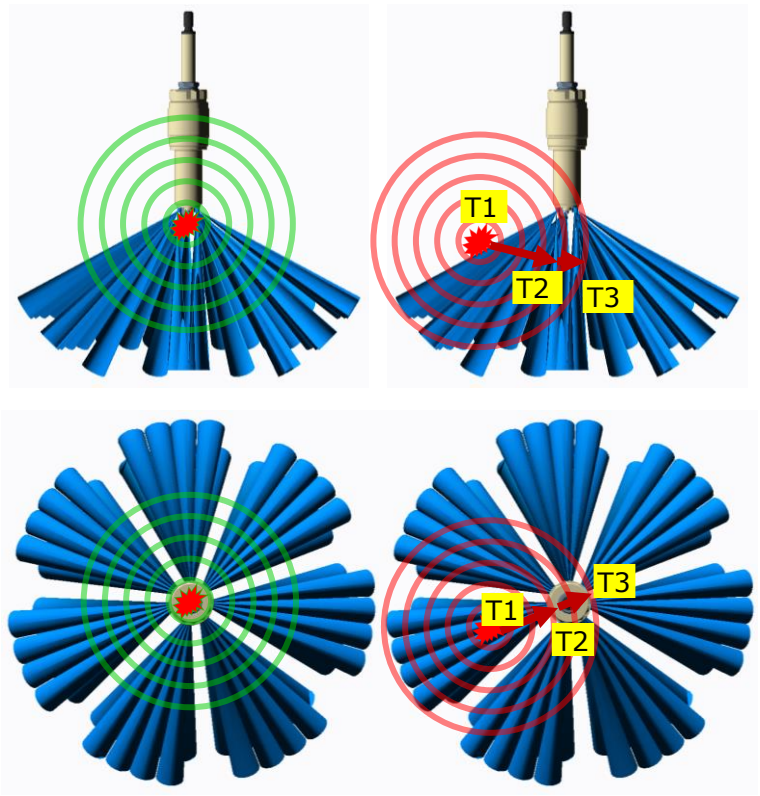

Figure 4-6 Concept showing ignition and flame kernel growth of regular (left) and irregular combustion

The concept of Figure 4-6 presumes the same premixed type turbulent flame front propagation in both regular and irregular ignition situations. Sensor signal sequence (see Figure 4-7, Figure 4-8 and Figure 4-9) and rate of signal expansion into neighbor channels are used to locate pre-ignition centers.

The following Figure 4-7 shows the flame signals of a regular ignition – combustion situation. The green - red colour scaling shows the transition from dark background (in green) to flame radiation (in red) for each sensor channel. With this scaling the first appearance of light is easily detected. The blue bar shows the spark discharge time. In Figure 4-7 the first appearance of flame radiation is seen a few deg CA after spark timing as is expected in a normal spark ignition flame. The polar signal maps show the typical appearance and growth of the flame kernel centred around the spark plug.

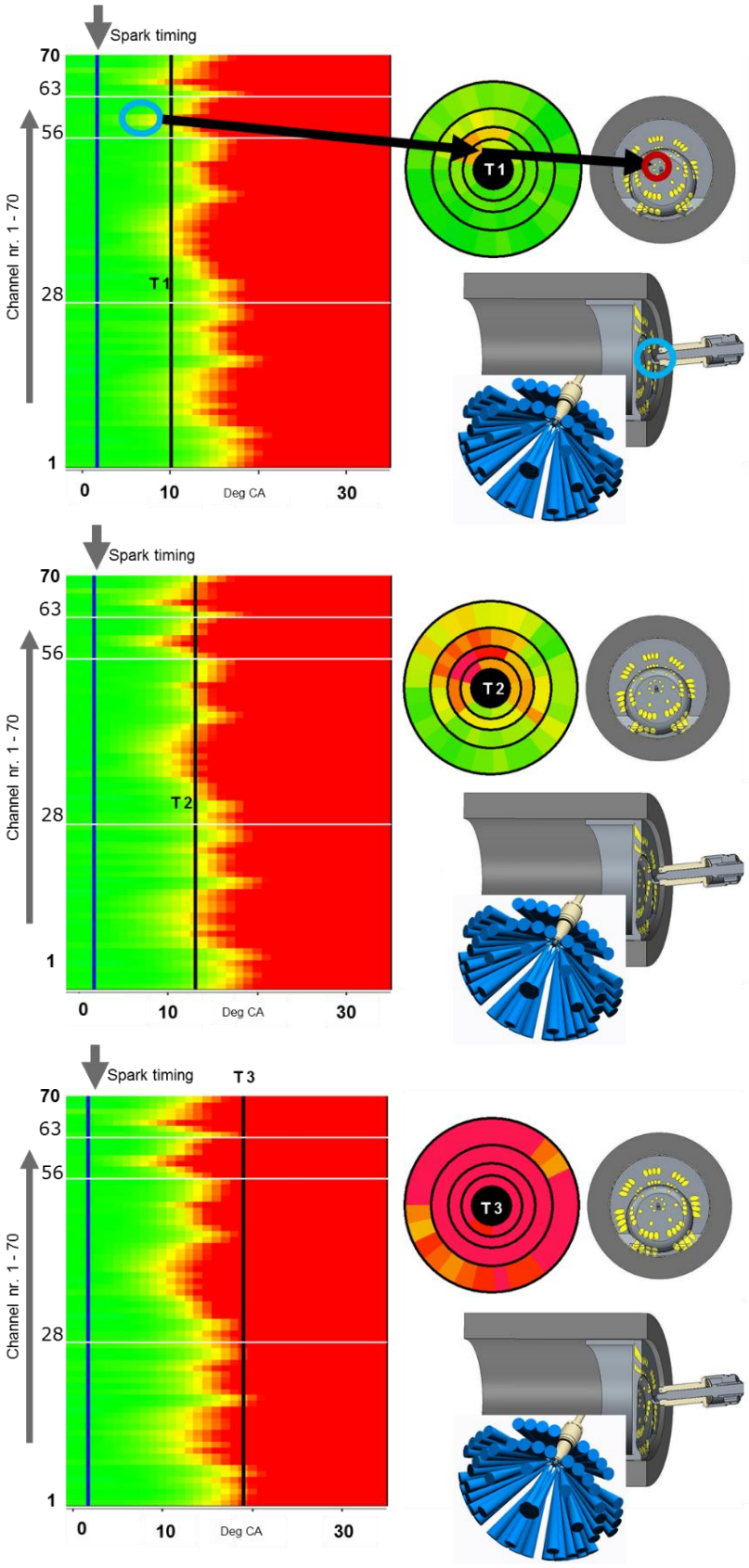

Figure 4-7 Visiolution signals of regular ignition and flame growth

The example of an irregular ignition event with flame growth starting at the combustion chamber periphery is given in Figure 4-8. Note that this PI event occurs more than 10 $deg\ CA$ before spark discharge.

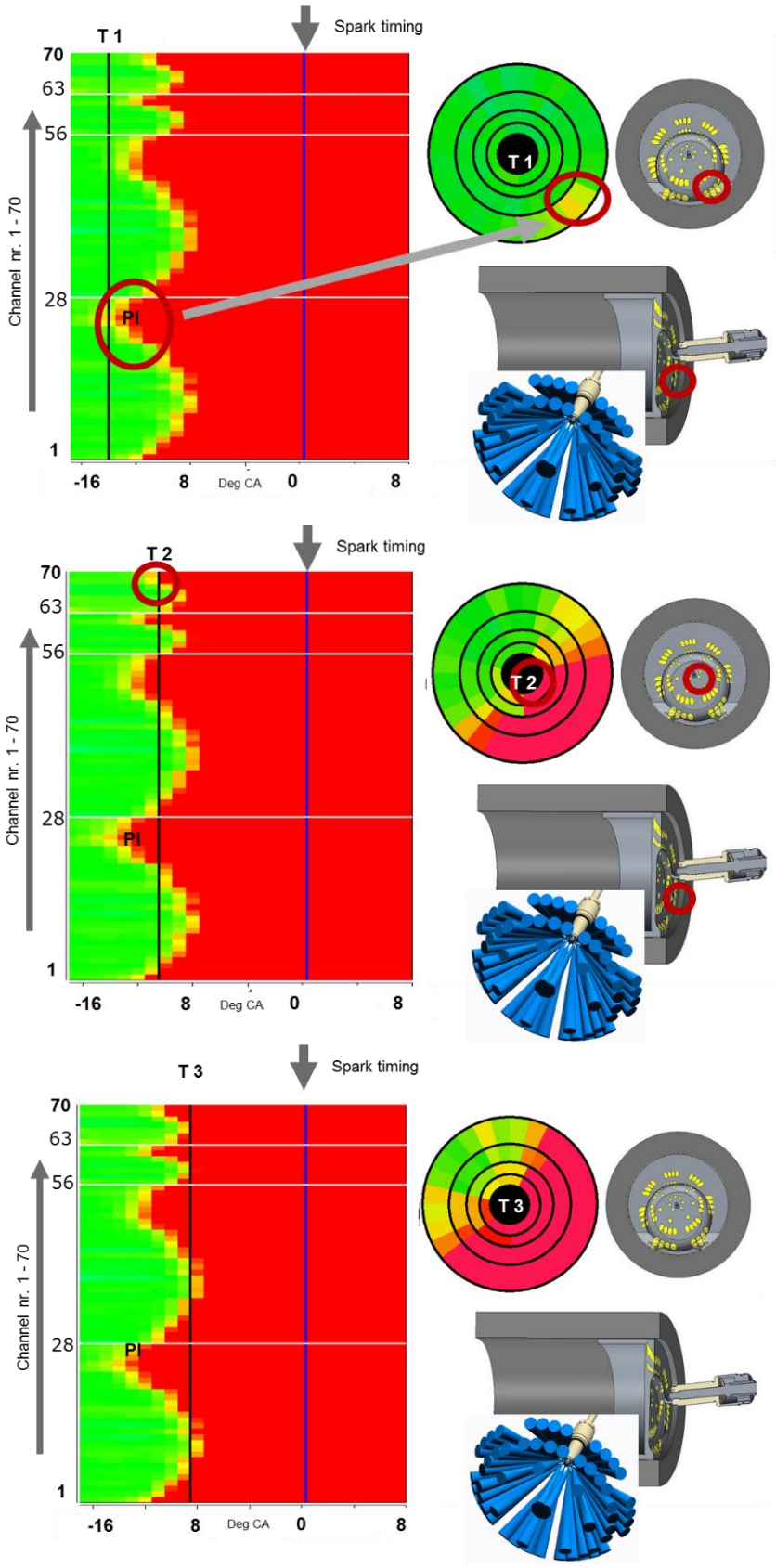

Figure 4-8 Signal signature of a pre-ignition event

The picture series in Figure 4-9 shows an irregular combustion cycle with two pre-ignition events occurring in the same cycle. The location of these PI events is shown in the polar diagrams of Figure 4-9.

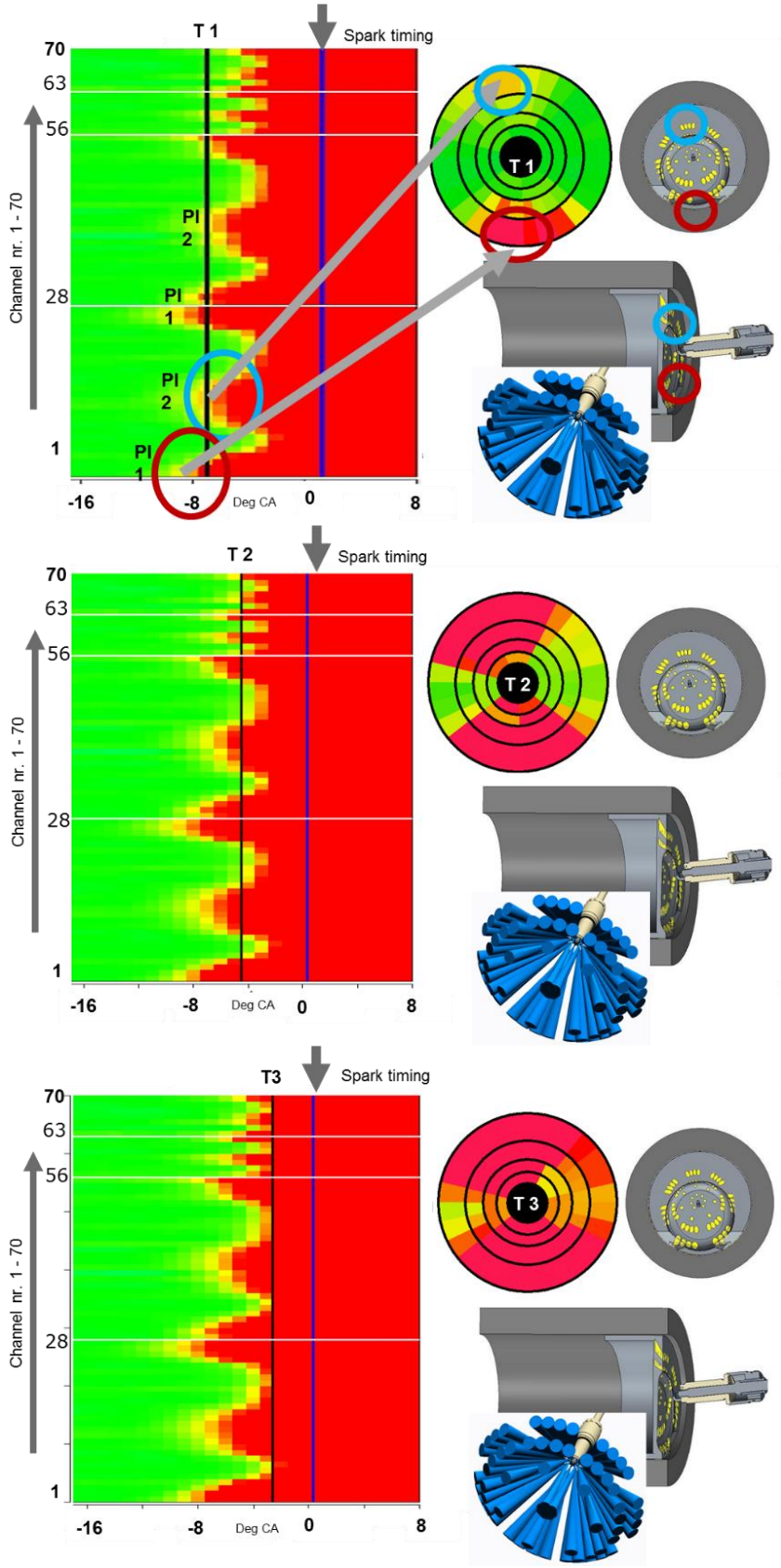

Figure 4-9 Pre-ignition example with two ignition centers and their flame kernels propagating across the combustion chamber

4.5 How to locate PI events?

The flame radiation signals recorded with the spark plug fiber sensors identify the direction at which a PI event occurs, the time of its occurrence T_1 and the time it takes to pass across the diameter of the spark plug T_2 and T_3, see Figure 4-10. With the assumption that flame front speed is constant, the velocity derived from the time it takes the flame kernel to pass across the spark plug is used to calculate the distance the flame had to travel before passing into the spark plug area. The result derived for the signals in Figure 4-10 is given in Figure 4-11 with equation (4-3) describing the evaluation procedure.

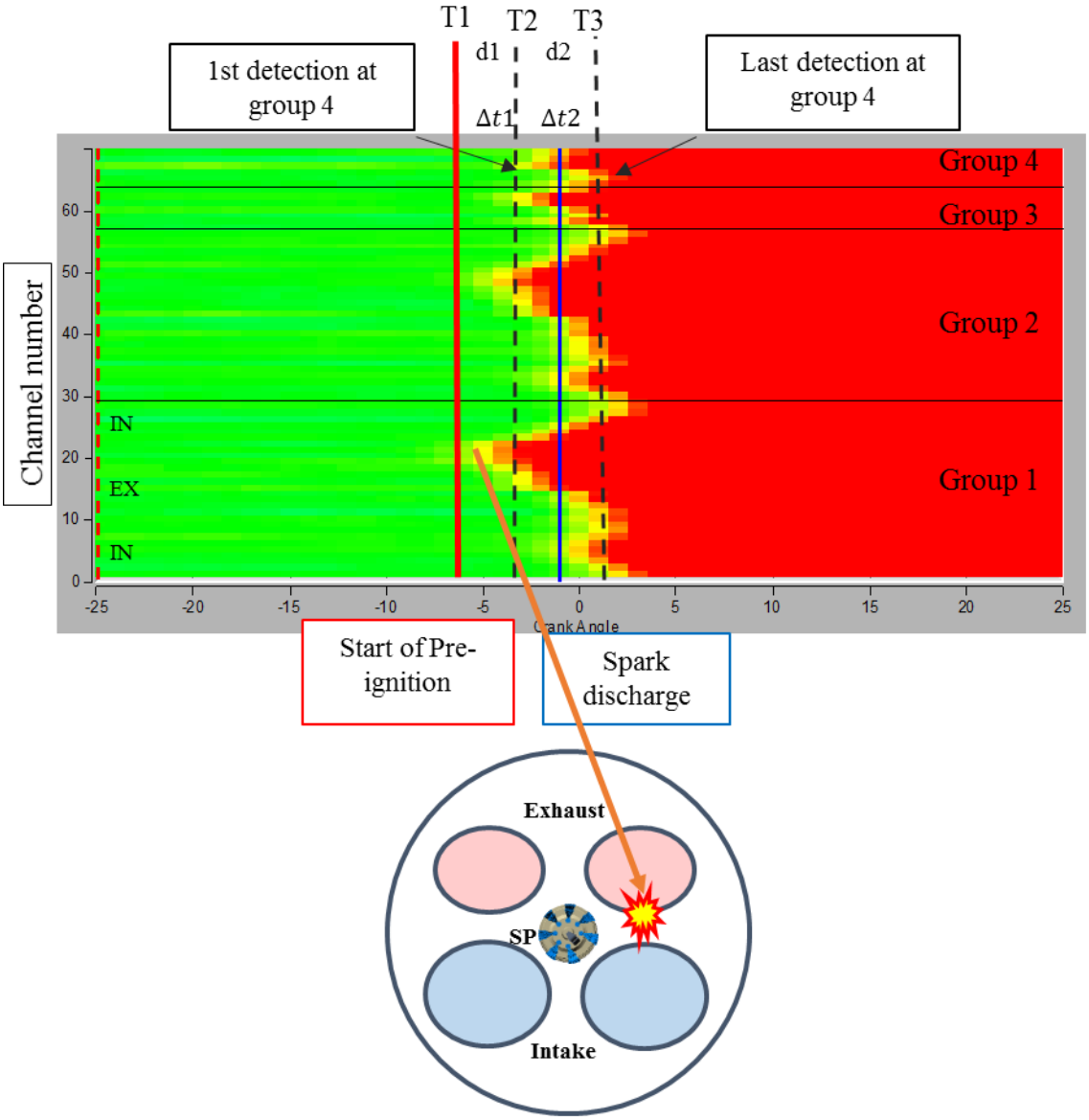

Figure 4-10 PI location evaluation

Evaluation steps for Figure 4-10 thus comprise:

1. Identification of first signal channel to recognize ignition: channel 22
2. Flame propagation velocity $v_f = 18\ m/s$ as per equ. (4-1)
3. Distance between spark plug sensor channel and PI location: $d1 = 6\ mm$

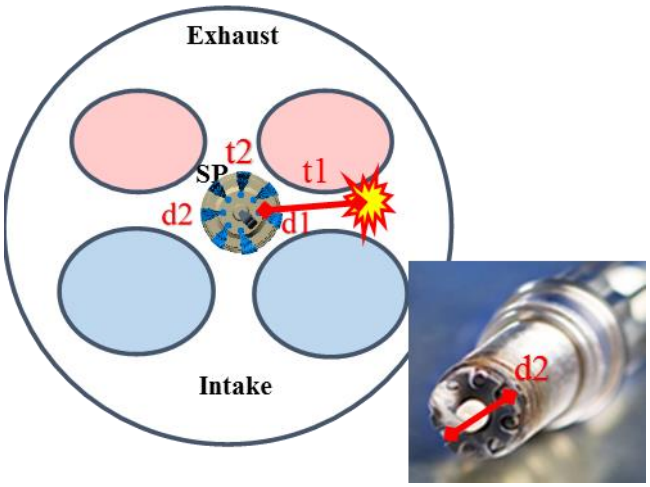

$$v_f = \frac{d}{\Delta t} = constant \qquad (4\text{-}1)$$

$$\frac{d1}{\Delta t1} = \frac{d2}{\Delta t2} \qquad (4\text{-}2)$$

$$\mathrm{d1} = \frac{\Delta t1}{\Delta t2} \cdot \mathrm{d2} \qquad (4\text{-}3)$$

Figure 4-11 PI localization

With:

$d1$ ... distance of pre-ignition area to spark plug

$d2$ ... distance between the sensor lenses

$\Delta t1$ ... time flame need from pre-ignition location to spark plug

$\Delta t2$ ... time flame to pass the lenses

The distance $d2$ between the sensor lenses is given by the design of the spark plug with $8\ mm$, the time intervals $\Delta t1$, $\Delta t2$ are taken from the CA scale of the light signals.

With $\Delta t1 = 3\ \mathrm{deg}\,CA$, $\Delta t2 = 4\ \mathrm{deg}\,CA$ and $d2 = 8\ mm$ the distance between spark plug sensor channel and PI start location is $d1 = 6\ mm$.

4.5.1 PI location - Accuracy considerations

Above procedure to identify PI location depends on

1. Measurement of time events T1, T2, T3 to yield $\Delta t1$ and $\Delta t2$
2. Distance between t2 and t3 sensor channels
3. Assumption of spherical flame propagation
4. Assumption that flame velocity is constant between T1 and T3

The time events $T1, T2, T3$ are identified as flame radiation signals exceed the background noise level. Prerequisite to this evaluation is the equilibration ("calibration") of sensor channel sensitivities, see calibration procedure in chapter 3.3.2.

As initial flame signals need to exceed the background noise, a threshold must be selected to identify such initial flame signal. Figure 4-12 compares the effect of threshold levels. A best

practice threshold level was found to be a factor of 2 above noise level. Any higher threshold yields the same PI position, but would delay PI time evaluation.

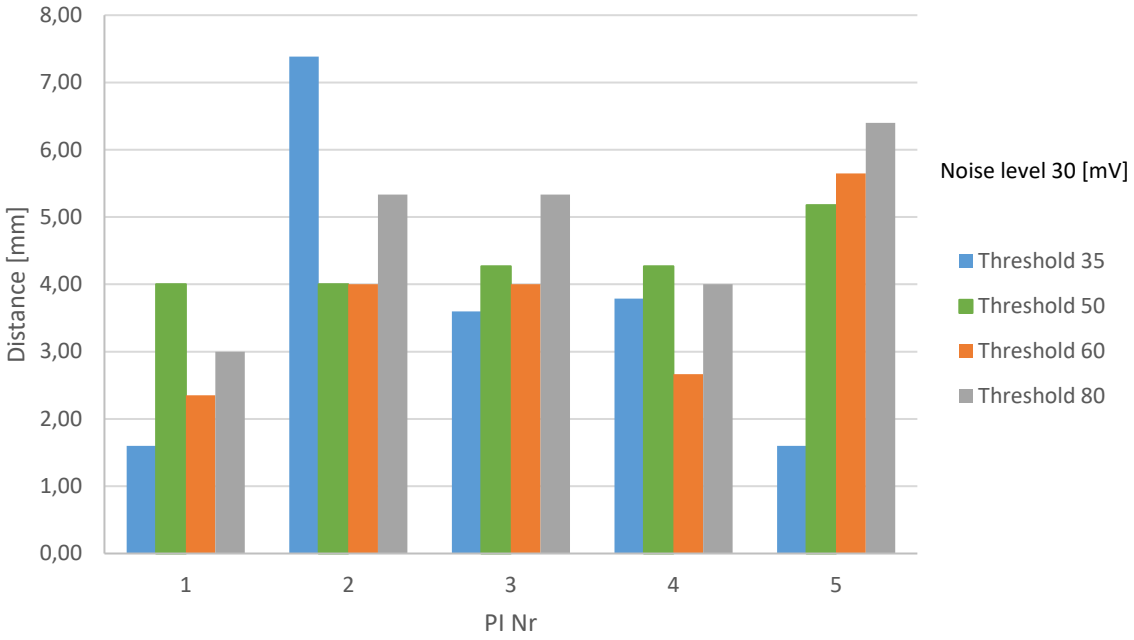

Figure 4-12 Influence of threshold choice on PI position evaluation. Signals are taken from Fig. 4-14 examples

An evaluation of PI locations under influence of signal threshold choices is given in Fig. 4-12 for the group of 5 PI events of Fig. 4-14. The data confirm that signal evaluation at about twice threshold level yields reliable position results. The data comparison in Fig. 4-12 shows a position spread of about 2 mm per each of the 5 PI events for threshold choices of 50, 60, 80 units.

The direction at which PI occurs is detected with the sensor channel orientation. This geometric sensor channel information is established as the sensor is mounted into the engine, see chapter 3.3.2.

4.5.2 Can we trust the flame velocity evaluation procedure?

The validity of above light signal evaluation for flame velocity can be checked with a comparison to turbulent flame velocity data as available in literature.

For the example of Figure 4-10 the flame speed is calculated with:

$$v_f = \frac{d2}{\Delta t} \tag{4-4}$$

With the values: $d2 = 8\,mm$, $\Delta t = 4\,\mathrm{deg}\,CA$ and $engine\ speed\ =\ 1500\,rpm$

$$v_f = \frac{8 \cdot 0.1\ [cm]}{4 \cdot \frac{1500}{60} \cdot 360[s]} = \ 1800\ \frac{cm}{s} = 18\ \frac{m}{s}$$

The flame propagation speed measured with the Visiolution sensor signals and above procedure yields $v_f\ =\ 18\ \frac{m}{s}$.

A comparison of this velocity with the data of chapter 2.3 is given in Table 4-1. The result is within reasonable agreement with published data, thus supporting the proposed procedure to locate the radial position of such PI events along a sensor channel's line of sight.

Table 4-1 Comparison of turbulent flame speed calculations

Theory	Calculation	Result at 1500 rpm
Visiolution	$v_f = \frac{d2}{\Delta t}$	$18\ \frac{m}{s}$
Winklhofer (3)	$v = \frac{engine\ speed}{100}\ \left[\frac{m}{s}\right]$	$15\ \frac{m}{s}$
Damköhler (5)	$s_t = \left(1 + C\frac{u'}{s_l}\right)^n s_l$	$14\ \frac{m}{s}$

4.5.3 Method verification

In order to verify above presented method to identify PI location areas, an experimental engine with a cylinder head as described in chapter 3.3 has been used. This engine allows introduction of pre-ignition by means of a glow plug, see Figure 3-4.

At sufficiently high glow plug temperature, the charge is igniting near the tip of the glow plug prior to spark ignition. Measurement of this event with the spark plug fiber sensor, thus is expected to demonstrate the feasibility of the presented method.

In each cycle a single image has been taken with an IR sensitive camera which was triggered to record flame radiation just before spark discharge, see Figure 4-13. Thus, in case of pre-ignition a flame signal is expected to be recorded with the camera in a single shot record and with the fiber optic sensor channels in continuous signal traces.

The results of these measurements are given in Figure 4-13 for a reference cycle with normal, regular ignition. A flame kernel is not yet present, the IR image thus only shows a weak signal arising from the glow plug surface.

PI cycle results are given in Figure 4-14. Each of the 5 PI cycles shows the same flame kernel position along the optical field between endoscope and glow plug. Flame kernel size and brightness are different from cycle to cycle due to variations of the PI events.

The fiber optic sensor signals show the continuous evolution of each PI event. Pre-ignition is first detected with the sensor channels including the glow plug position inside their field of view and PI flame kernel growth is seen with the flame signatures expanding into more and more channels.

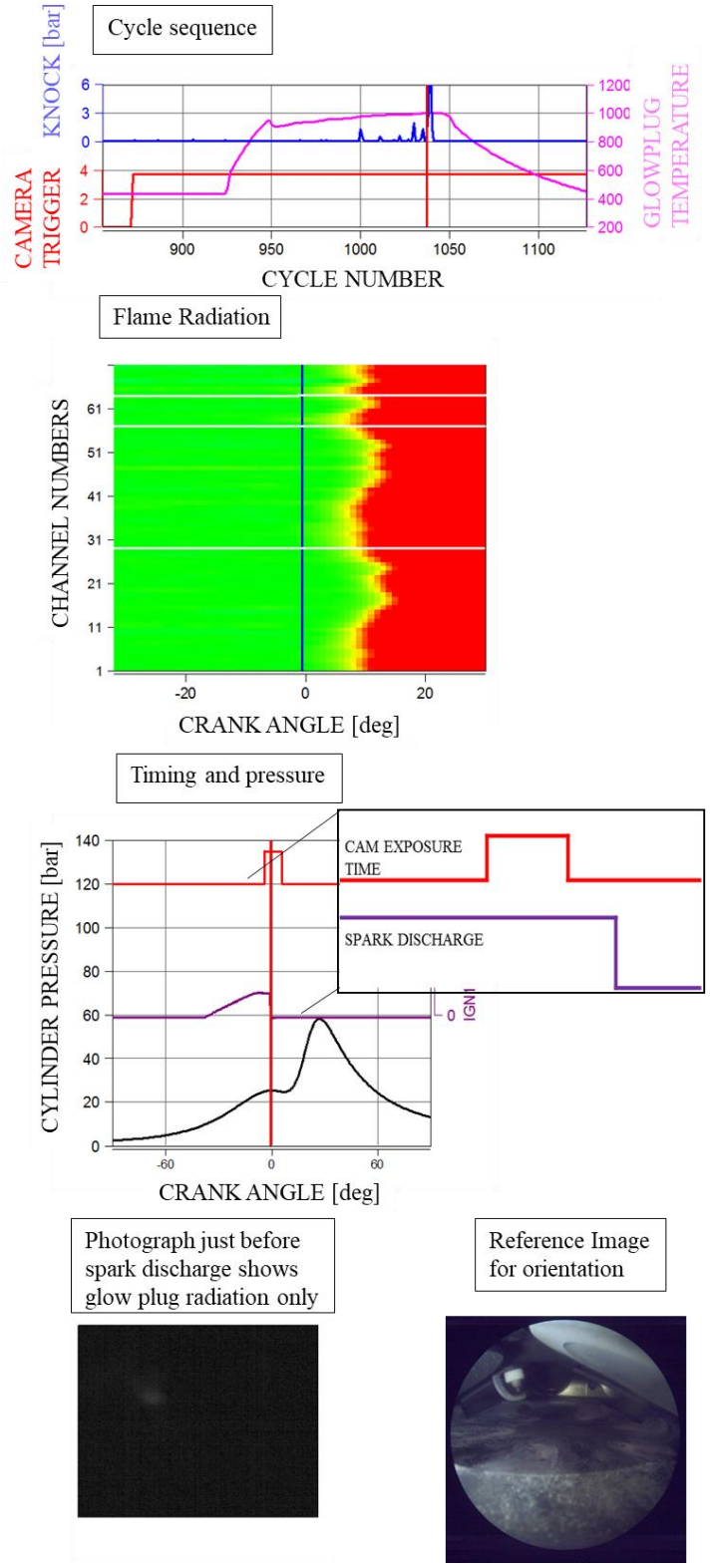

Figure 4-13 Cycle sequence with regular and irregular combustion events. Cycle example shows data for regular ignition.

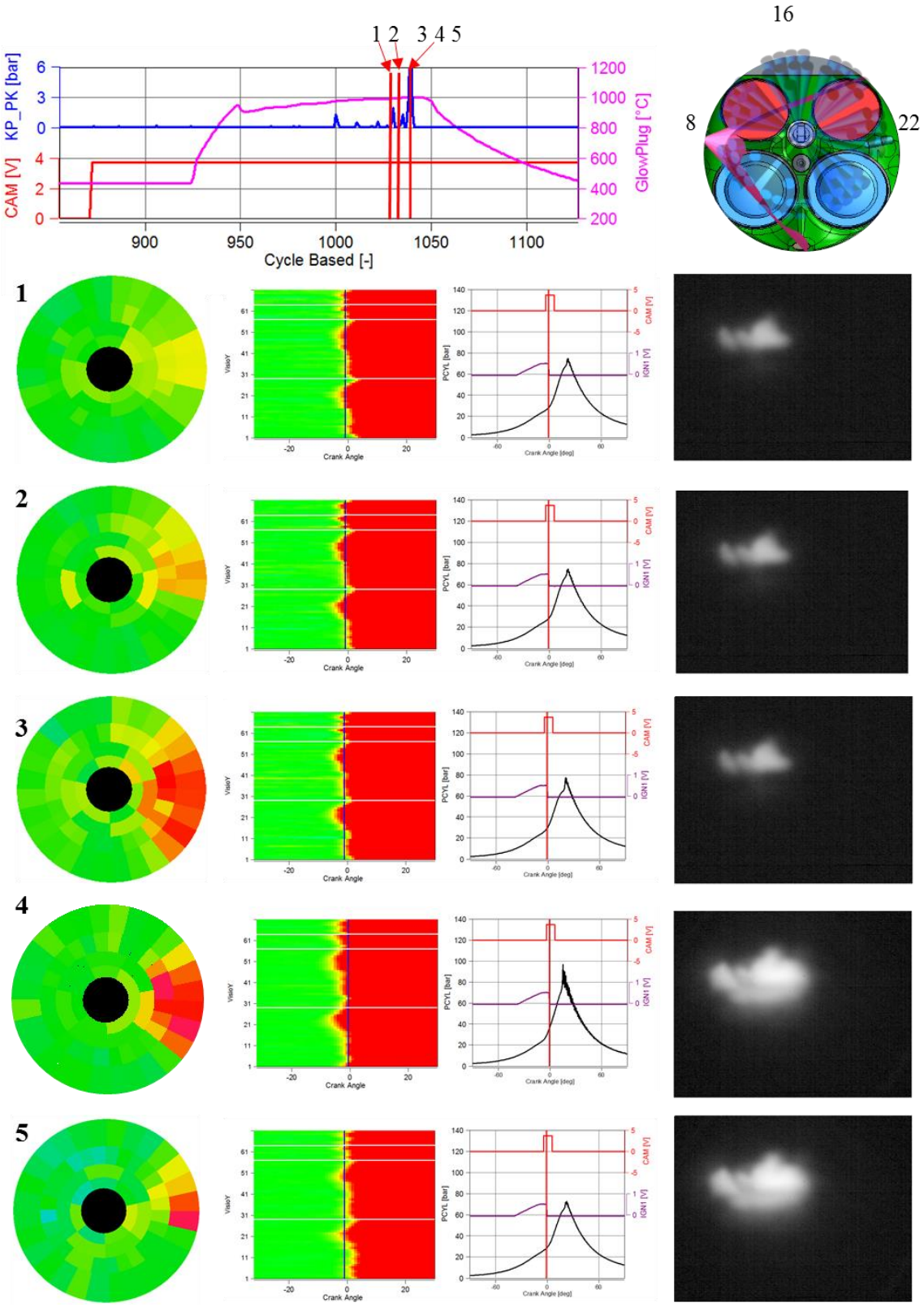

Figure 4-14 Cycle sequence with regular and irregular combustion events. Cycle examples show data for irregular ignition. Flame kernel is seen in IR photograph recorded before spark discharge

PI Nr	T1 [deg CA]	T2 [deg CA]	T3 [deg CA]	D1
1	-2	-0.75	3.5	2.4
2	-2.5	-0.5	3.5	4.0
3	-2.5	-0.5	3.5	4.0
4	-6.5	-5	-0.5	2.7
5	-3.5	-0.5	3.75	5.7

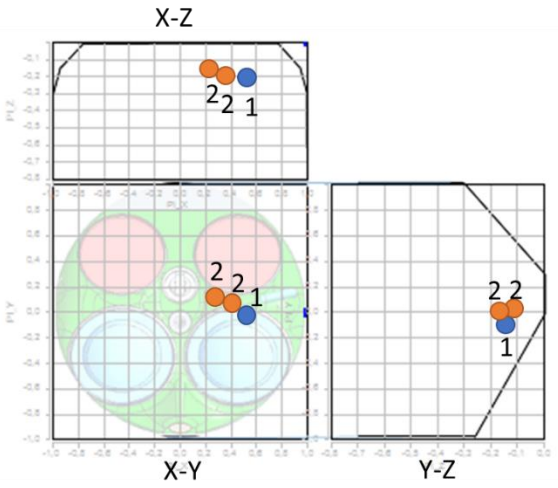

Figure 4-15 Local distribution of the PI events events, data of Fig. 4-14

Evaluation of the fiber sensor data with the method explained in chapter 4.5 shows the location of PI events in the graphics of Figure 4-15. For position accuracy see Fig. 4-12.

5 Pre-ignition mechanism

In chapter 2 basic concepts have been presented to describe the input of activation energy into premixed charge and to explain “in principle” activation energy sources arising from a spark plasma, gas compression, or external sources like hot spots or residuals. Chapter 5 now discusses pre-ignition mechanisms in view of thermodynamic conditions present in engine operation.

5.1 Arrhenius Equation

Compression of the in-cylinder charge raises the gas temperature. This temperature rise introduces kinetic energy into the gas and reactive gas molecules (oxygen and fuel) may respond with exothermal reactions. The relation between reactive gas properties, temperature and the time τ it takes to convert the reactants into products is described by the Arrhenius equation (4).

$$\tau = \mathrm{A}\, \mathrm{p}^{-\mathrm{n}}\, e^{\frac{B}{T}} \tag{5-1}$$

where $A,\ n\ and\ B$ are fuel specific parameters, with B representing the reactants’ activation energy. T is the gas temperature and p the cylinder pressure.

Activation energies for various HC fuel – air mixtures have been measured in shock tube tests of Yates et al (20) with results given in Fig. 5-1.

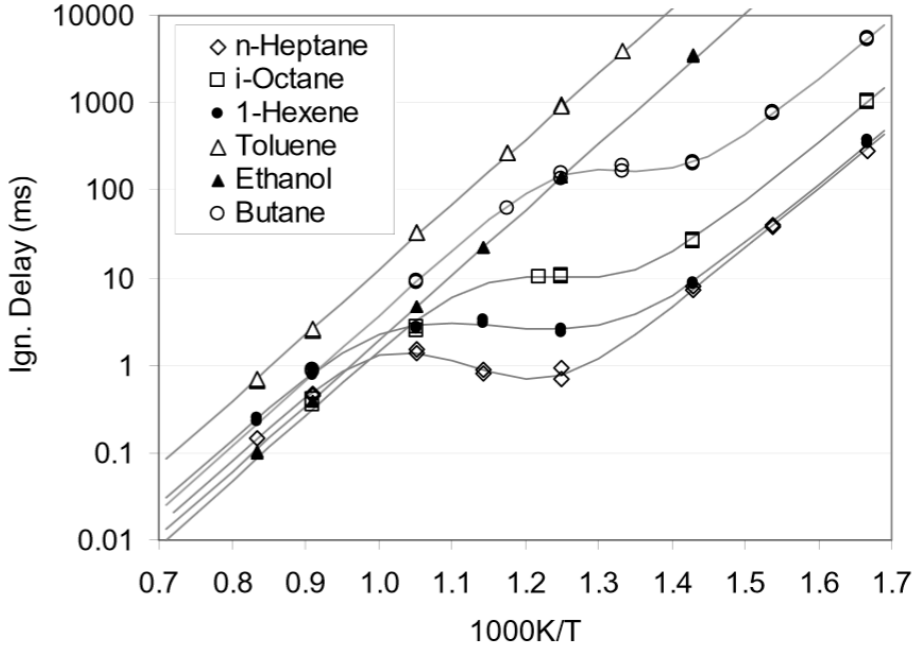

Figure 5-1 Ignition delay times of different kinds of fuels (20)

Table 5-1 Several Arrhenius equations from literature

Source	Arrhenius equation	Parameter A, n, B
Douaud and Eyzat (4)	$\tau = 17.68 \left(\frac{ON}{100}\right)^{3,402} p^{-1,7} e^{\frac{3800}{T}}$ (5-2)	$A = 17.68 \left(\frac{ON}{100}\right)^{3.402} = 14.84$ with $ON = 95$ $n = -1.7$ $B = 3800$
Zhou et al (21) **2 stage LW-integral**	$\tau_i = Cp^{\alpha} \left(\frac{T}{T_{ref}}\right)^{\beta} e^{\frac{\theta_a}{T}}$ (5-3) $\tau = \{(\tau_1 + \tau_2)^{-1} + (\tau_3)^{-1}\}^{-1}$ (5-4)	$A = C \left(\frac{T}{T_{ref}}\right)^{\beta}$ $n = \alpha$ $B = \theta$

i	1	2	3
C	$6.62e^{-43}$	$1.12e^{10}$	$6.57e^{9}$
β	49.24	-1.87	-10.98
n	-0.26	-1.86	-1.11
B	45640	-5350	1520

Elmqvist et al. (5)	$\tau = 0.021\ p^{-1,7} e^{\frac{3800}{T}}$ (5-5)	$A = 0.021$ $n = -1.7$ $B = 3800$
Yokoo et al. (22)	$\tau = 0.0186 \left(\frac{ON}{100}\right)^{3,402} p^{-1,7} e^{\frac{3800}{T}}$ (5-6)	$A = 0.01869 \left(\frac{ON}{100}\right)^{3.402} = 0.0156$ with $ON = 95$ $n = -1.7$ $B = 3800$
Yokoo et al. (22)	$\tau = 0.017 \left(\frac{ON}{100}\right)^{2.6} p^{-1,8} e^{\frac{3700}{T}}$ (5-7)	$A = 0.017 \left(\frac{ON}{100}\right)^{2.6} = 0.0147$ with $ON = 95$ $n = -1.8$ $B = 3700$
For this thesis used	$\tau = 55\ p^{-1,7} e^{\frac{3800}{T}}$ (5-8)	$A = 55$ $n = -1.7$ $B = 3800$

Table 5-1 gives a collection of various authors' Arrhenius coefficients A, n and B for RON 95 gasoline fuel.

Most authors' coefficients cover an unspecified temperature range and apply their data for purposes specific to individual applications as described in their references. Zhou et al. relate their parameters to selected temperature regimes (21). Yates et al (23) propose a two-staged low temperature and a single stage high temperature regime with:

$$\tau = \{(\tau_1 + \tau_2)^{-1} + (\tau_3)^{-1}\}^{-1} \quad (5\text{-}9)$$

Yates et al furthermore showed that a three stage Arrhenius model is representative for describing the ignition delay of a wide range of different fuels. Figure 5-2 shows an example of the ignition delay of a general type fossil fuel. Therein three temperature regimes are well separated. (23)

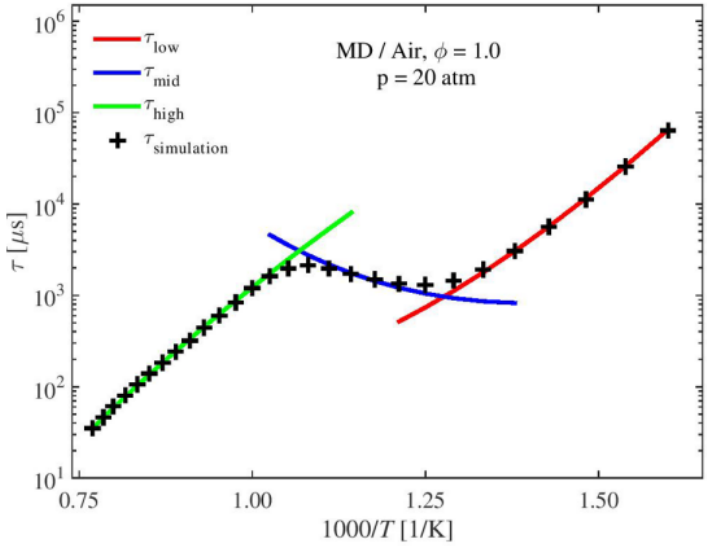

Figure 5-2 Three regions of the temperature regimes high (green), mid (blue) and low (red) for 20 atm cylinder pressure and a fuel air mixture of 1.0 (21)

A central part of this thesis relates to the numerical implementation of the LW integral and the Arrhenius function for the description of the ignition delay time τ. The parameter set of Douaud and Eyzat has been applied, however using a modification of the A parameter in order to best represent the self-ignition data collected in the experimental part of this work. Thus, throughout the scope of this manuscript, the Arrhenius expression as given in equ. (5-10) has been applied:

$$\tau = 55\, p^{-1,7}\, e^{\frac{3800}{T}} \tag{5-10}$$

5.2 Livengood-Wu-integral

As described in (4), Livengood and Wu have adopted Arrhenius' ignition delay equation for the conditions of internal combustion engines. Following their arguments, ignition of a fuel – air mixture occurs as soon as the integral relation starts to "explode" as defined by equ. (5-11):

$$\int_{\tau_0}^{\tau_e} \frac{1}{\tau\,(p, T, A, n, B)}\, dt = 1 \tag{5-11}$$

For any given fuel with parameters A, n, B this integral defines the time τ_e in a compression stroke when self-ignition conditions are achieved. Gas temperature and pressure are given by in-cylinder conditions at intake valve closing, by piston motion and heat transfer. Consequently, compression ratio, initial gas and engine conditions as well as engine speed contribute to above integral equation.

Following chapters give a discussion of the Livengood-Wu (LW) integral for various parameters relevant in engine design and operation.

5.3 Parameters in the LW integral

Throughout this thesis, Arrhenius parameters are as given in line 7 of Table 5-1with

- $A = 55$
- $n = -1.7$
- $B = 3800$

A, n and B are kept constant for any engine parameters to be discussed

In order to visualize the influence of typical engine and operation parameters on self-ignition events, the examples in Figure 5-3, 5-4 and 5-5 show the trends on how the LW integral responds to variations of compression ratio, intake air temperature and engine speed

1. Compression ratio (CR)

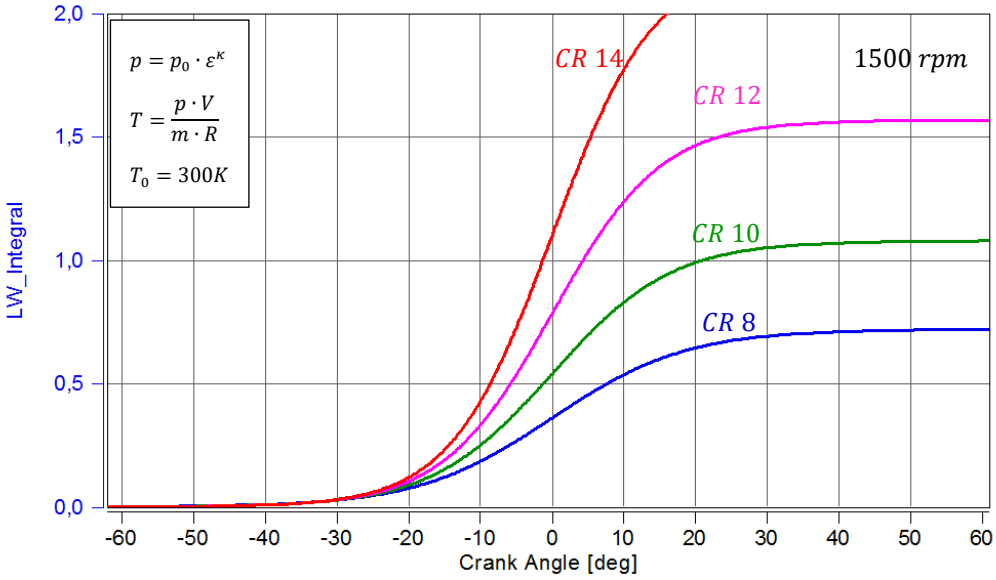

Figure 5-3 LW-Integral: Influence of compression ratios

2. Intake air temperature

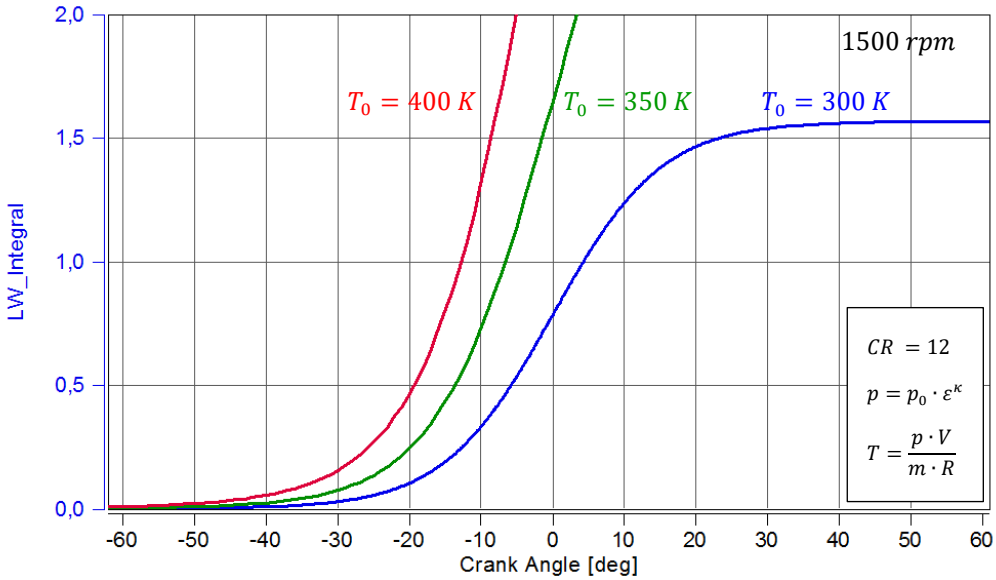

Figure 5-4 LW-Integral: Influence of intake air temperatures

3. Engine Speed

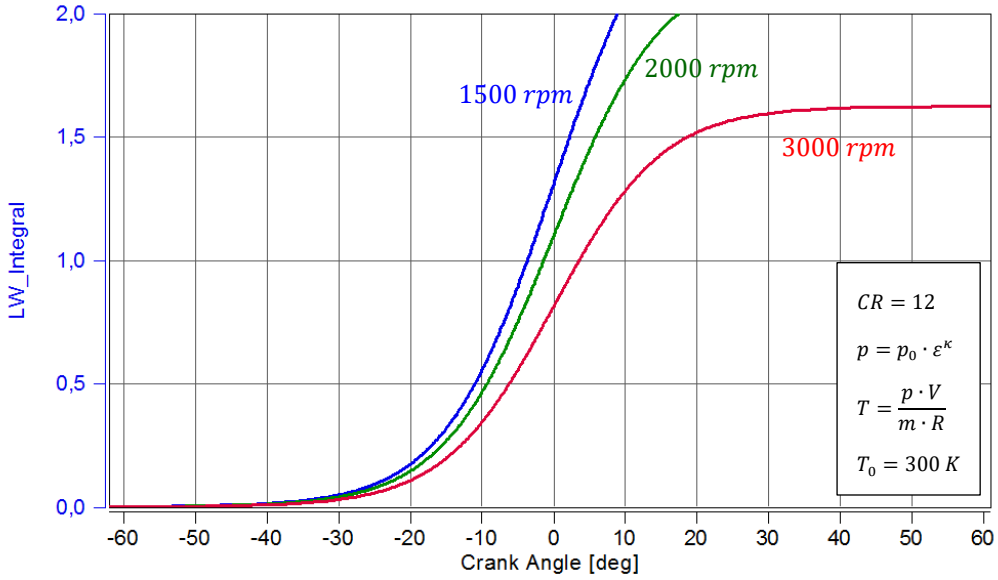

Figure 5-5 LW-Integral: Influence of engine speed

Whereas CR and intake air temperature show the impact of compression heating and gas temperature on self-ignition, the engine speed trend shows the time requirements to initiate self sustained exothermal reactions.

The consequences of such trends are obvious: any input of heat into the premixed charge increases the risk for self-ignition and low engine speed sets a natural limit to high load operation as it results in the well known LSPI (low speed pre-ignition) events.

Self-ignition summary

A summary of engine speed and intake air temperature influence on the self-ignition criterion LW = 1 is given in Figure 5-6. With increasing intake air temperature ignition delay is shorter as was already evident in Figure 5-4.

In view of a later discussion of surface temperature influence on PI, it is interesting to note that the charge temperature at self-ignition as is shown in the right hand scale of Figure 5-6 covers a range of about 650 to 1050 K as intake air and engine speed are varied within the given boundaries.

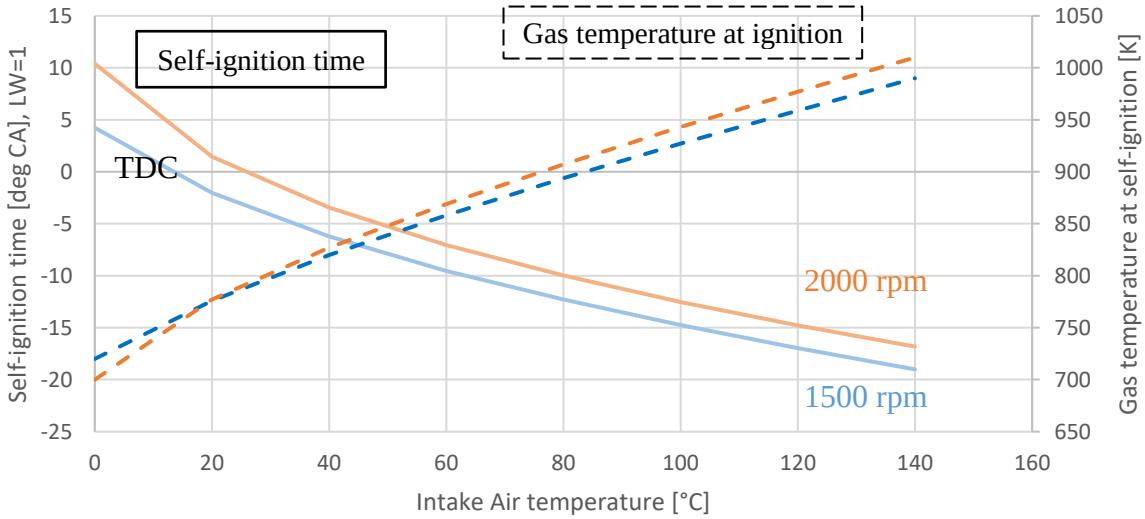

Figure 5-6 Start of combustion (SOC) and temperature at ignition - variation of intake air temperature

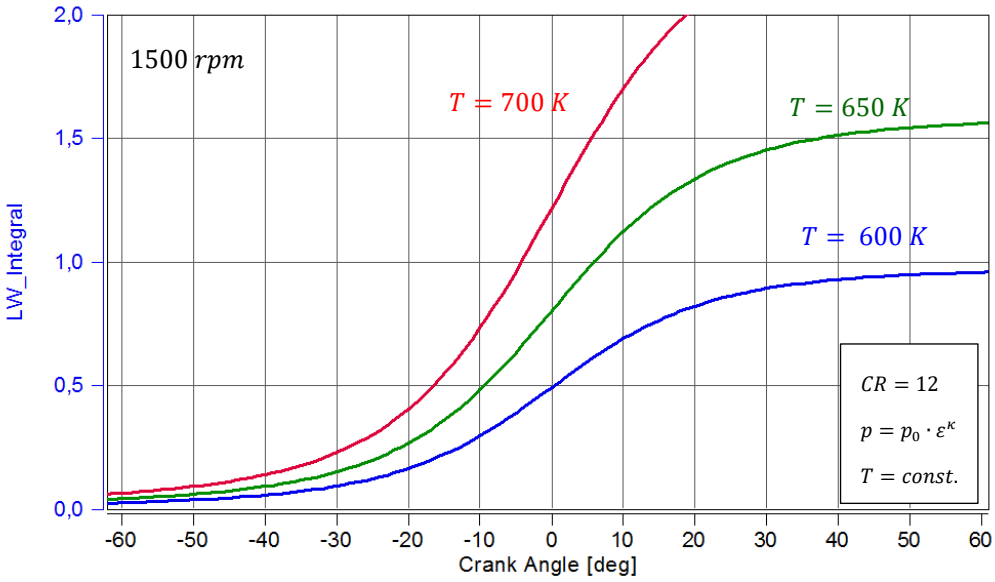

Figure 5-7 LW-integral: Simulation of gas on constant temperature being compressed by piston motion

Figure 5-8 shows the (artificial) situation of a gas of constant temperature being compressed by the piston motion at 1500 and 2000 rpm, respectively.

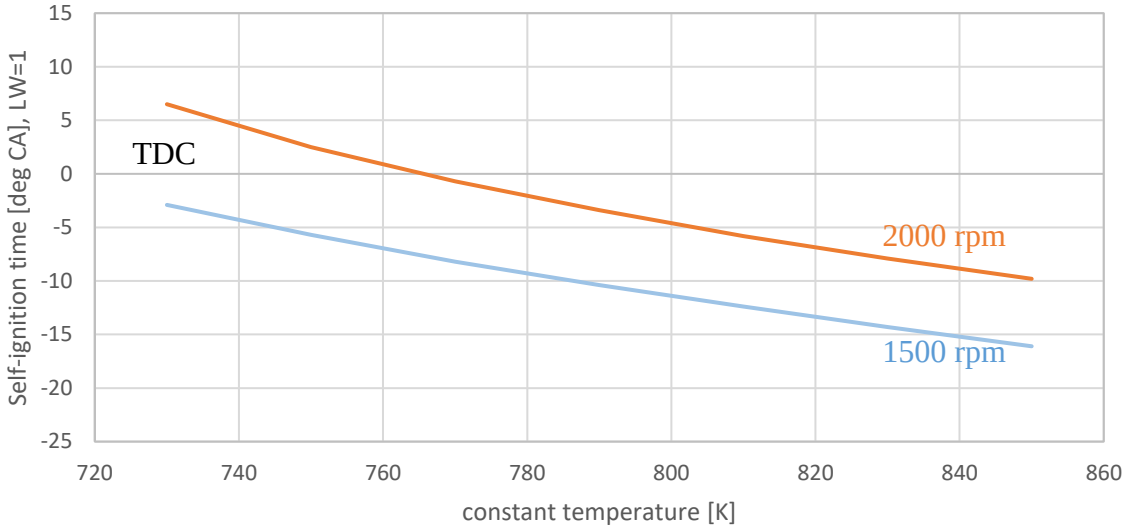

Figure 5-8 Start of combustion – variation of constant gas temperature

In Figure 5-6 the conversion from time to crank angle intervals is given by

$$\tau\,[°CA] = \frac{n \cdot 6}{1000}\left[\frac{°CA}{ms}\right] \cdot \tau\,[ms] \tag{5-12}$$

$$\tau_{1500rpm}[°CA] = 9\,\left[\frac{°CA}{ms}\right] \cdot \tau[ms] \tag{5-13}$$

$$\tau_{2000rpm}[°CA] = 12\,\left[\frac{°CA}{ms}\right] \cdot \tau[ms] \tag{5-14}$$

5.4 Pre-Ignition sources

Chapter 5.3 has given a view into parameters which take influence on the self-ignition criterion as described by the Livengood - Wu integral. In practical engine operation, a combination of such parameter effects as well as further sources for pre-ignition can be of interest. This chapter gives a list of potential sources, including above discussed thermodynamic and thermal effects and shows some typical situations found in engine operation.

Table 5-2 PI sources and influenced parameters of the ignition delay calculation

PI source	Symbol	Auto-ignition influence	Comment
Compression ratio	ε	p, T	Gas compression heating
Intake temperature	T_0	T	Gas compression heating
Engine load	-	p, T	Gas pressure/density, hot surfaces
Hot spot	T_x	T	Surface heat source
Glowing particles	T_y	T	Local ignition source
Fuel chemistry	-	A, n, B	Chemical kinetics of fuel
Lube oil	-	A, n, B_0	Chemical kinetics of oil
Deposits	T_z	T	Combination of combustion products, fuel and lube oil with specific heat capacity and heat transfer features
Engine speed	n	τ	Incubation time

- Charge temperature as a result of compression: compression ratio, intake air temperature
- Charge temperature as a result of heat transfer: surface temperature
- Engine load: the primary effect is heating of combustion chamber surfaces as a result of heat transfer imposed by high power density.

$$\dot{Q} = \alpha \cdot (T_{surface} - T_{water}) \tag{5-15}$$

Where $\dot{Q}$ is the heat transfer from combustion chamber into the coolant, α is the heat transfer coefficient and the temperatures of the combustion chamber surface $T_{surface}$ and the cooling water T_{water}. With higher load $\dot{Q}$ is increasing whereas α and T_{water} are constant. The result is that the cylinder wall temperature is increasing, too.

$$T_{cyliner\ liner} = T_{water} + \frac{\dot{Q}}{\alpha} \tag{5-16}$$

- Hot spots: due to heat transfer features, local areas of the combustion chamber such as spark plug, valves or piston can have significantly higher temperatures than the surrounding cylinder head or liner surfaces. Heat transfer and potential PI events due to such local heat sources are furthermore discussed in chapter 5.4.1.

- Deposits: the primary thermal mechanism is poor heat transfer with consequently high deposit temperatures. Chemical effects may include the storage of fuel and lube oil with consequent self-ignition of such species.

- Glowing particles: this refers to deposits which come free of their initial wall contact. Consequently, such particles (or flaking deposits) are heated by their gas environment and maintain high temperatures due to their heat capacity. Their position inside the combustion chamber is unspecified, PI consequently occurs at random positions.

- Fuel chemistry: as given by a fuel's ignition delay features, see chapter 5.4.3.

- Lube oil chemistry: as given by the lube oil's ignition delay features, see chapter 5.4.4.

- Engine speed: as engine speed defines the time for heat transfer into the charge and the progress of endothermal pre-reactions, it is a defining parameter for PI events.

5.4.1 Hot spot at local surface areas

Hot surface areas act as heat sources for the surrounding gas with potential consequences for pre-ignition. In cylinder surface temperatures are usually highest at protruding spark plug electrodes and on the insulator, at exhaust valves and on specific parts of the piston. Control of these components' peak temperatures is a central part in combustion system design. The risk for such hot spot pre-ignition rises with hot spot temperature, but PI need not necessarily arise at hottest parts as there is need for ongoing heat transfer from surfaces into the gas phase.

A thermal image in Figure 5-9 shows highest temperatures on the spark plug ground electrode (up to $800\ °C$), exhaust valves may be up to $650\ °C$, piston surface temperatures are typically below $400\ °C$. Such temperature features would suggest that PI should primarily occur at the spark plug and the risk for PI on valves or piston surfaces should be negligible. This, however, is contradictory to experimental evidence. (24), (25)

In a simplified expression, the heat transfer from the hot spot surface area into the gas is given by:

$$\dot{Q} = h\ A\ (T_s - T_g) \tag{5-17}$$

$\dot{Q}$ ... Heat transfer in $[W]$

h ... Heat transfer coefficient in $[\frac{W}{m^2 K}]$

A ... Surface in $[mm^2]$

T_s ... Surface temperature in [K]

T_g ... Gas temperature in [K]

This heat transfer is convected along with the gas flow and dissipated by heat transfer within the gas. In order for the gas to exceed the self-ignition limit as per the LW criterion, the gas temperature – time integral must be sufficiently high. This relates the heating of a gas volume element near a hot spot surface to both, temperature and the area of the hot spot, otherwise convection and dissipation would prevent the gas volume to exceed the ignition limit.

For considerations of heat flux across the spark plug and exhaust valve surfaces, some numerical estimates are given below:

$$\dot{Q}_{SP} = h \cdot A_{SP} \cdot (T_{SP} - T_g) \tag{5-18}$$

$$\dot{Q}_{EX} = h \cdot A_{EX} \cdot (T_{EX} - T_g \tag{5-19}$$

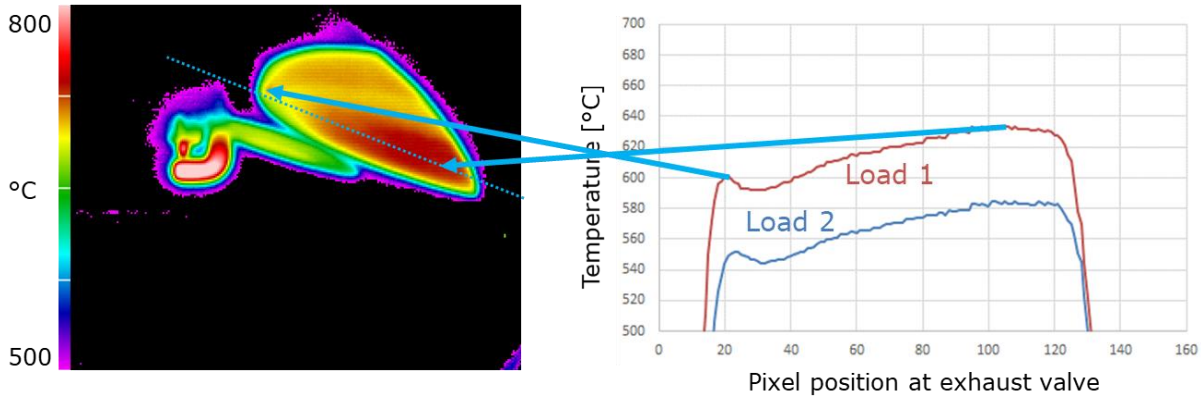

Figure 5-9 Surface temperature distribution at an exhaust valve under

The surface area of the spark plug electrode and one exhaust valve are estimated to be:

$$A_{SP} \sim 70\ mm^2$$

$$A_{ExValve} \sim 490\ mm^2$$

$$A_{glowplug} \sim 90\ mm^2$$

with an exhaust valve diameter of $d_{EX} = 25\ mm$

$$T_{SP} = 800\ °C$$

$$T_{EX} = 650\ °C$$

$$T_{GP} \sim 1000\ °C$$

$$T_{gas} = 400\ °C$$

With surface temperature data taken from Figure 5-9 and the surface area dimensions for spark plug and exhaust valve, respectively, the heat transfer comparison is given by following analysis:

$$T_{SP} = \frac{5}{4} T_{EX} \tag{5-20}$$

$$A_{SP} = \frac{1}{7} A_{Ex} \tag{5-21}$$

$$T_g = \frac{5}{8} T_{EX} \tag{5-22}$$

Parameters (5-20) to (5-22) are set in the equations (5-18) and (5-19):

$$\dot{Q}_{SP} = \frac{5}{56} h\, A_{EX} \cdot T_{EX} \tag{5-23}$$

$$\dot{Q}_{EX} = \frac{3}{8} h\, A_{EX} \cdot T_{EX} \tag{5-24}$$

$$\frac{\dot{Q}_{SP}}{\dot{Q}_{EX}} = \frac{\frac{5}{56}}{\frac{3}{8}} \sim 23\% \tag{5-25}$$

The conclusion on this calculation is that not only the component temperature, but component temperature together with the area of the hot spot have influence to the PI behaviour.

This analysis is summarized in the graphics of Figure 5-10.

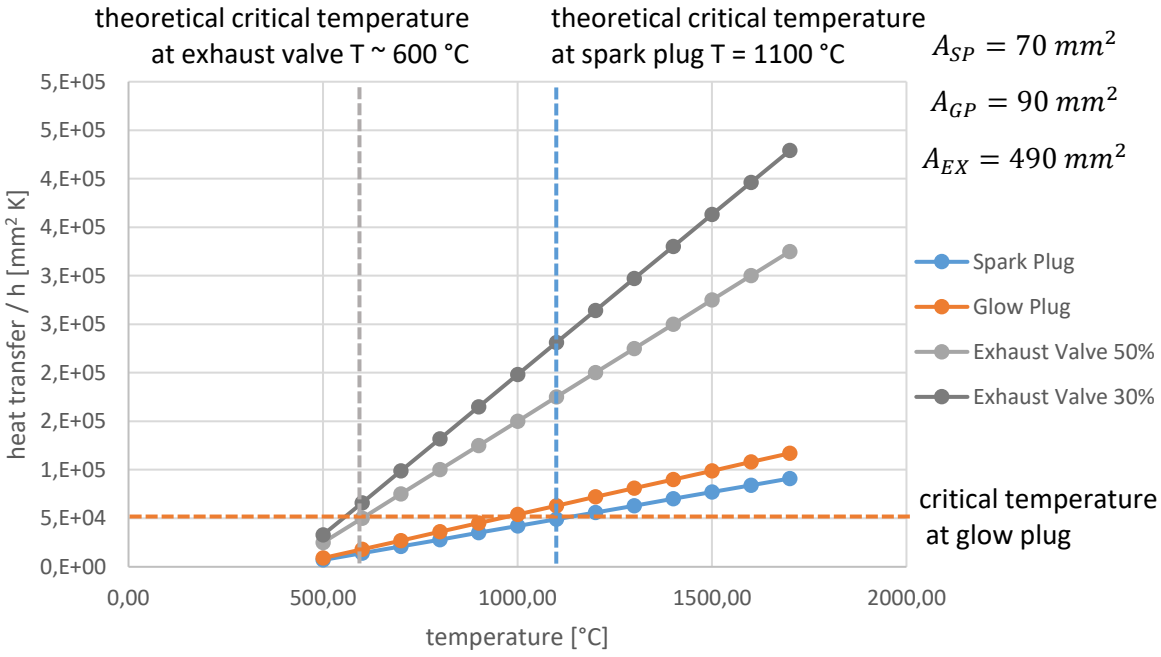

Figure 5-10 Heat transfer for various hot spot areas

On this topic, Döhler describes in (25):

- spark plug temperature in stationary wide open throttle (WOT) combustion is about $150\ °C$ higher than the temperature of the exhaust valve
- retarding of the spark timing: spark plug is still $50\ °C$ warmer
- during negative speed ramps starting at $5000\ rpm$ down to $1800\ rpm$ WOT the exhaust valve temperature is higher than the spark plug temperature
- thermal inertia of the spark plug, due to the smaller surface area, is lower than the exhaust valve
- a combination of the higher exhaust valve temperature with the low engine speed increases the risk of glow ignitions at the exhaust valve.

5.4.2 Deposits and glowing particles

Deposits are combustion residuals including unburned fuel, oil, carbon, etc., which are agglomerated at combustion chamber surfaces.

Their potential influence on pre-ignition includes:

- Chemical effects: activation energy of deposits could be sufficiently low to initiate PI at otherwise normal conditions
- Thermal effects related to heat transfer and heat capacity result in high temperature deposit layers
- Deposit breakoff giving rise to glowing particles: results in free floating particles which are heated during combustion and may pass into subsequent cycles. Their heat capacity together with low heat transfer allows them to act as ignition sources.

Examples for deposits and glowing particle signals are given in Figure 5-11 and Figure 5-12.

Figure 5-11 Deposits on intake valve

Deposits as seen on intake valves in Figure 5-11 may pass into the combustion chamber and act as ignition source in subsequent cycles.

Figure 5-12 shows the light radiation data of a mega-knock event. The light signals of a 40 channel Visiolution sensor show a free moving glowing trace of a particle which finally gives rise to pre-ignition. This event is interpreted as the result of some deposits being knocked off an intake valve or any other combustion chamber surface.

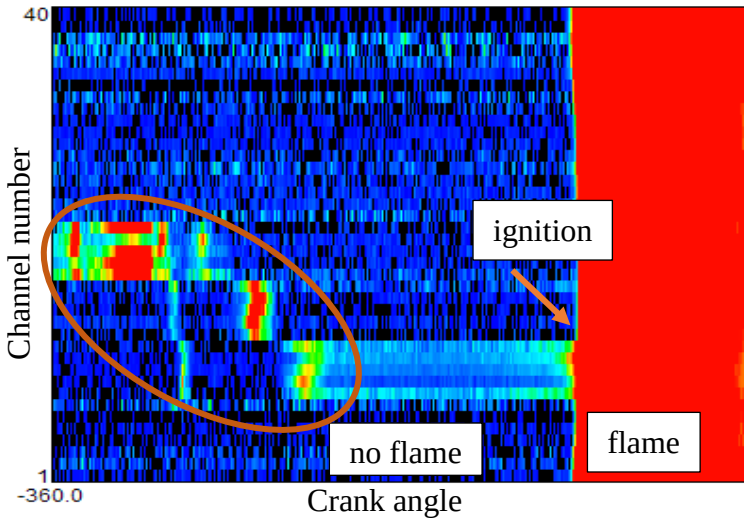

Figure 5-12 Traces of glowing particles during gas exchange and compression stroke (Visiolution signals)

5.4.3 Fuel

The pre-ignition behavior of fuel strongly depends on the fuels chemical composition. Günther et al. showed in (26) that with adding of up to 20% of ethanol to E0 RON95 fuel the glow ignition tendency is decreased. Higher ethanol concentrations (E85 and E100), however, are mentioned to decrease the effect. In (27) and (28) it is described, that even with similar RON the self-ignition behavior can be significantly different. (29), (30), (31), (32)

Furthermore an optimization of the direct injection parameters can decrease the liner wetting in the combustion chamber. (33), (34) This reduces the build-up of deposits and furthermore can reduce pre-ignition tendency, see chapter 5.4.2.

5.4.4 Lube oil

Spicher describes in (33) the oil influence on pre-ignition phenomena. Similar investigation have been done by Luef with a description of oil parameters effects such as: (8), (32), (35)

- Composition of the lubricant base (36)
- Molecular mass (C_xH_y)
- Viscosity of the lubricant base
- Boiling behaviour
- Evaporation behaviour
- Concentration of the lubricant base

These parameters are sorted with their PI-relevance from high to low. In the experiments of Luef it was shown that not every oil droplet leads to a pre-ignition event. A specific oil mass is needed with defined chemical structures and a minimum of ignition energy to ignite the fuel air mixture. Luef summarized that the main reason for pre-ignition is the quality of the base oil, where the aliphatic, the paraffinic hydrocarbons and high n- and iso-alkalis have the highest damage potential. (29), (37)

Metal additives have shown a strong influence on LSPI phenomena. In particular potassium and calcium increase the LSPI frequency whereas molybdenum dithiocarbonate and magnesium decrease the frequency. (38), (39)

Further mechanisms of pre-ignition occurrence based on oil are mentioned in (40), (41) and (36). In these publications various aspects of oil transport mechanisms such as oil film build up or flying oil droplets are described.

5.4.5 Engine Speed

Engine speed influence is most evident at LSPI – low speed pre-ignition events. They are a natural limit to high load – low speed operation as the time - temperature effects on the compressed charge available to initiate PI are competing with the spark discharge event.

In high rpm hot spot PI events, speed has a twofold influence: high flow velocities related to high rpm operation support heat dissipation within the charge, thus reducing local gas overheating. High rpm – high load operation otherwise increases combustion chamber surface temperatures and the risk of hot spot pre-ignition.

5.5 Detection of pre-ignition events in engines

As pre-ignition occurs in SI engine, it can result in various cylinder pressure related phenomena. Most noticeable is of course the occurrence of so called “mega knock” events as this introduces a strong acoustic response of the engine structure. However, pre-ignition may also result in events which are otherwise unnoticed. Following chapters give an overview of signals to recognize PI occurrence and furthermore analyse PI details.

5.5.1 Cylinder pressure indication

The pressure diagrams in Figure 5-13 give a comparison of motored and fired cycle signals with one cycle showing the typical PI pressure curve with strong knock amplitudes. As main objective is in understanding PI root causes, timing and location of the pre-ignition event are of interest.

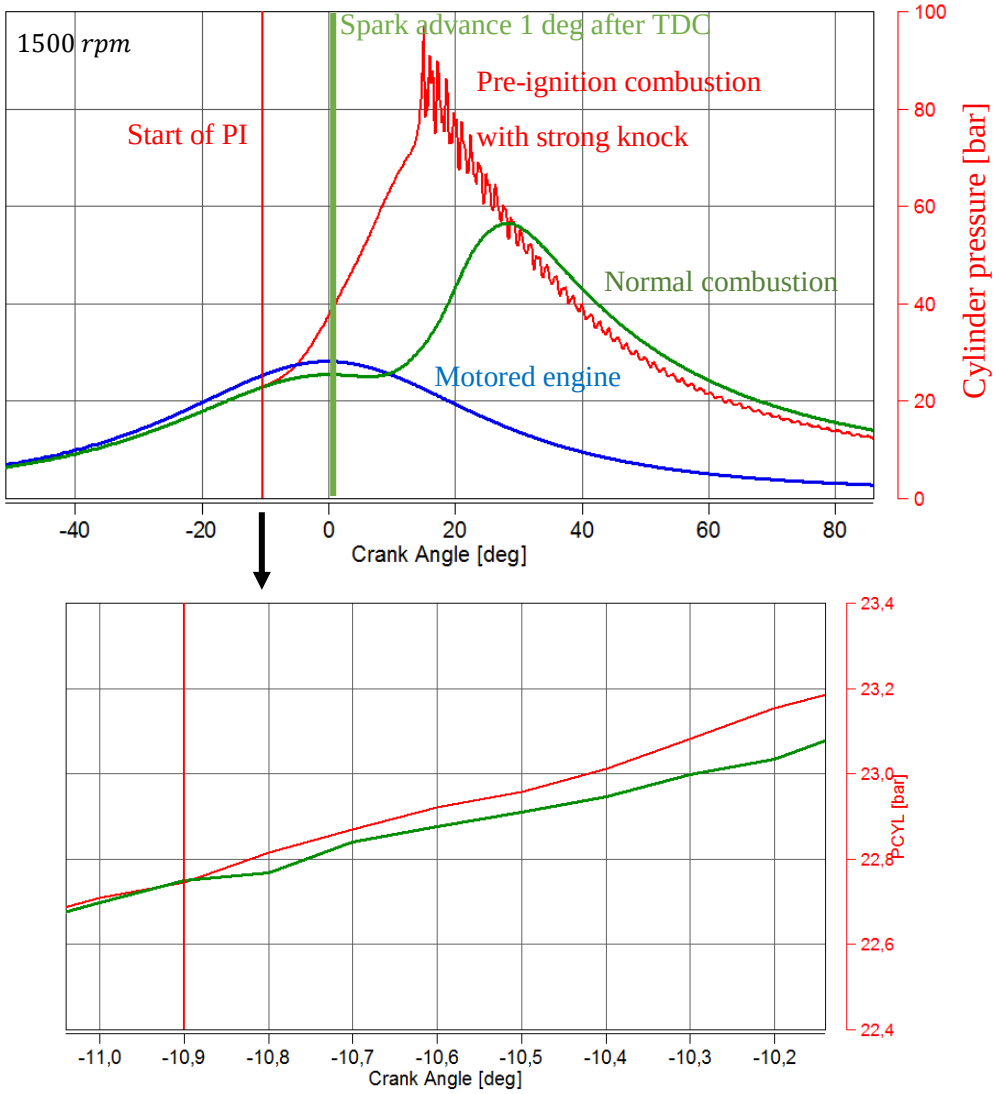

Figure 5-13 Cylinder pressure traces of motored and fired cycles. PI timing is seen in the comparison of fired cycle pressure traces

With above given pressure signals, PI is seen to occur at around $-10.9\ deg\ CA$. How does this compare with rate of heat release evaluation and furthermore with a comparison of flame radiation recorded with fiber optic sensors?

5.5.2 Rate of heat release

Rather than comparing pressure traces of PI and non PI cycles for evaluation of start of combustion (SOC), a rate of heat release (RoHR) evaluation is as well suited to identify SOC, see Fig. 5-14. As this methods avoids the comparison of two independent cycles, it also avoids errors arising from cycle to cycle variations. It of course requires an accurate selection of RoHR evaluation parameters to provide reliable identification of the RoHR trace rising above its zero line. Thus the time resolution of the RoHR signal is lower than the pressure signal, a reliable SOC information is given.

With knowledge of start of combustion and spark timing, the ignition delay parameter can be used to characterize combustion cycles in more detail:

$$ID = SOC - SA$$

ID ... Ignition delay

SOC ... Start of Combustion

SA ... Spark Advance

With this definition, negative ignition delay refers to PI cycles, positive ignition delay to normal, regular combustion cycles and cycle with $ID = 0$ or close to zero are described as "borderline" PI cycles. Such reference to ID data is later used to classify cycles as PI, borderline or normal. (42)

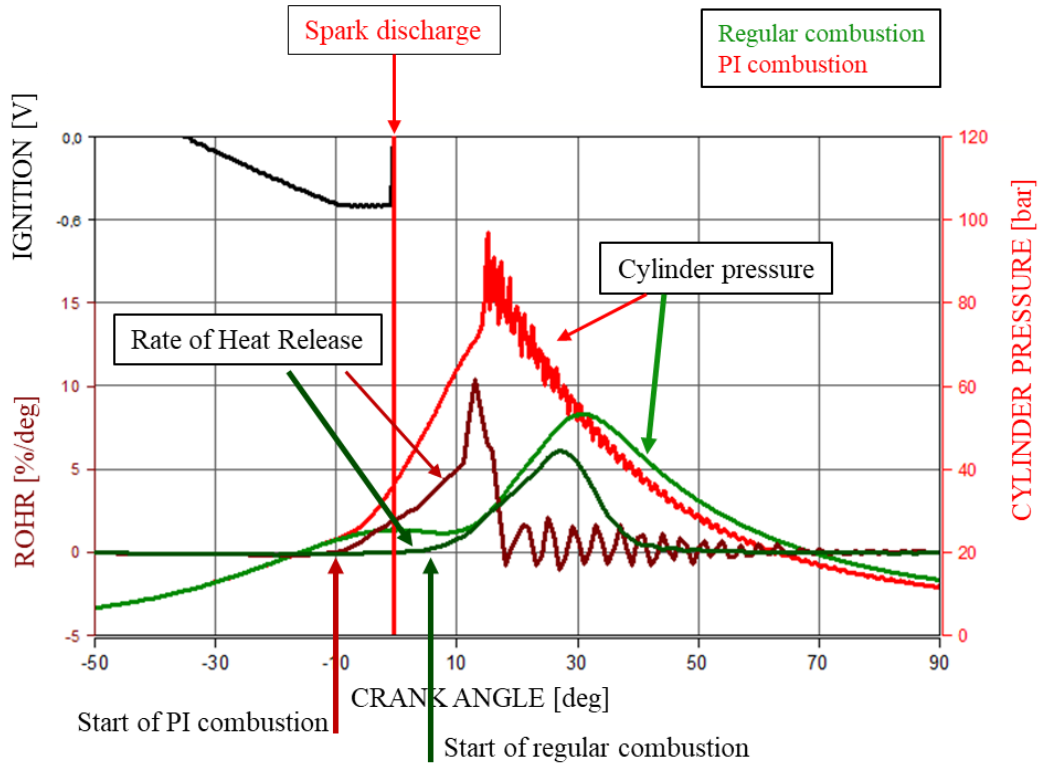

Figure 5-14 Comparison of the RoHR of a PI cycle with a normal combustion cycle

5.5.3 Optical detection

Occurrence of flame radiation is used to identify the time of self-ignition. This simple concept requires an optical sensor's field of view to coincide with the self-ignition area. The concept, furthermore, allows to locate the PI area provided that multichannel sensors can be used to record locally separated combustion chamber areas.

The flame signals in Figure 5-15 are recorded with Visiolution spark plug sensors for the PI cycle shown in Figure 5-13. The transition from no flame to flame radiation is easily seen in each sensor channel. A limit to identify the onset of flame signals is only given by background signal noise, see chapter 4.5.1.

In a comparison with pressure and rate of heat release signals we recognize following:

The pressure sensor responds to the change of gas pressure, the optical sensor responds to the appearance of optical radiation. These signals are not necessarily co-incident, but depend on spectral sensitivity of the optical signal path and on dynamic sensitivity of optical as well as pressure sensors.

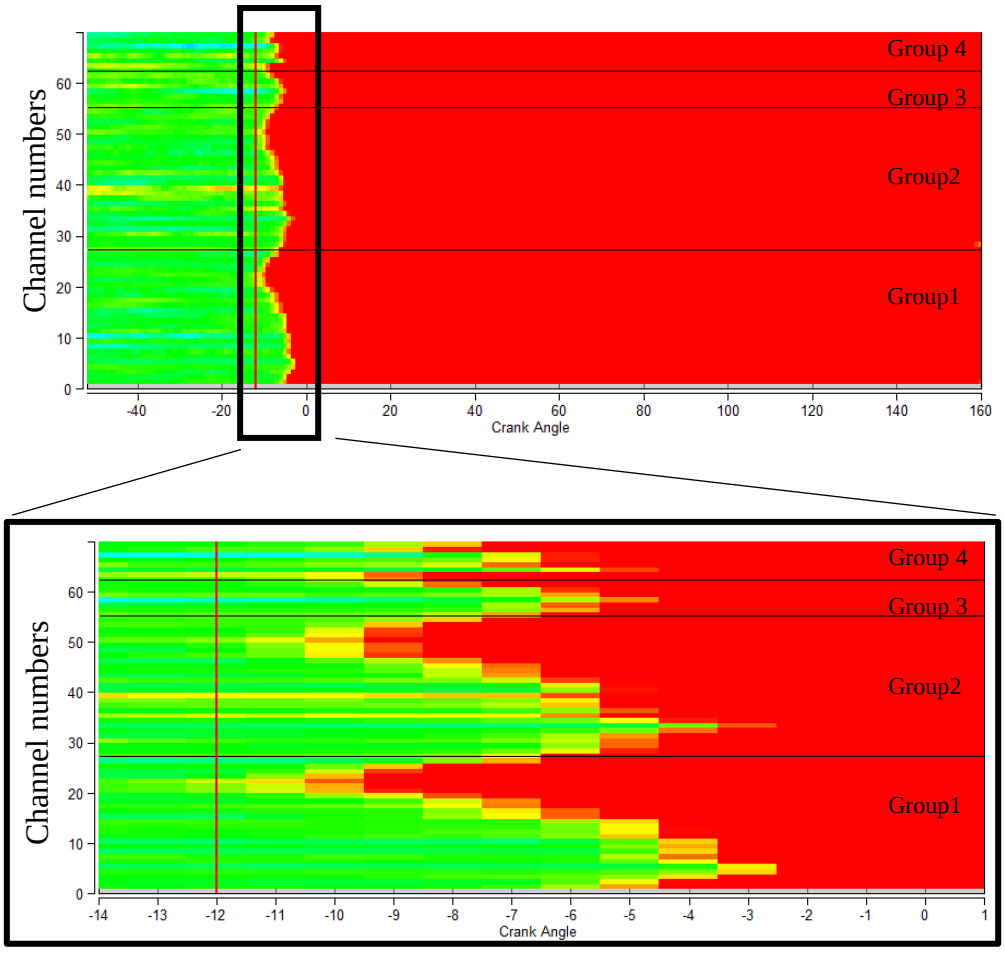

Figure 5-15 Light intensity signals of an irregular combustion cycle, scaled in no light intensity (green) and light (red)

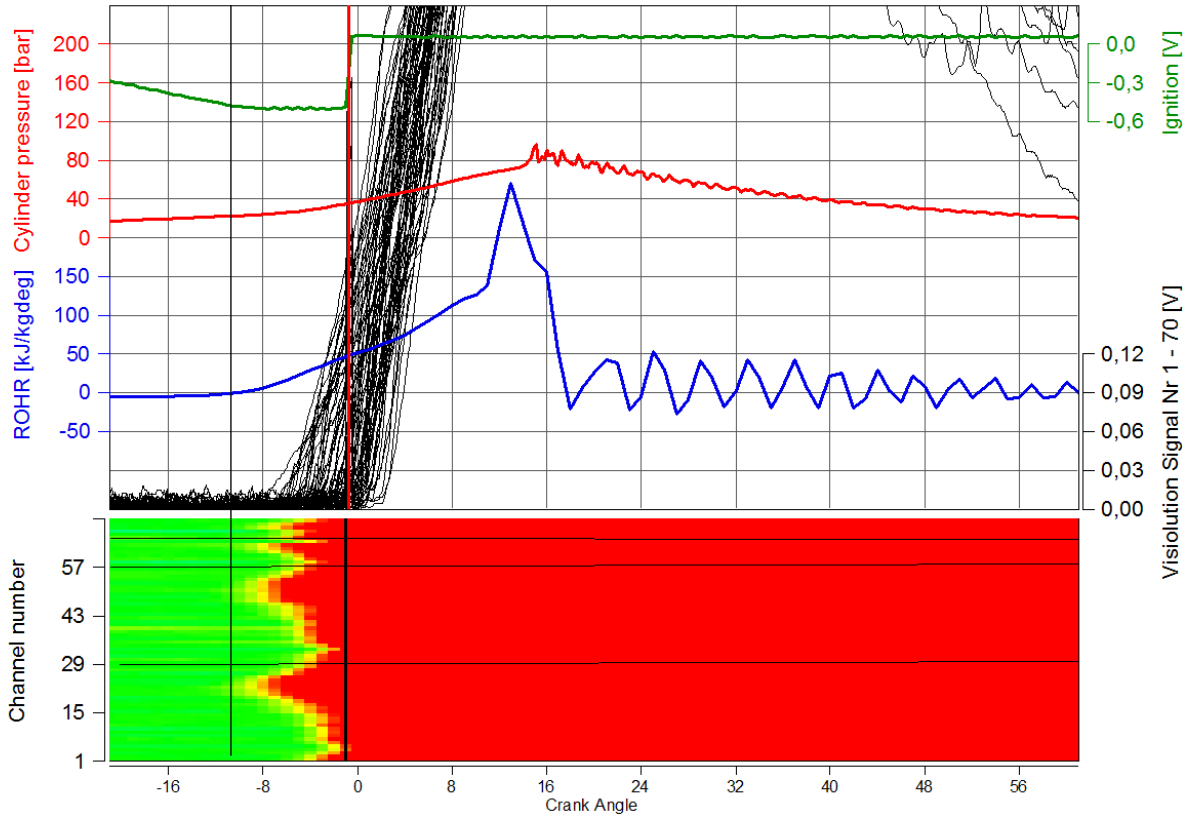

Figure 5-16 Comparison of the different methods for the determination of the ignition time

Figure 5-16 gives a comparison of start of combustion evaluation. The figure shows that the start of combustion is visible with the RoHR as well as the visiolution flame signals. These signals rise at the same time, about 12 $deg\ CA$ before TDC.

5.5.4 Knock sensor

A knock sensor is well suited to detect mega knock events, see Figure 5-17, however detection of the pre-ignition event itself is beyond the scope of such sensors.

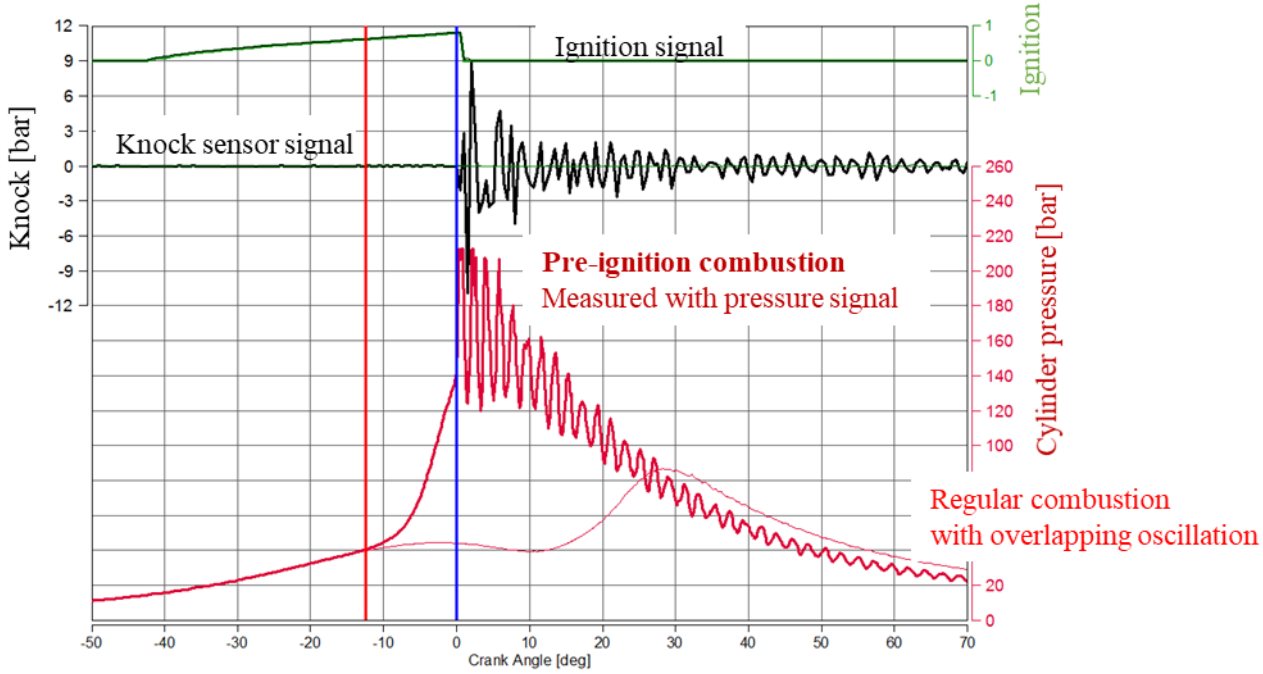

Figure 5-17 Example of a pre-ignition recorded with knock sensor and cylinder pressure indication

In summary, signals recorded with a cylinder pressure sensor allow identification of PI timing, either by direct comparison with normal fired cycles or with a well calibrated rate of heat release evaluation. Optical sensors are very well suited to identify PI timing provided their field of view coincides with the PI area. Multichannel sensors furthermore allow evaluation of PI location, see chapter 4.5. Knock sensors are suited to detect the knock event introduced by PI, but are unsuited to identify PI timing.

6 Project examples

This chapter describes pre-ignition tests which were performed in two types of SI engines:

1. A single cylinder engine with special access to the combustion chamber to initiate controlled surface ignition with a glow plug and to observer in-cylinder events by means of endoscope and glass fiber sensors, see chapter 3.1.
2. A single cylinder engine with large optical windows for direct view into the combustion chamber to visualize combustion events by means of a high speed camera

6.1 PI surface ignition measurements

In a single cylinder research engine a glow plug was used to initiate pre-ignition events. The combustion chamber geometry is shown in Figure 3-4. The glow plug temperature was controlled with a current regulator, its temperature was measured with a thermocouple inserted in a bore near the tip of the glow plug.

The engine was operated under boosted conditions in the speed range from 1200 to 3000 rpm. In order to initiate pre ignition, the glow plug was heated up to target temperatures for a duration of 10 to 20 seconds. Experimental parameters are given in Table 6-1.

Table 6-1 Measurement parameters

Engine Speed [rpm]	Engine Load [bar IMEP]	Glow Plug Temperature [°C]	Glow duration [sec]
1200	**16**	700	**10**
1500	**18**	**900**	**15**
2000	**20**	**1000**	**20**
2500	**22**	-	-
3000	**24**	-	-

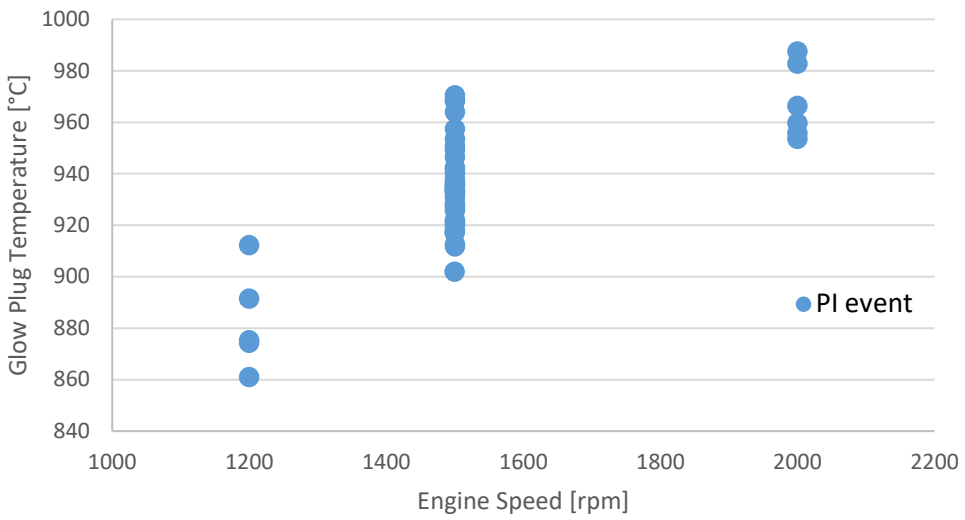

Figure 6-1 PI events for given engine speed and glow plug temperature, as per Table 6-1, $n = 50$ PI events were detected in total

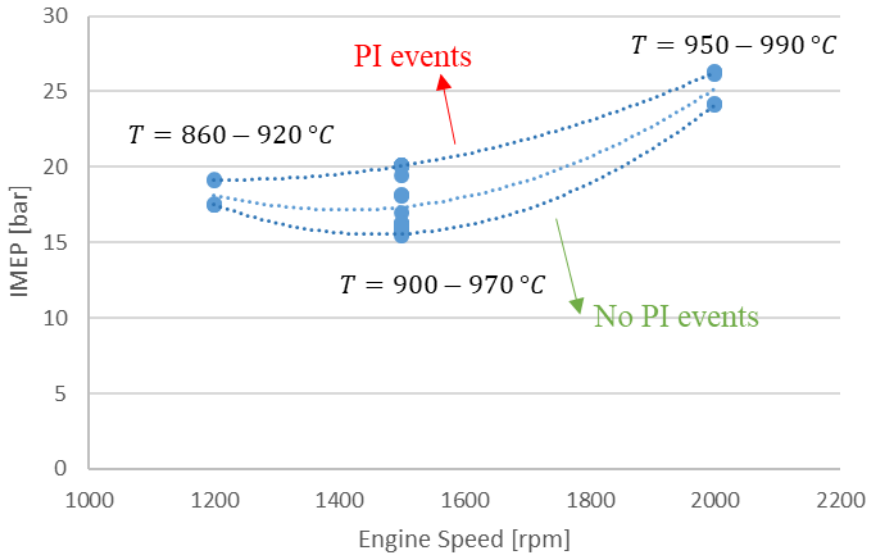

Figure 6-2 IMEP limits for PI at given engine speed and glow plug temperature

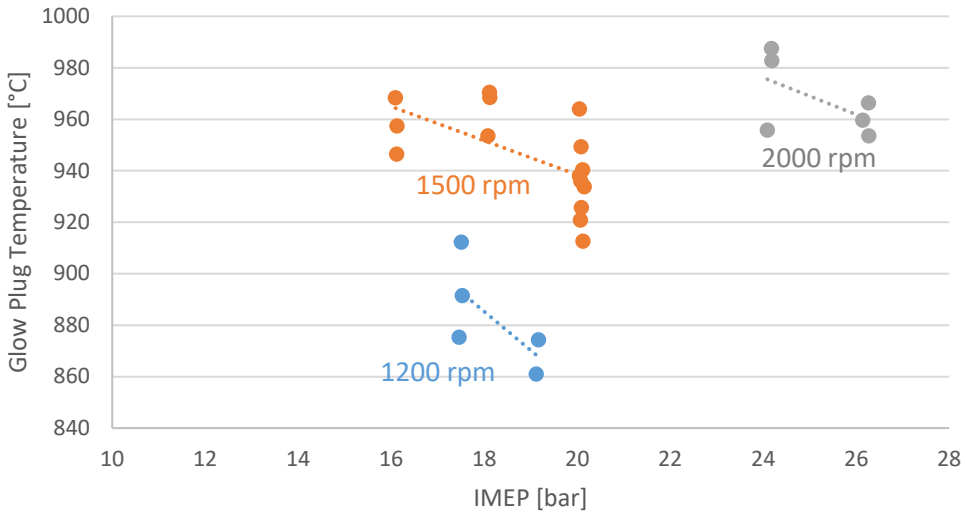

Figure 6-3 PI events for given IMEP and glow plug temperature at $1200\ rpm$, $1500\ rpm$ *and* $2000\ rpm$

With the boundary conditions given by engine load, glow plug temperature and heating time, the PI event statistics in Fig. 6-1, 6-2, 6-3 show and confirm that hot spot PI risk rises with:

- Hot spot temperature
- Time available to heat the charge
- Engine load

These features are well reflected in the figures' trend analysis and are in good accordance with the considerations discussed in chapter 5.

In the test engine, heating of the charge results from compression, heat transfer from surfaces into the charge and from the hot spot introduced with the glow plug. It is obvious to expect that pre-ignition occurs at the glow plug surface.

However, the optical instrumentation allows to actually "see" the area of self-ignition and thus to evaluate how close the PI kernels are really located to such local heat source.

6.2 Glow plug measurement

The procedure to handle the engine near PI conditions and to measure relevant signals is explained in Figure 6-4 with an example operating point of 16 $bar\ IMEP$ at $1500\ rpm$. After engine stabilization, the glow plug is heated and within about 20 cycles, glow plug temperature rises from 500 to over $1000\ °C$.

This glow plug heating first initiates some knocking cycles before it causes PI combustion with consequent mega-knock pressure events, see the upper part of Figure 6-4 with cylinder pressure signals for the PI cycle compared to a normal reference cycle. Fuel injection and spark discharge events are the same for each cycle.

In response to the mega-knock pressure signal, the engine controller introduced a fuel cut to protect the engine from subsequent "run-away" PI combustion cycles.

Signals were recorded with a conventional crank angle based engine data recorder (AVL Indimodul). The engine controller activated fuel injection and ignition. A real time signal processor was used to identify engine knock with the knock index (k_{pi}) and maximum cylinder pressure (p_{max}) derived from the pressure trace. (The knock index is defined as the maximum value of a high pass filtered cylinder pressure signal.) A threshold for k_{pi} and p_{max} was set to identify mega-knock and initiate the fuel cut.

Table 6-2 Signals recorded for the PI tests

Signal	sensor
Ignition	Current clamp
Injection	Current clamp
Cylinder pressure	Pressure sensor
Glow plug temperature	Thermocouple
Intake air pressure	Pressure sensor
Lambda	Lambda sensor

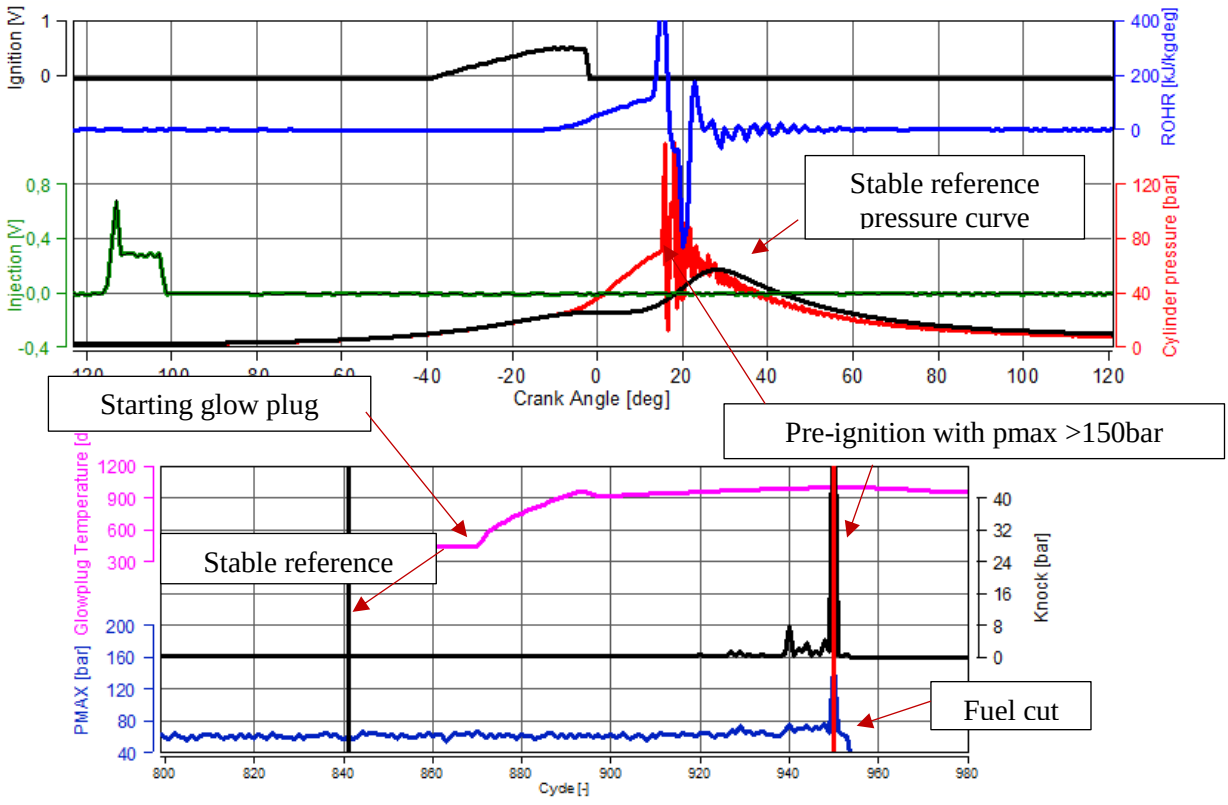

Figure 6-4 Indicating data of test cycle with PI event

The cycles in above PI test have also been studied with a “single shot” camera which is sensitive in the IR (infrared) part of the optical spectrum. Access to the combustion chamber was accomplished with an endoscope, see Figure 3-6. This IR camera ensures recording of flame kernels in premixed charge which otherwise would be invisible with an endoscope access and a passive camera.

In order to visualize any PI event, the camera was triggered to record an image of the combustion chamber just before spark discharge. The recordings in Table 6-3 were achieved with a camera shutter duration of $100\ \mu s$, the time delay between camera closing and spark discharge was $11\ \mu s$.

The black / white photographs in Table 6-3 show PI flame kernels in cycle 940, 942, 944, 948 and 950. The flame kernel images are superimposed on a photograph of the combustion chamber in order to provide geometric orientation. This background photograph was taken in a normal combustion cycle.

The PI flame kernels found in the IR photographs are each related to a pressure event which is furthermore identified by the knock pressure analyser. Most of these cycles show pressure traces with a knock index (k_{pi}) in the range of $2 - 6\ bar$ until cycle 950 yields a strong megaknock event with a KP index of $81\ bar$ and a peak pressure spike of $150\ bar$.

Each of the flame kernel photographs, as expected, shows the flame appearance within the same area between spark plug and glow plug.

Table 6-3 IR-picture series of PI-events related to Figure 6-4

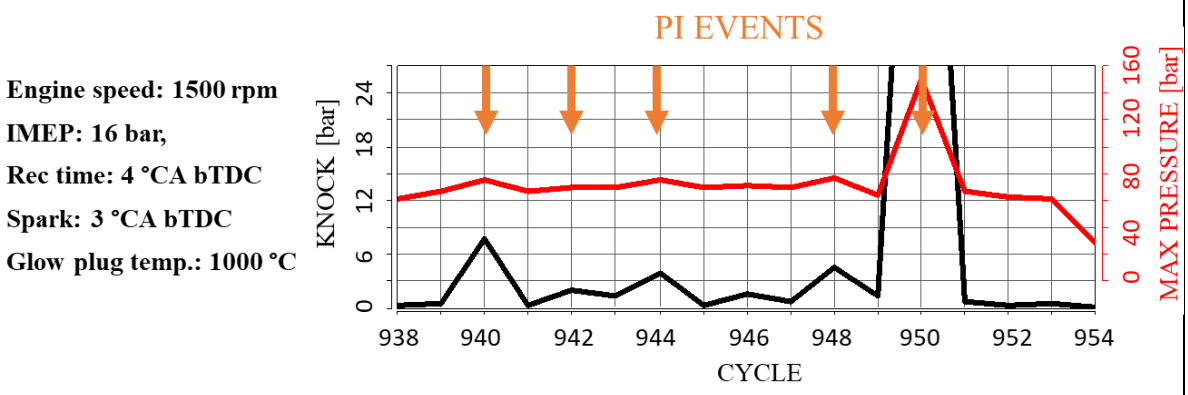

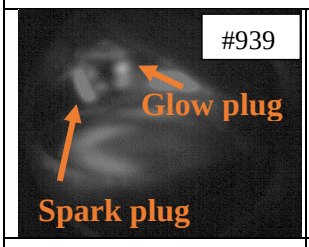	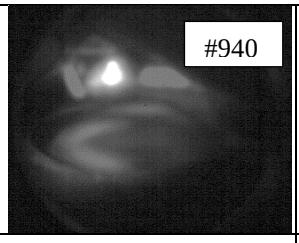	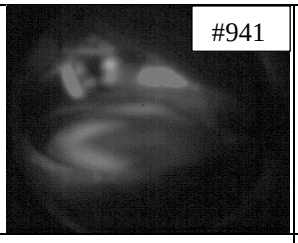	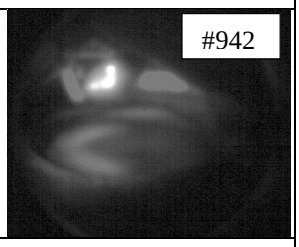
	PI EVENT		**PI EVENT**
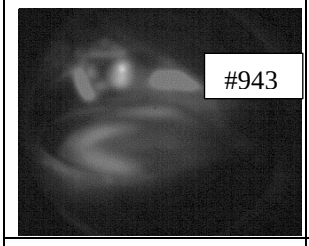	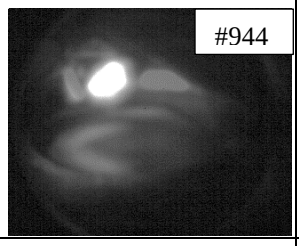	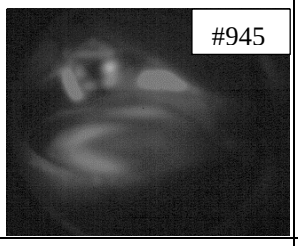	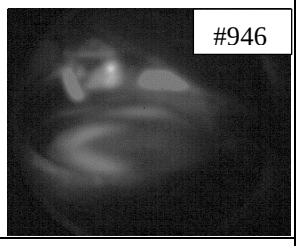
Small PI event	**PI EVENT**		
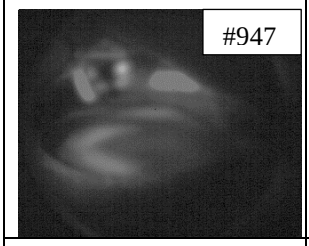	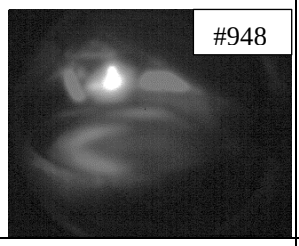	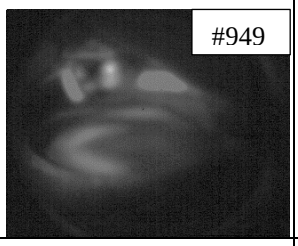	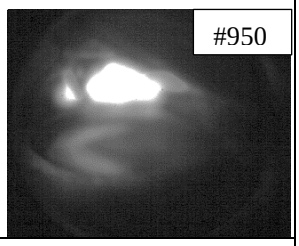
	PI EVENT		**PI EVENT**
	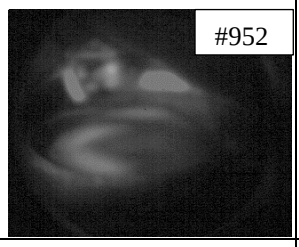	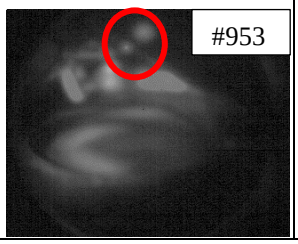	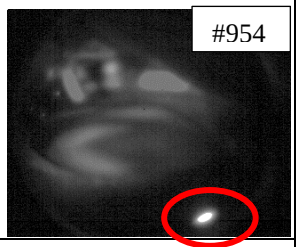
	Fuel cut	Glowing particles after PI events and injection stop	

Figure 6-5 to Figure 6-8 give a more detailed discussion of some selected cycles with features as listed in Table 6-3 at 1500 rpm, $IMEP = 16\ bar$. Ignition delay (ID) is defined with the crank angle difference between the start of combustion (detectable with the rise in RoHR) and spark timing. It identifies combustion conditions to be normal ($ID > 0$), borderline ($ID = 0$) and PI ($ID < 0$).

Table 6-4 Cycles selected for discussion in Fig 6.5 to 6.8

Cycle nr	Feature	Comment	p_{max} [bar]	ID = ignition delay [deg CA]
939	Regular combustion	reference	67.1	5
950	PI cycle	Hot spot ignition with glow plug	150.5	-5
953	PI cycle	Glowing particle	61.3	0
954	Fuel cut effective with ignition out	misfire	28.3	-

The cycles have been selected to provide pressure trace examples together with a snapshot of the combustion chamber just before spark discharge as already explained above. As an example, cycle nr. 950 shows the PI event identified with a RoHR evaluation to occur some 5 $deg\ CA$ before spark discharge, followed by a remarkable “mega knock” amplitude. The flame kernel present just before SA has already been shown in Figure 6-6 above.

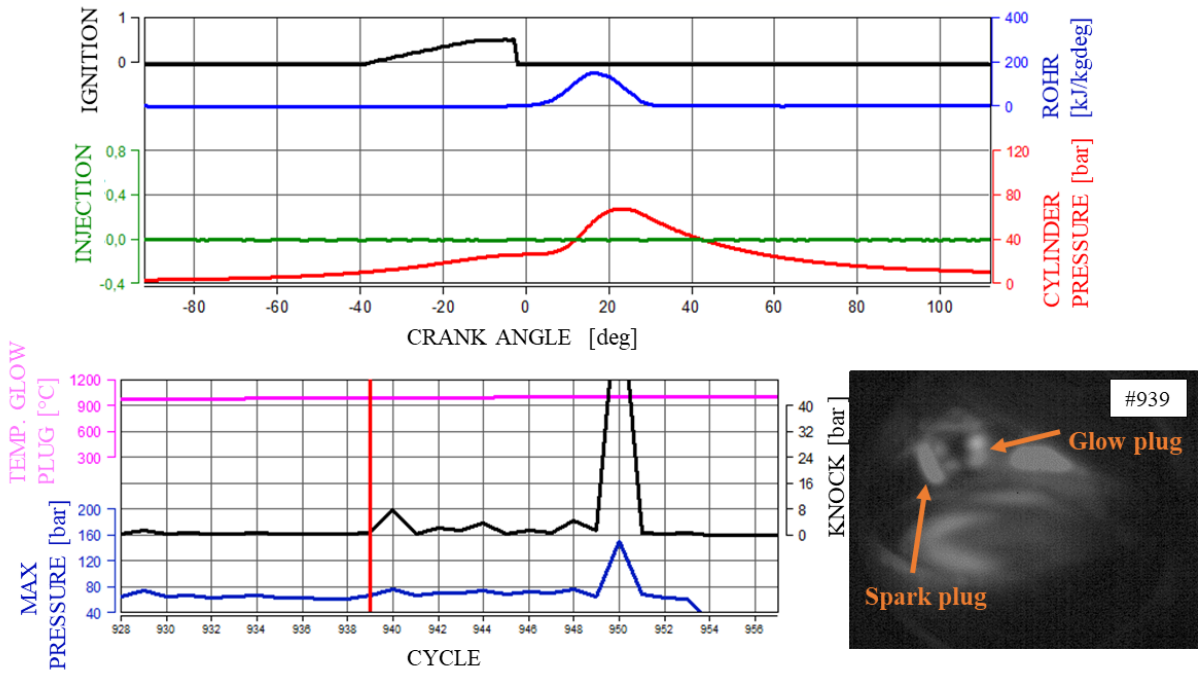

Figure 6-5 Cycle example of normal combustion with glow plug operation

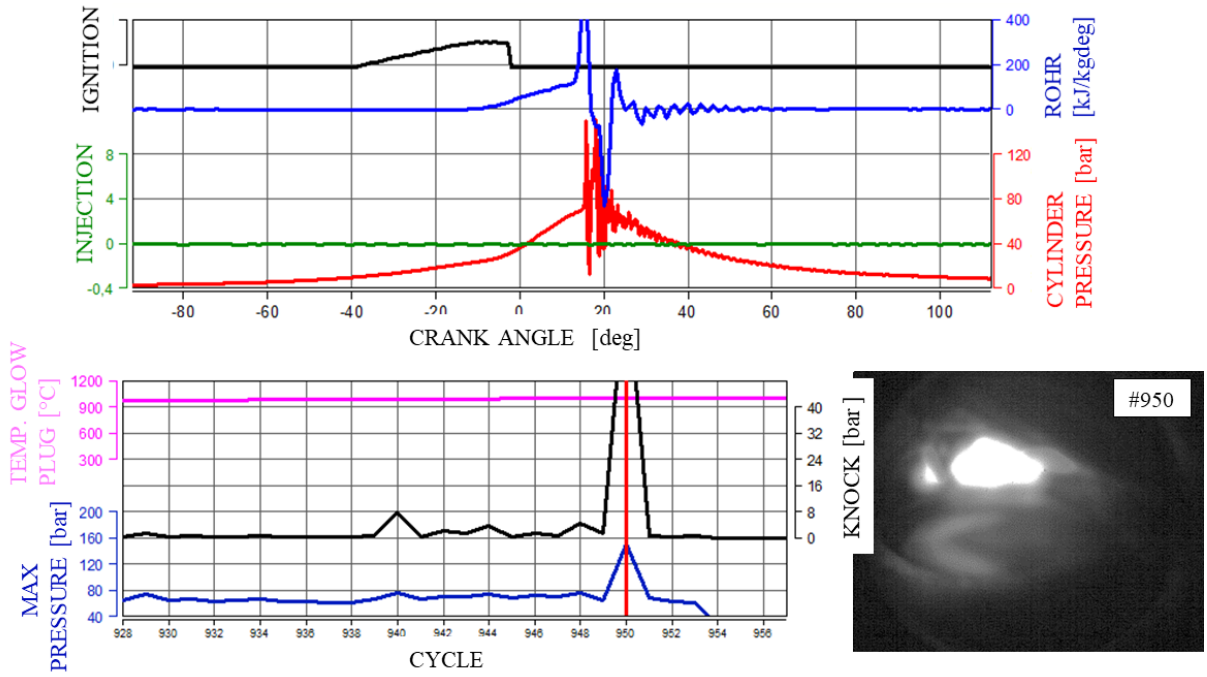

Figure 6-6 Cycle example of strong pre-ignition event

The photographs for cycles 953 and 954 were found to show traces of glowing particles. The pressure trace evaluation for cycle 953 shows a typical "borderline" PI event with start of combustion after, but close to, spark discharge.

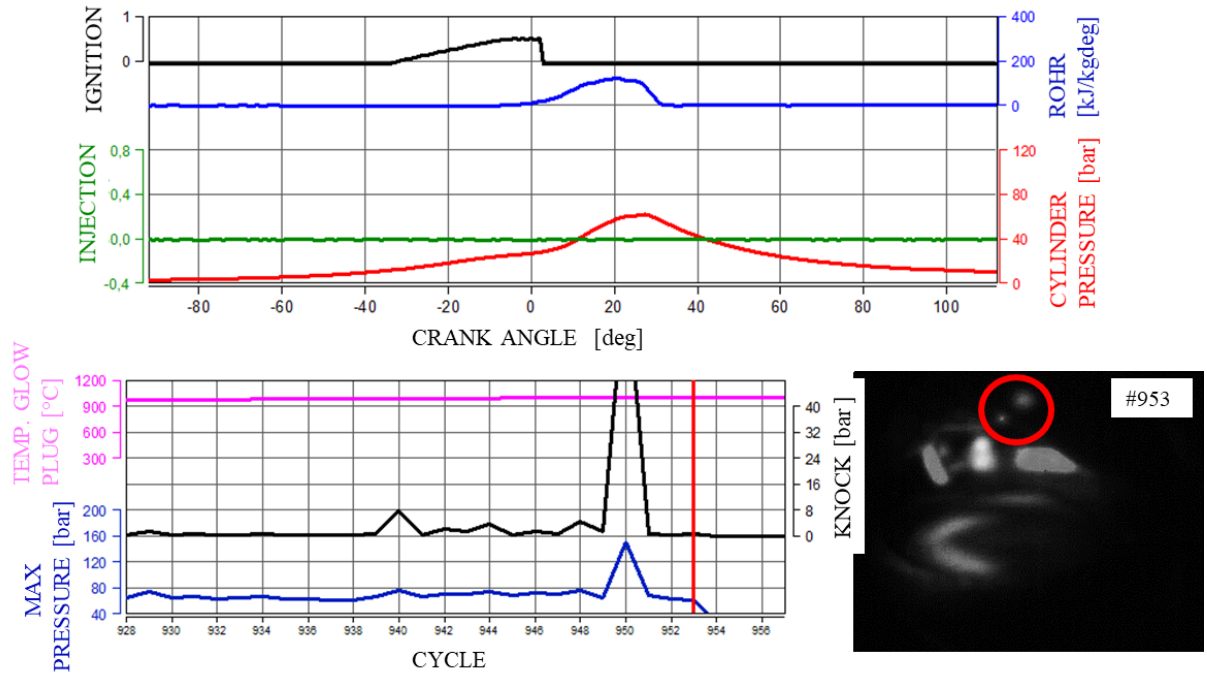

Figure 6-7 Cycle example after Pre-ignition event with glowing particles

In the next cycle nr 954, the engine controller's safeguard function has terminated both fuel injection as well as spark discharge.

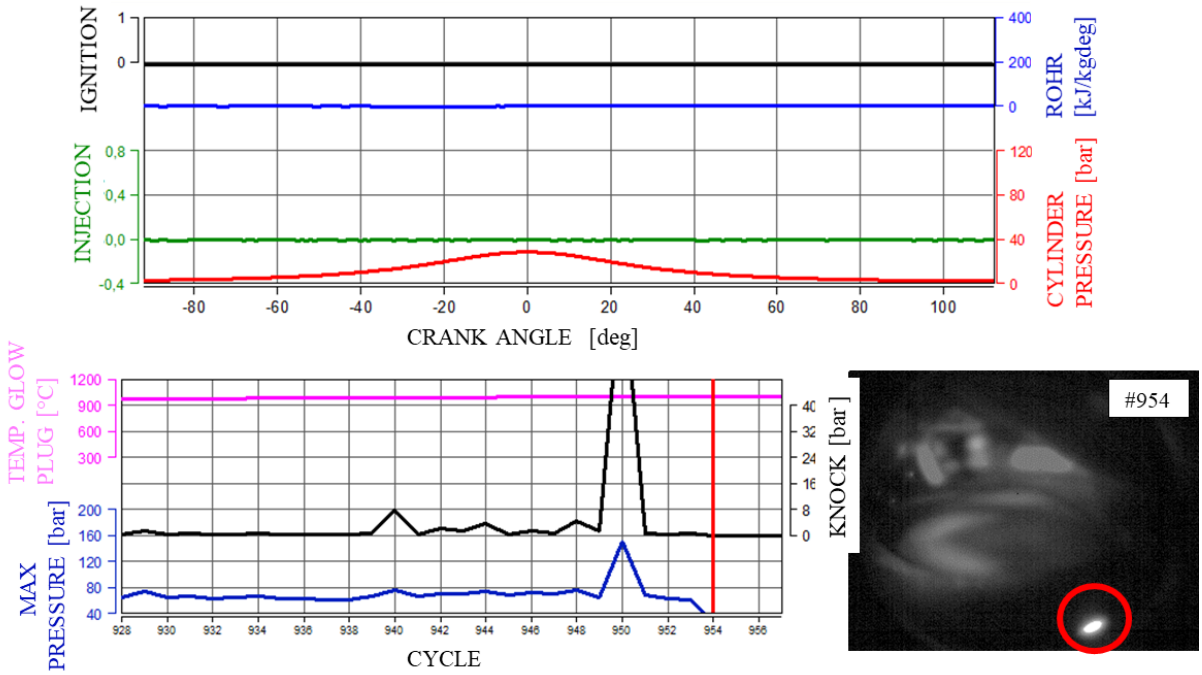

Figure 6-8 Cycle example after fuel cut with glowing particle

Concluding this chapter:

- A glow plug was used as an artificial heat source to initiate hot spot ignition events
- Occurrence of PI events, as expected, depends on glow plug temperature and the time available to initiate self-sustained flame kernel growth
- Location of visible PI flame kernels is near hot spot surface. It is, however, not necessarily identical with the hot spot surface. For an exact ignition localisation measurements with fiber optical spark plug sensors have been done, see chapter 6.2.2.
- After a strong mega-knock event, it was found that following cycles showed some radiating particles. Most likely as a result of deposits which were knocked off their surface contact by the pressure oscillations.

6.2.1 Data evaluation charge ignition temperature

For each of above cycles ignition timing has been derived from the cycles' pressure traces and RoHR. As the LW integral defines ignition conditions on basis of the Arrhenius parameters and the charge temperature, a numerical temperature variation can be used to adjust the LW ignition timing to the actual ignition timing of each cycle. This yields the charge ignition temperature T_i. The procedure thus comprises of: (1)

1. Evaluation of pre-ignition timing t_i
2. The Arrhenius relation $\tau = 55\, p^{-1,7}\, e^{\frac{3800}{T}}$ with parameters (A, B, n) and the simplistic assumption of constant charge temperature T_i. Charge pressure is given by the cylinder pressure trace.
3. The LW integral for given engine speed
4. Then the free parameter T_i is adjusted to yield $LW = 1$ for the ignition timing t_i
5. Identified for each cycle.

Such T_i evaluations for numerous cycles are shown in the diagrams of Figure 6-9 -Figure 6-10.

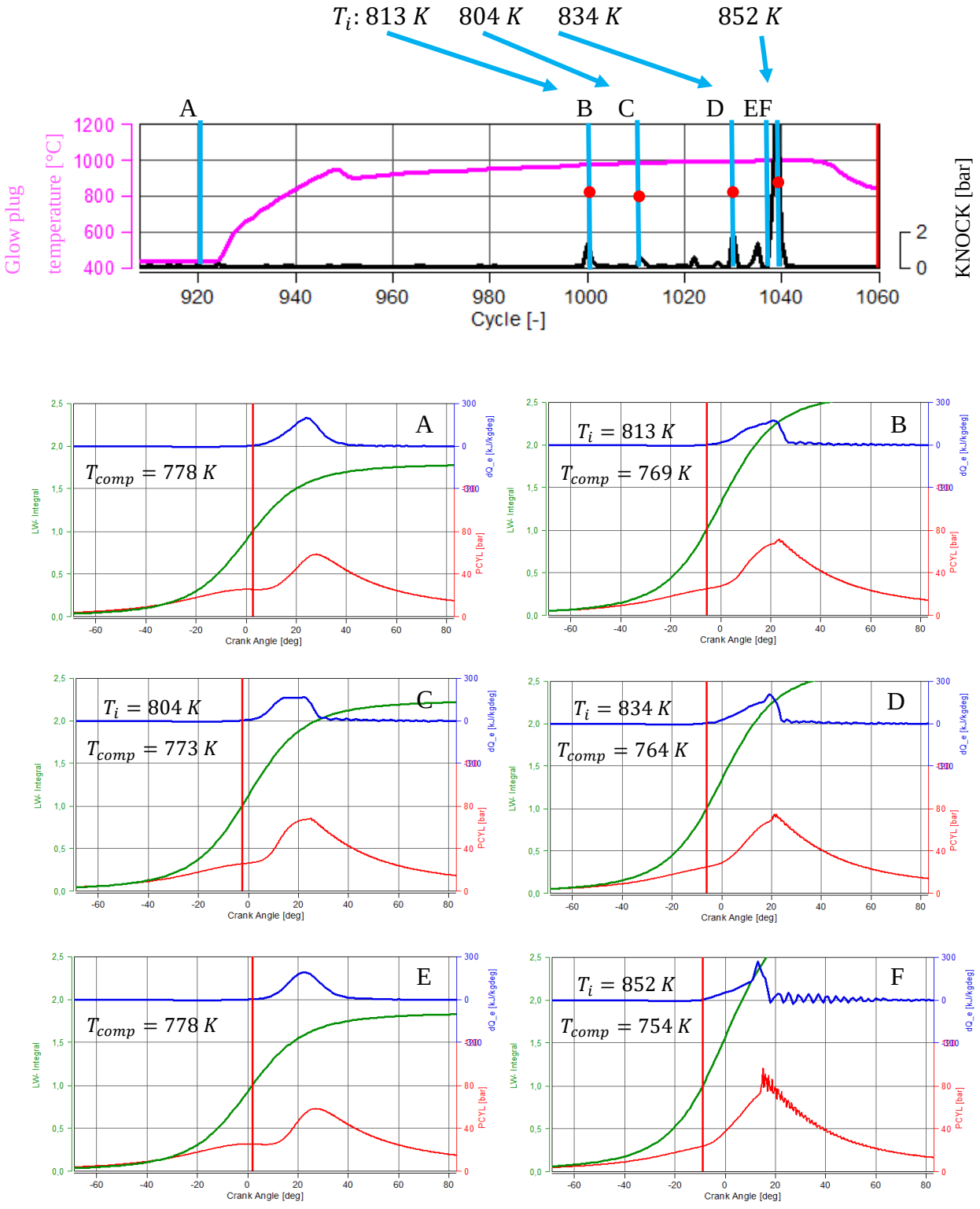

Figure 6-9 Data set 1: 1500 rpm, 16 bar IMEP, 1000 °C glow plug temperature, SA 0 deg CA: Ignition temperature T_i is evaluated from ignition timing (via rate of heat release) and the LW integral equation.

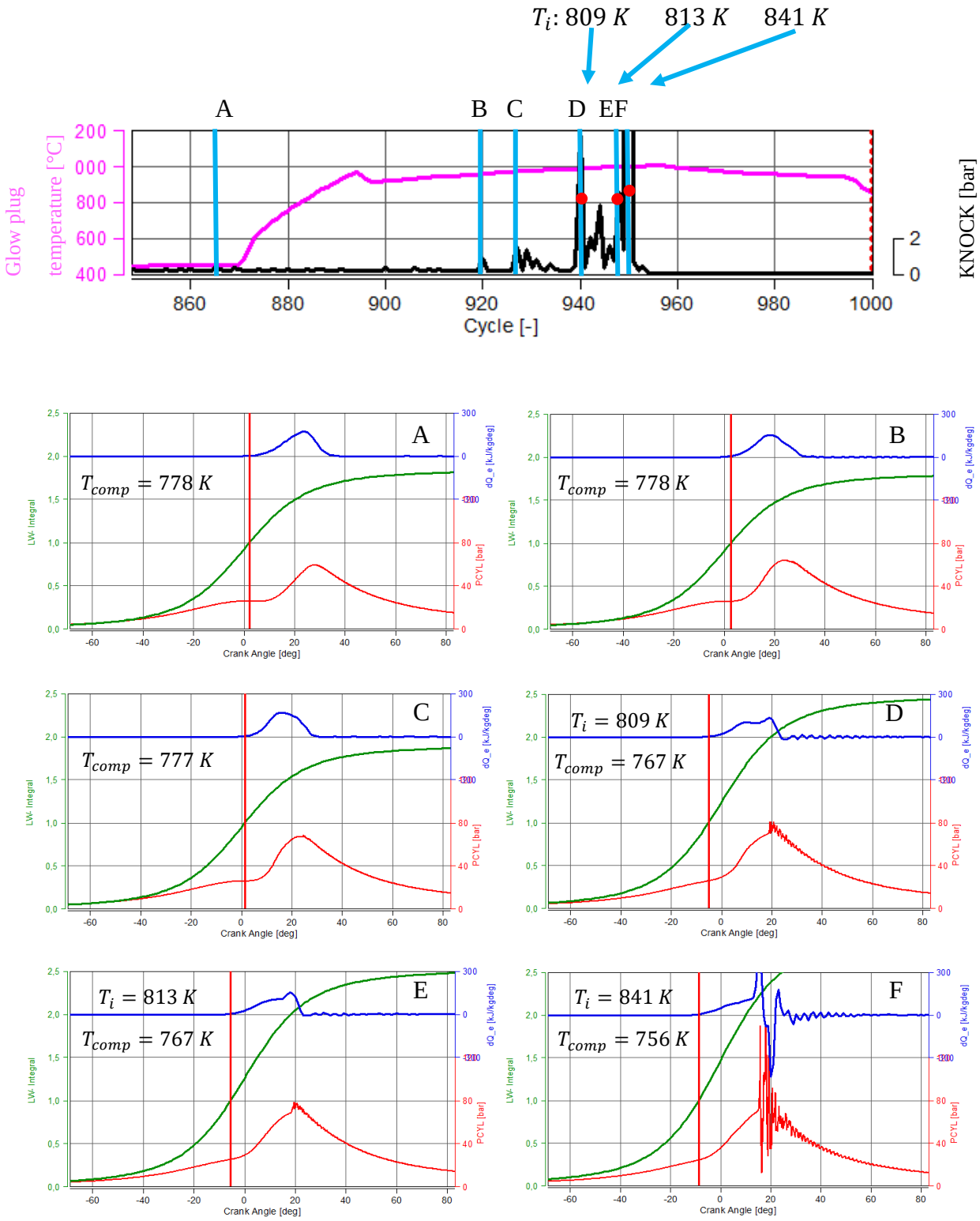

Figure 6-10 Data set 2: 1500 rpm, 16 bar IMEP, 1000 °C glow plug temperature, SA 0 deg CA: Ignition temperature T_i is evaluated from ignition timing (via rate of heat release) and the LW integral equation.

The T_i charge temperature evaluation shows a temperature spread in the range of $775\ K$ for weak PI cycles to $855\ K$ for strong PI cycles with an ignition delay of up to $-10\ deg\ CA$. For comparison, charge temperature due to compression is up to $775\ K$ and the hot spot glow plug temperature is up to $1275\ K$.

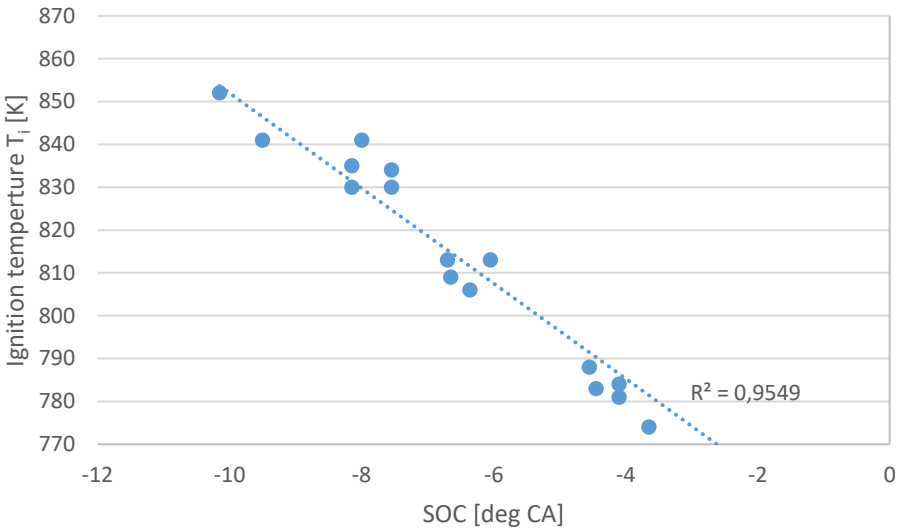

Figure 6-11: Ignition temperature T_i over the start of combustion: 20 measurement points of Figure 6-9 and Figure 6-10, 16 bar IMEP and 1500 rpm

In summary, the temperature values given in Figure 6-9 relate to:

1. T_{comp} Charge temperature due to compression $up\ to\ 775\ K$
2. T_{glow} Glow plug temperature $1075\ K - 1275\ K$
3. T_i Temperature of charge element which passes the ignition limit $775\ K - 855\ K$

Some spread of the ignition temperature T_i at a similar start of combustion is due to intake air pressure fluctuations.

6.2.2 Ignition location measurement with Visiolution spark plug

Self-ignition events have been recorded with a Visiolution spark plug sensor, ignition location is evaluated as has been described in chapter 4.5. The configuration of the combustion chamber with spark plug and glow plug positions is seen in Fig. 6-12.

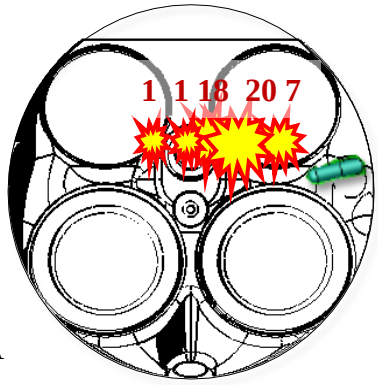

A

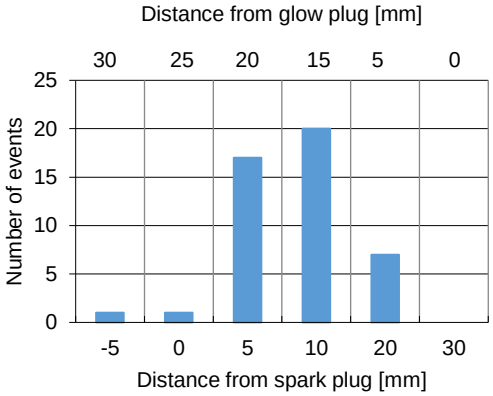

B

Figure 6-12 Position of PI events in combustion chamber (Visio evaluation)

The test series produced 46 PI events in total. Their positions have been identified as is given in the graphics of Fig- 6-12. Here, it is evident that location of a PI flame kernel is not necessarily identical with the hot spot glow plug surface, even if heat transfer from the glow plug into the charge is the root cause for pre-ignition.

The data set of Fig. 6-12 has been further evaluated for the charge “parcel” temperature initiating the pre-ignition event. Such temperature is evaluated as described in chapter 6.2.1. The data in Figure 6-13 confirm that an early start of combustion (SOC) requires higher “initiation” temperatures than retarded SOC at otherwise similar boundary conditions (rpm, charge density).

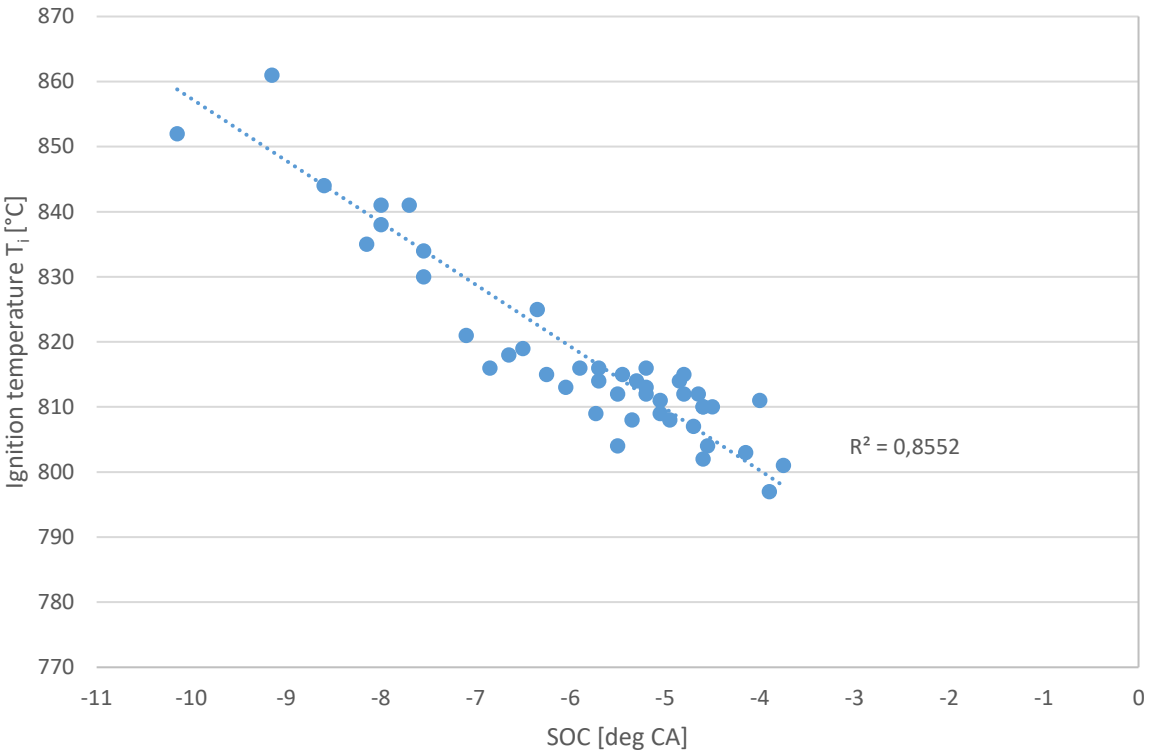

Figure 6-13 T_i statistics for ignition charge kernel temperature over start of combustion

The resultant knock intensity is related to ignition timing as would also be expected in normal spark ignition cycles.

Figure 6-14 to Figure 6-16 give a further breakdown of PI statistics with respect to glow plug temperature, knock intensity parameter as well as distance to spark plug. It is not evident that there would be any correlation of PI location with either of these parameters.

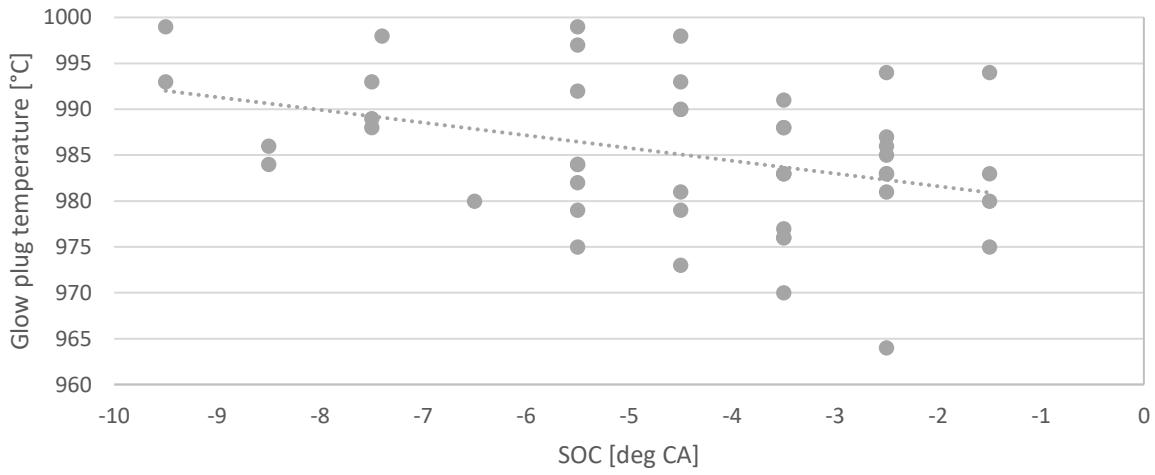

Figure 6-14 Glow plug temperature over start of combustion

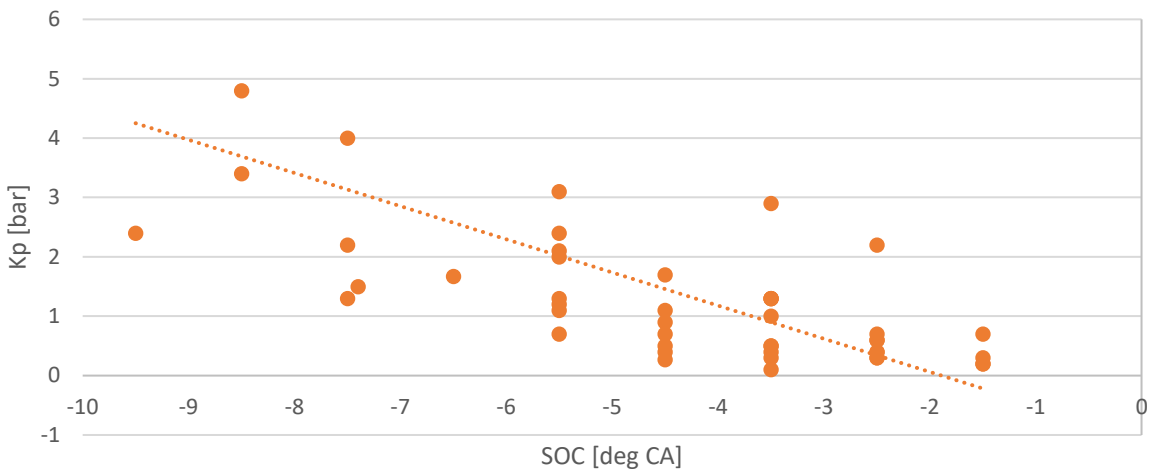

Figure 6-15 Knock value over start of combustion. Note that acceptable knock amplitude would be at 1.5 bar

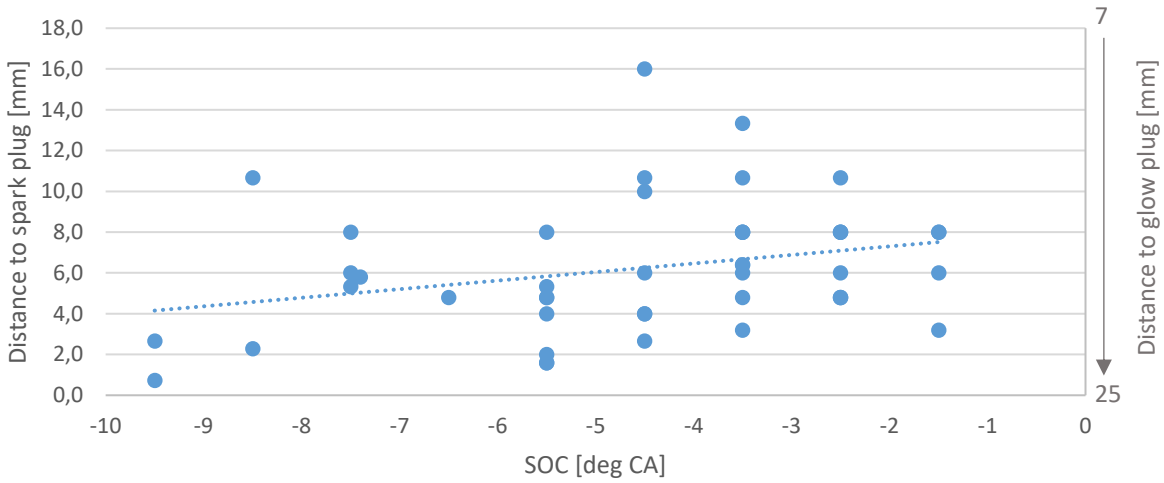

Figure 6-16 Distance to spark plug over start of combustion

The conclusions derived from these tests are as follows

- Heat transfer from hot surface into the gas is evolving over time, and is under influence of the parameters given by Arrhenius and Livengood-Wu
- Heat transfer requires a critical level to initiate ignition
- During heat transfer and the heated gas “parcel” becoming exothermal, convective gas transport can result in the PI event to occur at some distance away from the hot spot surface
- Turbulent gas motion most likely reduces PI probability as it enhances heat dissipation within the gas

6.3 Pre-ignition in engine with glass piston

Visualization tests for spark ignition and self-ignition events have been performed in a single cylinder research engine which allowed the view into the combustion chamber by means of an optical piston, see Figure 6-18. Ignition and flame growth were recorded with a high speed camera at a resolution of 2 $deg\ CA$. The operating conditions, see Table 6-5, allowed regular engine operation for about 100 fired cycles which occasionally included some PI cycles.

Table 6-5 Engine operation conditions at transparent Engine

Engine Speed [rpm]	Intake air pressure above ambient [mbar]	Coolant water Temperature [°C]	Spark advance [deg CA bTDC]	IMEP [bar]	MFB 50% [deg CA]
1500	750	60	-11	14.5	33

Figure 6-17 Design of glass piston for transparent engine

Figure 6-18 shows the view through the piston into the combustion chamber.

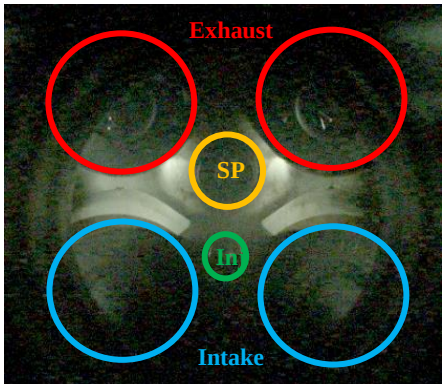

Figure 6-18 Reference picture for orientation with marked exhaust valves, intake valves, spark plug and injector

The photographs in

Figure 6-19 to Figure 6-21 show flame kernel growth under regular and irregular ignition conditions. See flame kernel growth with the spark plasma igniting the charge in Fig. 6-19. Two more examples are given with evidence of separate ignition centres and their individual flame kernels in Fig, 6-20 and 21.

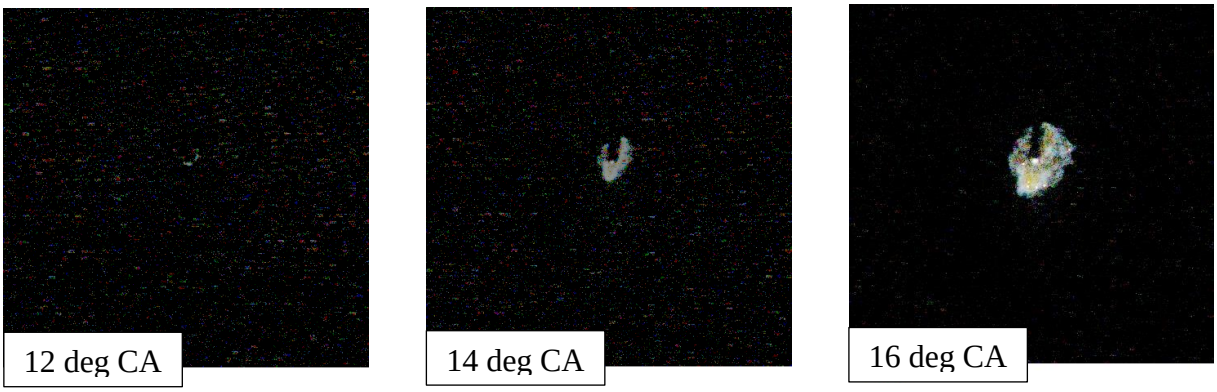

Figure 6-19 Flame kernel formation of regular combustion in 2deg CA step

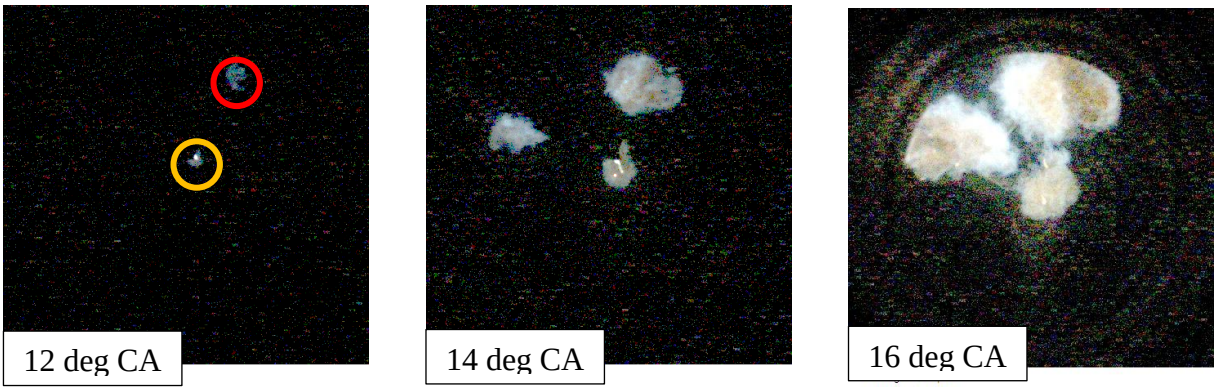

Figure 6-20 Flame propagation at irregular ignition with finally 3 flame kernels

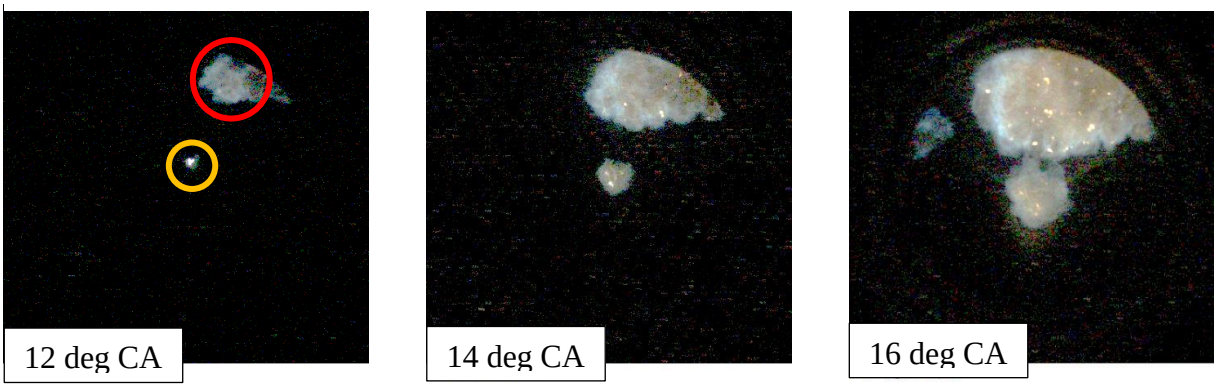

Figure 6-21 Flame propagation at irregular combustion in 2 deg CA step

The flame kernels initiated by the PI events show the very same premixed turbulent flame structure as is given by the normal plasma ignited flame.

With the engine and fuel conditions as given in Table 6-5, the self-ignition temperature as derived from the LW condition (5-10) would have to be 730 K. The charge temperature given by compression is 720 K at TDC. Thus the heat input required to initiate the PI events arises from another source. As is easily seen in the flame photographs, the PI ignition kernel is located near the intersection of the glass surface with the metal piston casing. Most likely this area is well heated in previous cycles and acts as hot spot ignition source.

The flame videos give evidence of single and multiple ignition sources especially under conditions where regular and irregular combustion events start at about the same time. This allows to address the question if such simultaneous, multiple ignition sources would be recognized in a rate of heat release analysis which is the usual path to such evaluation in normal engines. The data are shown in Figure 6-22.

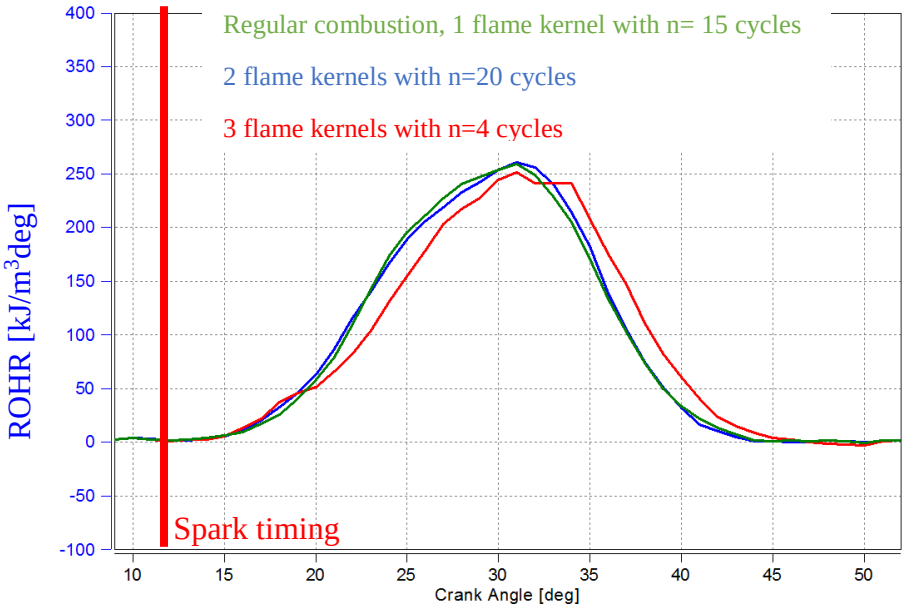

Figure 6-22 Mean values of the RoHR of combustion cycles with 1, 2 and 3 flame kernels

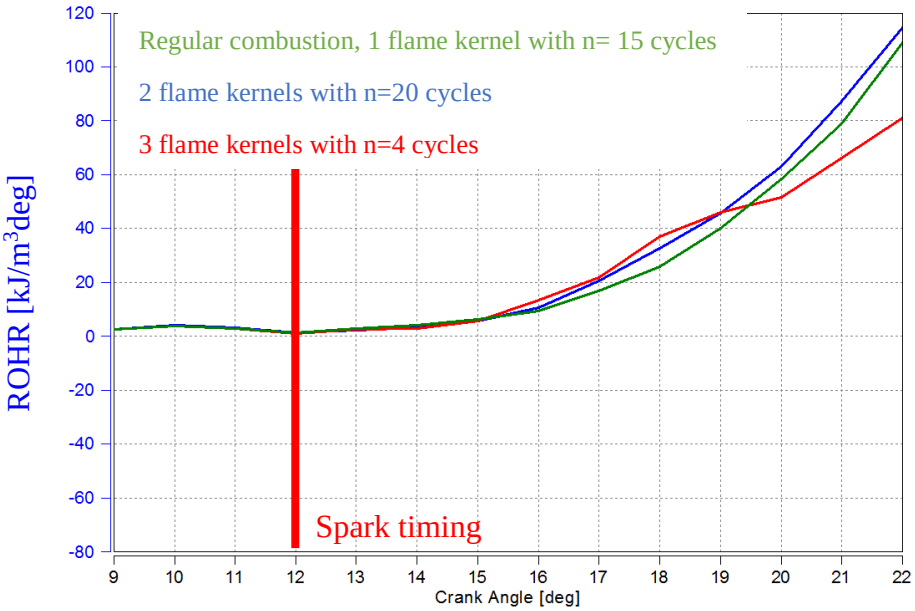

Figure 6-23 Detail view of the start of combustion of Figure 6-22

The conclusion based on above data is that on average and against expectations, there is no significant increase in the rate of heat released in any phase of combustion.

7 Procedure for the reduction of pre-ignition phenomena in normal engines

For the task of addressing and improving pre-ignition situations in normal engines the most important questions are:

- Which engine operating conditions lead up to PI events?
- Where do the pre-ignition events start?
- What is the root cause for these pre-ignition phenomena?

An experimental procedure to work on this topic comprises of activities as are summarized in Fig. 7-1.

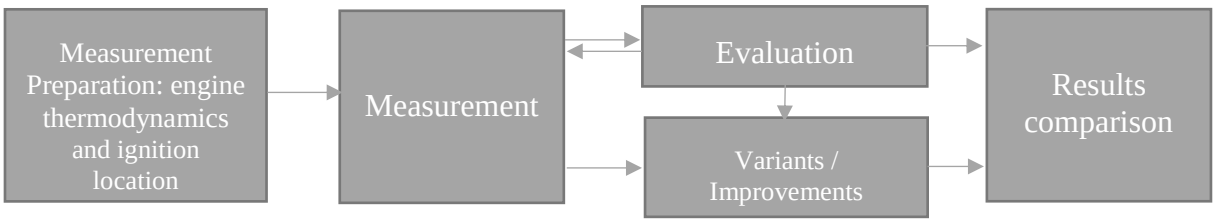

Figure 7-1 PI analysis procedure

7.1 Measurement preparation

- Clarify which engine operation condition result in PI events and how these PI events can be initiated in an engine test sequence.
- An evaluation of PI conditions will need 20 or more PI cycles. Clarify how to achieve such PI repetitions.

The analysis equipment includes

- Pressure sensors (not spark plug) in the cylinders of interest
- Fiber optic (Visiolution) spark plug sensors with appropriate heat values, length dimensions and spacers for length variation
- Signal measurement and evaluation system

Testbed requirements:

- Cylinder pressure indication system
- Open ECU, access to ignition and injection parameters
- A “safeguard” system to protect the engine from run-away combustion cycles

Engine test operation may include methods to provoke PI events:

- Later ignition time → warmer engine conditions, higher boost pressure to reach the same load and exhaust valves as hot spot
- Higher intake temperature → warmer engine conditions
- Increased engine load → higher combustion temperatures
- Increased cooling water temperature → higher engine component temperature
- Change injection timing to high diffusion flame combustion → creation of deposits
- Decrease of cooling water temperature → creation of deposits
- Transient modes of engine operation: Speed up / speed down

7.2 Measurement and data generation

Measurement of sporadic PI cycles needs signal recording procedures which continuously collect data in a first in first out (FIFO) transient memory configuration. Once a PI cycle is identified, the FIFO content is put into permanent memory, always including a group of cycles before and after the PI event. The trigger to identify PI cycles is derived from a real time comparison of pressure traces with target pressure levels.

Example:

- Engine with
  - Visiolution measurement system with 70 Channel Spark plug sensor
  - Cylinder pressure measurement
- Engine operation
  - under cold engine conditions
  - full load acceleration ramps from idle speed to $2000\ rpm$

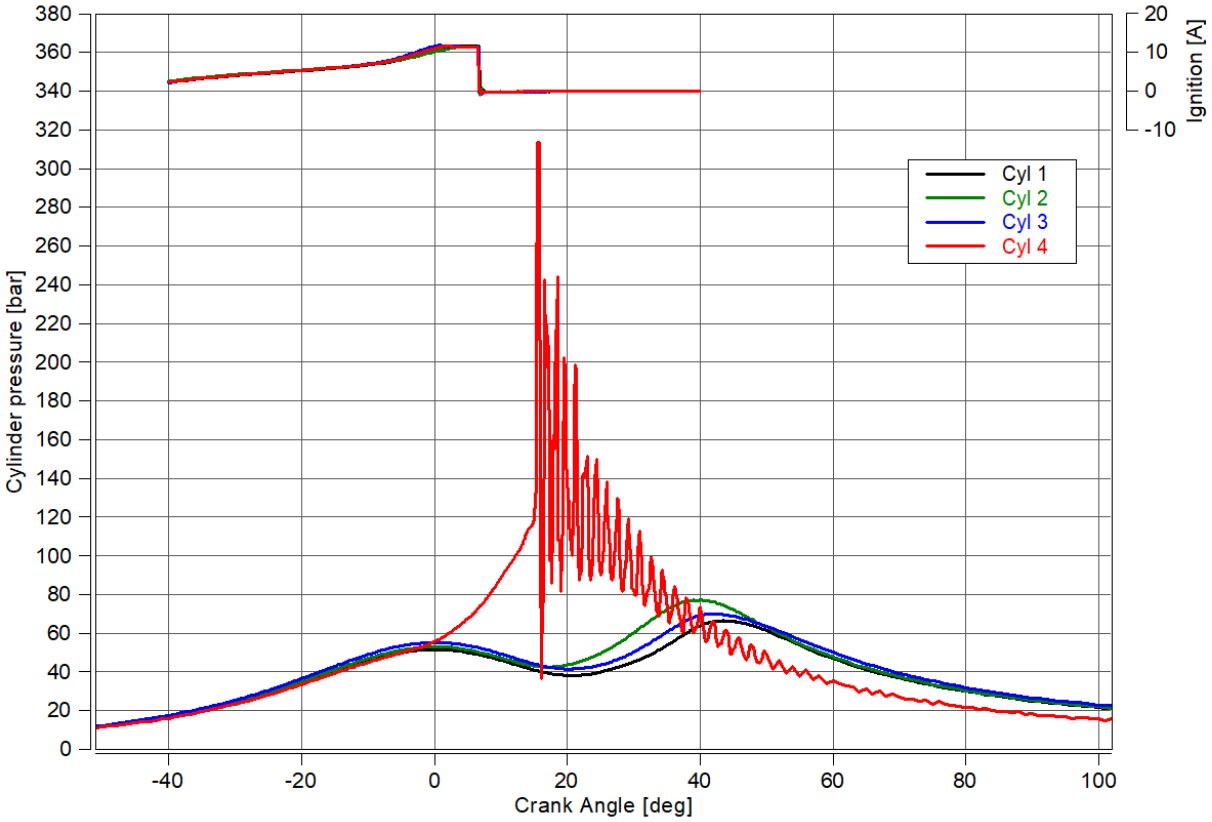

Figure 7-2 PI-event example at cylinder 4

Figure 7-2 shows an example of an PI event which occurred during the measurements. The statistic of all measurements, see Figure 7-3, during the first test shows a higher occurrence of PI centers in the central combustion chamber area close to the cylinder head.

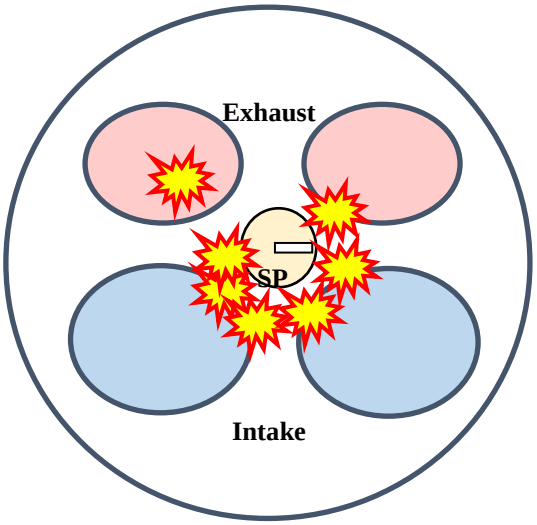

Figure 7-3 location of PI events shows agglomeration near spark plug area

7.3 Improvements

In the next step variations for combustion improvements are done to reduce PI occurrence. Possible variants may include:

- Reduce the temperature around the spark plug area by means of:
  - Late, multiple injection
  - Cooling water management
- Reduce component temperature:
  - heat value of spark plugs (43)
  - material for valve sealing rings
- Less deposits
  - By means of injection parameters
  - By means of fuel and lube oil additives

Example related to page 82:

The PI location results as shown in Fig. 7-3 suggest to reduce the surface temperature of the spark plug and around the spark plug thread. Two options were tested: less spark plug protrusion for a better heat transfer to the cylinder head and triple injection for charge cooling during the late compression stroke. In Figure 7-4 the resulting statistics is presented to show the effect of these measures. Between the testing's a back check of the base conditions was done for comparison purposes.

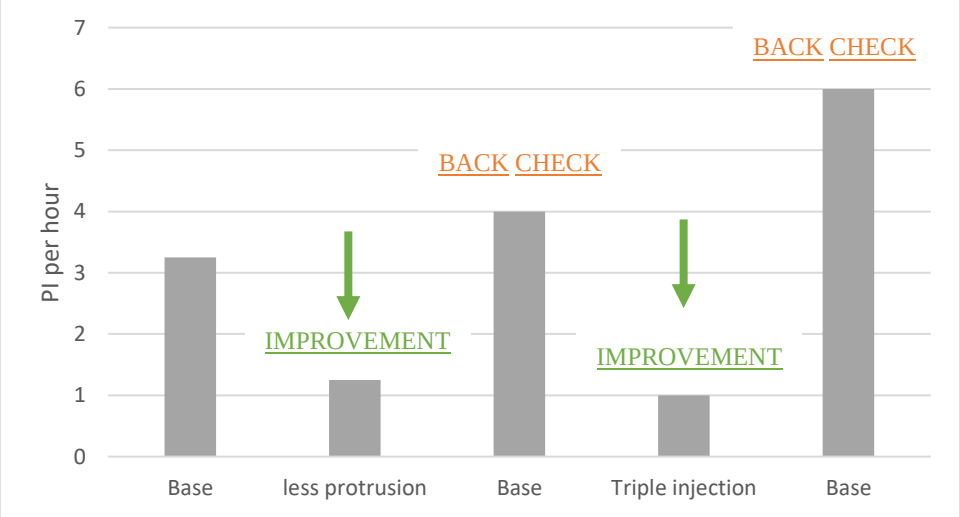

Figure 7-4 Test sequence results: comparison of test variants with repetitions of base conditions

8 Summary

Pre-ignition is driven by the input of activation energy, other than the spark plasma, into the in-cylinder charge. It has become an issue especially in turbo charged gasoline direct injected (GDI) engines which operate a high compression ratios and at high torque levels in a wide engine speed range.

The work presented in this thesis has focused on:

- A discussion of basic ignition and combustion phenomena
- A numerical analysis of potential activation energy sources based on the Arrhenius and Livengood-Wu concepts
- An experimental analysis of PI phenomena in various engines with focus on
    - Evaluation of PI ignition time, mainly derived from rate of heat release analyses
    - Evaluation of PI ignition location by means of fiber optic spark plug sensors

Evaluation of experimental data and analysis of ignition conditions with the Livengood-Wu integral has allowed to determine the temperature of a charge “parcel” at its time of self-ignition.

The measurement of the position of the self-ignition flame kernel then allows to relate the PI event to a potential root cause:

- Heat input from a local hot spot: in a controlled hot spot test by means of a glow plug it was shown that whereas heat input into the charge appears across the glow plug surface, self-ignition of the heated charge “parcel” can occur at some distance to the hot spot location.
- For a hot surface area to act as PI source it needs both surface temperature and size of the hot area in order to provide the heat transfer required to achieve PI.
    - A consequence of this effect is that large area exhaust valves have a higher potential to initiate PI as compared to the high temperature yet smaller spark plug surfaces
- In any LSPI (low speed pre-ignition) situation, the main parameter is the time available to heat the charge before its regular ignition with the spark plasma. Consequently hot areas and their heat transfer at low engine speed need specific attention.
- Engine operation and vehicle drive situations together with lube oil and fuel selection have an impact on the chemistry parameters of in-cylinder charge and surfaces. PI analysis provides data on PI timing and location and thus gives guidance for improvements
- The presence of “glowing particles” as potential ignition sources is detected with the optical spark plug sensors.

9 Sources

1. **Grüneberger, P. and Winklhofer, E.** *Charge temperature evaluation in self ignition events.* s.l. : The International Journal of WKM, 2018, https://doi.org/10.1007/s41104-019-00046-w.

2. **Warnatz, J., Maas, U. and Dibble, R.W.** *Combustion.* Heidelberg : Springer-Verlag, 2006.

3. **Brandstätter W., Pitcher G., Tatschl R., Winklhofer E.** *Modellierung der homogenen Verbrennung im.* MTZ Motortechnische Zeitschrift 58. 1997, p96 - 101.

4. **Heywood, J.** *Internal Combustion Engine Fundamentals.* Signapore : McGraw-Hill International Editions, 1989.

5. **Merker, G. and Schwarz, C.** *Grundlagen Verbrennungsmotoren.* Wiesbaden : Vieweg+Teubner, 2009.

6. **Pischinger, R., Klell, M. and Sams, T.** *Thermodynamik der Verbrennungskraftmaschine.* Wien : Springer-Verlag, 2009.

7. **Kuboyama, T., Moriyoshi, Y. and Morikawa, K.** *Visualization and Analysis of LSPI Mechanism Caused by Oil Droplet, Particle and Deposit in Highly Boosted SI Combustion in Low Speed Range*. s.l. : SAE Int. J. Engines, 2015.

8. **Luef, R.** *Entwicklung einer Prüfmethode zur Bestimmung des Öleinflusses auf irregulare Verbrennungsphänomene bei hochaufgeladenen DI-Ottomotoren.* Graz : Technische Universität Graz, 2015.

9. **McAllister, S., Chen, J.-Y. and Fernandez-Pello, C.** *Fundamentals of Combustion Processes.* New York Dordrecht Heidelber London : Springer, 2011.

10. **Metghalchi, M. and Keck, J. C.** *Burning Velocities of Mixtures of Air with Methanol, Isooctane and Indolene at High Pressure and Temperature.* Combustion and Flame 48, 191–210. 1982.

11. **Metghalchi, M. and Keck, J. C.** *Laminar burning velocity of propane-air mixtures at high temperature and pressure.* s.l. : The Combustion Institute, 1980.

12. **Damköhler, G.** *Der Einfluss der Turbulenz auf die Flammengeschwindigkeit in Gasgemischen.* Zeitschrift für Elektrochemie und angewandte physikalische Chemie. 1940, Bd. 46, 11.

13. **Wirth, M.** *Die turbulente Flammenausbreitung im Ottomotor und ihre charakteristischen Längenskalen.* Dissertation. RWTH Aachen : s.n., 1993.

14. **Dolt, R.** *Indizierung in der Motorentwicklung - Messtechnik, Datenauswertung, Anwendung und Kombination mitoptischen Messverfahren.* München : verlag moderne industrie, 2006. 3-937889-31-0.

15. **Vision Research, Inc.** *Phantom v7.3.* Wayne : s.n., 2013.

16. **Reling, J., Flögel, H.-H. and Werschy, M.** *Technische Endoskopie, Grundlagen und Praxis endoskopischer Untersuchungen* . Renningen : expert Verlag, 2001.

17. **Xenics.** *Xeva-1.7-320 VisNIR - Advanced research in SWR imaging.* Leuven : s.n., 2008.

18. **Kohlrausch, F.** *Praktische Physik.* Stuttgart : Vieweg+Teubner Verlag, 1996. ISBN 978-3-322-87208-1.

19. **Hirsch, A., Rzehorska, M. and Winklhofer, E.** *Flame and Radiation measurement techinques for Dynamic Emission Calibration in Gasoline Engines.* s.l. : PTNSS CONGRESS, 2007.

20. **Yates, A. D. B., Swarts, A. and L., Viljoen C.** *Correlating Auto-Ignition Delays And Knock-Limit Spark-Advance Data For Different Types Of Fuel.* s.l. : SAE 2005-01-2083, 2005.

21. **Zhou, A., Dong T., Akih-Kumgeh B.** *Simplifying ignition delay prediction for homogeneous charge compression ignition engine design and control.* International Journal of Engine Research. 2016, Vol. 17(9) 957–968.

22. **Yokoo, T., et al.** *Research on the Improvement of the Knovking Prediction Accuracy by Considering the Effect of Negtive Temeprature Coefficient for High Compression Ratio Engine.* [Buchverf.] A. Leipertz. *Engine Combustion Processes - Current Problems ans Modern Techniques.* Erlangen : ESYTEC Energie- und Systemtechnik GmbH, 2017.

23. **Yates, A., Vilijoen, C. und Swarts, A.** *Understanding The Relation Between Cetane Number And Combustion Bomb Ignition Delay Measurements.* s.l. : SAE 2004-01-2017, 2004.

24. **Winklhofer, E., et al.** *TC GDI Engines at Very High Power Density – Irregular Combustion and Thermal Risk*. s.l. : SAE International, 2009.

25. **Döhler, A. und Schaffner, P.** *Optical Diagnostic Tools for Detection and Evaluation of Glow Ignitions*. [Buchverf.] M. Günther und M. Sens. *Knocking in Gasoline Engines.* Cham, Switzerland : Springer International Publishing AG 2018, 2017.

26. **Günther, M., Uygun, Y., Kremer, F. and Pischinger, S.** *Vorentflammung und Glühzündung von Ottokraftstoffen mit Bioanteilen.* s.l. : MTZ, 2013.

27. **Dedl, J., et al.** *Kraftstoffkennzahlen zur Beschreibung von Vorentflammungen in Ottomotoren.* s.l. : MTZ, 2018.

28. **Dahnz, C., et al.** *Investigations on Pre-Ignition in Highly Supercharged SI Engines.* s.l. : SAE 2010-01-0355, 2010.

29. **Martin, C., et al.** *Development of New Test Methods to Describe Knock and Pre-Ignition Behaviour of Fuel and Oil in Highly Charged Gasoline Engines.* 35. Internationales Wiener Motorensymposium 2014 : s.n., 2014.

30. **Pischinger, S., Hoppe, F., Krieck, M. et al.** *Behaviour of Fuel and Oil in Highly Charged Gasoline Engines "Tailor-Made Fuels from Biomass"*. 37. Internationales Wiener Motorensymposium 2016 : s.n., 2016.

31. **Adomeit, P., et al.** *Effect of fuel and combustion system on the pre-ignition of boosted SI engines.* s.l. : 34. Internationales Wiener Motorensymposium, 2013.

32. **Luef, R., et al.** *Development of a New Test Procedure to Determine Fuel and Oil Impact on Irregular Combustion Phenomena with Focus on Highly Boosted Downsized S.I. Engines.* s.l. : 23rd Aachen Colloquium Automobile and Engine Technology, 2014.

33. **Spicher, U., et al.** *Die Bedeutung des Motoröls bei der Entstehung der Vorentflammung.* s.l. : MTZ , 2016.

34. **Berg, T., Seefeld, S. and Thiele, O.** *Quantitative Optical Measurement Techniques for Mixture Formation and Combustion Process Analysis.* s.l. : Springer International Publishing AG, 2018. M. Günther and M. Sens (eds.), Knocking in Gasoline Engines, https://doi.org/10.1007/978-3-319-69760-4_12.

35. **Willand, J et al.** *Die Grenzen des Wownsizings bei Ottomotoren durch Vorentflammungen.* s.l. : MTZ, 2009.

36. **Wigger, S., et al.** *Visualization of Fuel Wall Wetting, Oil Dilution by Fuel, and Oil Transport Mechanisms in an Optically Accessible Engine by LIF Imaging.* s.l. : Springer International Publishing AG, 2018. M. Günther and M. Sens (eds.), Knocking in Gasoline Engines, https://doi.org/10.1007/978-3-319-69760-4_10.

37. **Alger, T. F., Briggs T. E.** *Chemical Analysis of Potential Initiating Fluid for Low-Speed Pre-ignition.* s.l. : Springer International Publishing AG, 2018. M. Günther and M. Sens (eds.), Knocking in Gasoline Engines, https://doi.org/10.1007/978-3-319-69760-4_7.

38. **Leach, B. et al.** *Management of Low Speed Pre-Ignition via Fuel and Lubricant Formulation.* 26th Aachen Colloquium Automobile and Engine Technology : s.n., 2017.

39. **Mayer, M., et al.** *Vorentflammungseinfluss des Motoröls bei hochaufgeladenen Ottomotoren mit direkter Einspritzung.* s.l. : MTZ, 2016.

40. **Lauer, T., et al.** *Modellansatz zur Entsehung von Vorentflammungen.* s.l. : MTZ, 2014.

41. **Kassai, M., Shiraishi, T. and Noda, T.** *Fundamental Mechanism Analysis on the Underlying Processes of LSPI Using Experimental and Modeling Approaches.* s.l. : Springer International Publishing AG, 2018. M. Günther and M. Sens (eds.), Knocking in Gasoline Engines, https://doi.org/10.1007/978-3-319-69760-4_6.

42. **Hirsch, A., Kapus, P., Winklhofer, E.** I*rregular combustion events in RDE test situations, Diagnostics – Analysis – Improvements*. Berlin : 5. Internationale Tagung Ottomotorisches Klopfen 12. und 13. Dezember 2017, 2017.

43. **Iwatsuka, T., et al.** *Study of HSPI/LSPI from Spark Plugs on Turbocharged Gasoline Engines.* Knocking in Gasoline Engines, : Springer International Publishing AG , 2018. https://doi.org/10.1007/978-3-319-69760-4_5.